DOCTORAL DISSERTATION

Advances in soil-structure interaction modelling for seismic analysis of offshore wind turbine pile foundations. Parametric assessment of soil heterogeneity, non-linear behaviour, and pile group effects

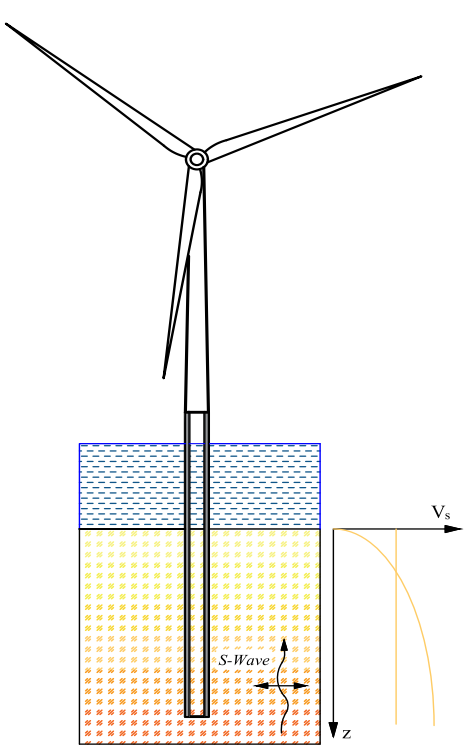

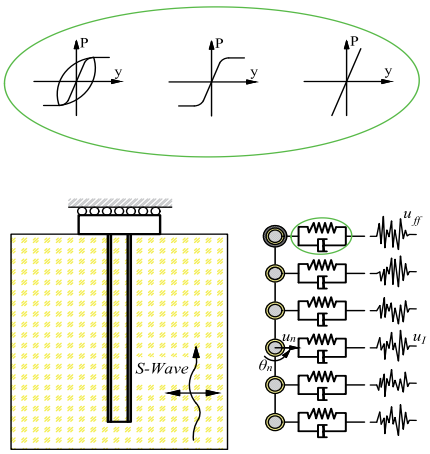

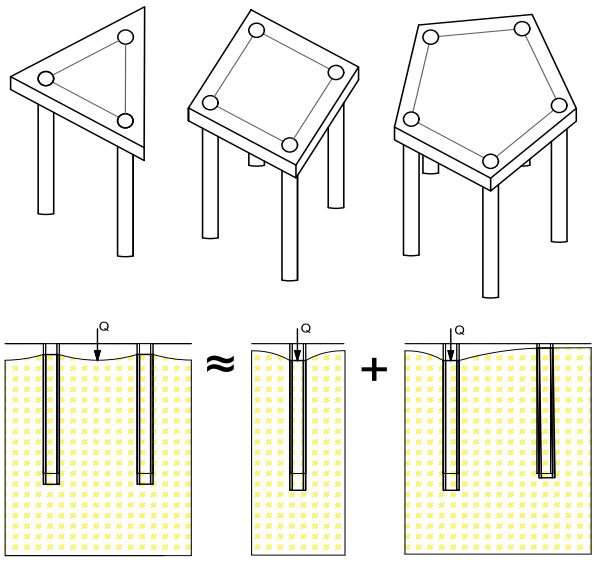

Eduardo Rodríguez Galván

Continuum Mechanics and Structures Division

Las Palmas de Gran Canaria • October 2025

INSTITUTO UNIVERSITARIO SIANI INGENIERIA COMPUTACIONAL

ULPGC Universidad de Las Palmas de Gran Canaria

Programa de Doctorado: Tecnologías de Telecomunicación e Ingeniería Computacional

Advances in soil-structure interaction modelling for seismic analysis of offshore wind turbine pile foundations. Parametric assessment of soil heterogeneity, non-linear behaviour, and pile group effects.

Eduardo Rodríguez Galván

RODRIGUEZ GALVAN EDUARDO - 45375946M

Firmado digitalmente por RODRIGUEZ GALVAN EDUARDO - 45375946M
Fecha: 2025.10.16 12:49:21 +01'00'

Universidad de Las Palmas de Gran Canaria
Escuela de doctorado

Programa de doctorado
Tecnologías de Telecomunicación e Ingeniería Computacional

Director:
Guillermo Manuel Álamo Meneses

ALAMO MENESES GUILLERMO MANUEL - 44739814F

Firmado digitalmente por ALAMO MENESES GUILLERMO MANUEL - 44739814F
Fecha: 2025.10.16 12:55:32 +01'00'

Director :
Juan José Aznárez González

AZNAREZ GONZALEZ, JUAN JOSE (FIRMA)

Firmado digitalmente por AZNAREZ GONZALEZ, JUAN JOSE (FIRMA)
Fecha: 2025.10.16 13:10:51 +01'00'

Las Palmas de Gran Canaria, October 2025

Acknowledgements

Firstly, I would like to express my deepest gratitude to my supervisors, Guillermo Álamo and Juan José Aznárez, for granting me the opportunity to carry out this work. I am profoundly grateful to them for offering me their assistance and guidance right from the start. Without their invaluable support and dedication, this work could not have been accomplished.

I am also extremely thankful to Orlando Maeso, who was the first to place his trust in me and gave me the opportunity of being part of such an excellent research group. Together with Guillermo Álamo, he has guided me since my Bachelor and Master's theses, always willing to offer his support, guidance and advice. Without their encouragement and motivation, I might never have undertaken this doctoral journey.

I would also like to express my gratitude to the entire Continuum Mechanics and Structures Division for being such a fantastic group to work with. Starting with Luis A. Padrón and Cristina Medina for being always there and ready to help with anything that was required; and continuing with my colleagues Carlos Romero, Borja Benítez, Samuel González and Óscar Ramón for always creating such a positive and supportive work environment. I am also grateful to Fidel García for his support and facilitating my teaching activities in the Department of Civil Engineering at ULPGC.

I am deeply grateful to Sandro Carbonari for welcoming me so warmly at Universtà Politecnica delle Marche. I would like to extend my gratitude to Francesca Dezi from University of Camerino. I am immensely thankful for granting me the extraordinary opportunity to collaborate with them and benefit from their expertise. I will never forget all the kindness I received in Ancona from every member of the Dipartimento di Ingegneria Civile, Edile e Architettura, who made me feel like home.

Lastly, though never enough, I would like to express my immense gratitude to my family, especially to my parents and my brother, for their unconditional support and love, which have been essential in helping me get to this point. Their constant encouragement and belief in me have been an invaluable source of strength and motivation. This work would not have been possible without the values, dedication, and example they have instilled in me.

This work has been funded by Ministerio de Ciencia e Innovación and Agencia Estatal de Investigación (MCIN/AEI/10.13039/ 501100011033) of Spain and FEDER through research project PID2020-120102RBI00 and predoctoral research scholarship PRE2021-099200 (Eduardo Rodríguez Galván), also funded by European Social Found Plus (FSE+). The research scholarship also provided financial support for the short-therm research at Università Politecnica delle Marche. In addition, this work has been partially supported by ACIISI, Spain-Gobierno de Canarias and European FEDER Funds Grant EIS 2021 04. Finally, throughout the grant period, the Research Group to which the author belongs has received founding from one national research project PID2023-151635OB-I00, founded by Ministerio de Ciencia, Innovación y Universidades and Agencia Estatal de Investigación (MCIU/AEI/10.13039/501100011033) and the FSE+.

Las Palmas de Gran Canaria, October 2025

Eduardo Rodríguez Galván

CONTENTS

Contents i

1 Introduction and background 3
1.1 Introduction 3
1.2 Literature review 5
1.3 Aims and objectives 8
1.4 Research group 8
1.4.1 Research Project PID2020-120102RB-I00 9
1.5 Published works derived from the PhD Thesis 9
1.5.1 Contributions in JCR journals 9
1.5.2 Conference contribution 10
1.6 Justification of the thematic unity and coherence of the PhD Thesis 10

2 Publications 15
2.1 First publication: Rodríguez-Galván et al., 2023, Marine Structures 15
2.2 Second publication: Rodríguez-Galván et al., 2024, Computers and Geotechnics 33
2.3 Third publication: Rodríguez-Galván et al., 2025, Engineering Structures 49

3 Summary, conclusions, and future research directions 69
3.1 Summary and conclusions 69
3.2 Future research directions 72

A Resumen en castellano 75
A.1 Introducción 75
A.2 Objetivos 79
A.3 Publicaciones derivadas de la tesis doctoral 80
A.4 Justificación 81
A.5 Conclusiones 82

References 89

1. Introduction and background

1.1 Introduction
1.2 Literature review
1.3 Aims and objectives
1.4 Research group
1.5 Published works derived from the PhD Thesis
1.6 Justification of the thematic unity and coherence of the PhD Thesis

1.1 Introduction

Pile foundations are widely employed to support a broad range of civil and marine structures, such as buildings, bridges, and offshore platforms. Their use is particularly advantageous in situations where surface soils are weak or unstable, since they transfer loads to deeper and more stable strata. Among all their benefits, the most notable ones are: high load-bearing capacity, providing an excellent capability to resist horizontal forces while they support the vertical loads of the superstructure (a typical situation for tall structures exposed to environmental and seismic loads); adaptability to diverse geotechnical conditions; reduction of settlements; and suitability for submerged sites or offshore constructions [1, 2].

Within the offshore sector, pile foundations were initially employed for supporting oil extraction structures. However, in recent years, with the aim of achieving a global transition toward a more sustainable and low-carbon energy future, they have also become a common foundation solution for Offshore Wind Turbines (OWTs). Offshore wind energy presents a great advantage in terms of energy production in comparison to the onshore one, as offshore technology benefits from stronger and more consistent wind speeds, providing higher energy outputs and capacity factors. Nevertheless, offshore wind technology involves higher installation, operation, and maintenance costs due to more demanding environmental conditions and the technical complexity of the infrastructures. Despite these challenges, its potential is substantial, especially in areas with high energy demand near the coast. For all these reasons, offshore wind energy has been significantly increasing its representation in recent years, and it is expected to continue gaining popularity in the near future. Attending to the recent 2025 Global Wind and Offshore Wind reports ([3, 4], respectively), 8 GW of new offshore wind capacity was connected to the grid in 2024, raising a total installed capacity of 83.2 GW at the end of this year, which is equivalent to the electricity demand of around 73 million households annually. In this way, 2024 was the fourth highest year in the history of offshore wind development. Despite the crisis derived from the COVID-19, the three preceding years to 2024 were the most active in offshore wind history, ranked as follows in terms of new capacity additions: 2021 with 21.1 GW, 2023 with 10.8 GW, and 2022 with 8.8 GW. Regardless of the existing geopolitical uncertainty and supply vulnerability, this tendency is likely to persist over the next few years, as it was observed after the COVID-19 crisis.

A critical component of any OWT is its substructure, including the foundation, which acts as the interface between the seabed and the OWT transferring environmental, self-weight, and operational loads to the submarine ground. As offshore wind farms are installed further from the coast and into deeper seabeds, the complexity of the engineering challenges related with supporting this type of structures is greater. Substructure choice is influenced by different conditions, such as water depth, seabed properties, turbine dimensions, installation and transportation procedures, and other economic factors. Attending to these aspects there are several OWT substructure typologies with different characteristics and compatibilities with distinct site scenarios.

These substructures can be grouped into two main categories: bottom-fixed and floating substructures. On the one hand, floating substructures are suitable for deep-water installations, where bottom-fixed ones are not feasible (depths greater than 60-70 m). Nevertheless, they are still in active development and deployment, and their average lifetime costs are notably higher than bottom-fixed substructures. On the other hand, bottom-fixed substructures are employed for lower seabed depths (up to 60-70 m). They are more mature technology with established supply chains. This fact added to their simple installation and maintenance make them a cheaper solution. For all these reasons, bottom-fixed solutions continue to dominate the offshore wind sector, and they are expected to remain the prevailing choice in the near future. Following the statistics provided by the 2024 Offshore Wind Market Report [5], bottom fixed foundations represented more than 99 % of the reported operating substructures in 2023. Bottom-fixed foundations include various typologies, ranked in popularity according to 2024 Offshore Wind Market Report [5] as follows: monopile (69.7 % of the 2023 reported operating substructures), jackets (16.8 %), high-rise pile caps (9.5 %), tripods (1.9 %), and gravity-based (1.6 %). Firstly, monopile is the most typically used technology. It consists of a single large diameter steel tube driven into the seabed. It is the best option for shallow waters due to its cost effectiveness and speed of installation. Monopiles are expected to keep leading the offshore substructure representation. According to [5], 75 % of the next 72 GW of future offshore projects will be supported by monopile foundations. Secondly, jacket substructures are steel lattice structures used in deeper waters. Due to the need of installing OWTs further from the coast and, therefore, into deeper seabed depths, they have been gaining popularity over the years. This type of substructure is founded on pile groups or suction caissons disposed in a polygonal arrangement (generally between 3 and 5 piles or suction caissons). According to the 2023 substructure data provided by [5], suction caissons support 3.15 % of the 16.8 % of jacket representation. Suction caissons offer a quiet installation process and are relatively easy to deploy. However, pile groups are more commonly used as they can be installed in a wider range of soil conditions, and they provide higher bearing capacity due to their structural efficiency, greater slenderness, and vertical stiffness [6]. Afterwards, pile cap substructures consist of multiple piles driven into the sea ground and joined by a cap in their heads. Finally, tripods are central steel shafts connected to three legs, which are founded on piles or suction caissons. In this way, the significance role of pile foundations in the offshore wind sector is particularly noteworthy.

OWTs are constantly subjected to dynamic and highly variable loads: wind, waves and operational ones. Thus, the dynamic analysis of this type of structures is a fundamental requirement in their design and performance assessment, particularly in relation to their substructure and foundation. Moreover, as a consequence of the global expansion of OWTs, projects are being deployed in regions with significant seismic activity. For this reason, seismic loads derived from earthquake induced ground motions have also become an essential consideration to take into account, recently emerging recommended practices to reduce the earthquake risk of wind power plants [7]. All these dynamic loads induce vibrations that lead to fatigue damage and structural instabil-

ity, affecting the performance of the overall system and even conducting to failure over time. In addition, other crucial aspect in the design of this type of structures is ensuring that the system's natural frequencies are not close to those of the rotor operation, intermittent shading produced by blade rotation, and environmental loads. It is precisely in all these aspects where the consideration of the soil-structure interaction (SSI) is essential, since its inclusion notably affects the dynamic response of the overall system.

1.2 Literature review

The dynamic behaviour of OWTs has been extensively investigated during the first quarter of the 21st century [8–30]. In recent years, seismic loads have also been studied and incorporated to the environmental and operational ones to perform the analysis, as well as the design, of these structures [8, 10, 11, 14–31]. The incorporation of the seismic loads has arisen as a consequence of the growing recognition that, even for low intensity earthquakes, seismic actions must be considered to guarantee a suitable structural response, as it has been demonstrated in [8, 20, 30, 31].

To perform the dynamic analysis and design of these slender structures, which are usually founded on soft seabeds, the consideration of the SSI phenomena plays a key aspect. This is because SSI incorporation is crucial for accurately estimating the dynamic behaviour of these structures, and its consideration may result to higher dynamic responses than fixed-base assumptions [8–10, 21, 24, 25, 32, 33]. Regarding existing modelling techniques for reproducing SSI, they can be mainly divided into two large groups: linear and non-linear models, both of which can be used to capture SSI effects in single and multiple pile foundations.

On the one hand, SSI linear models [8, 22–26, 29, 34–41] assume that the behaviour of soil, pile, and their interaction remain elastic, and the stiffness and damping properties do not change with deformation or load intensity. One linear approach is the substructuring method, which employs a set of complex-valued impedance functions and kinematic interaction factors [22, 23, 25, 29], representing the soil-foundation stiffness and damping, and the foundation filtering effects over the ground movement, respectively. This formulation is applied in the frequency domain, making it suitable for analytical studies and simplified or initial design stages. Other typical technique is to employ lumped parameter models (LPMs) [8, 24, 26]. LPMs approximate the soil's dynamic behaviour by means of discrete mass–spring–dashpot systems whose parameters are calibrated to reproduce the target impedances over a certain frequency range. This allows to incorporate SSI effects directly into time-domain analyses with standard structural dynamics solvers. In these linear SSI models, the reference dynamic behaviour of the soil and foundation is usually computed by using previously developed models, such as elastic halfspace solutions, finite element and boundary element methods, or other alternative techniques [39, 42–45]. However, for pile group foundations, impedance functions can also be estimated using an alternative approach known as the

superposition method [35–40]. This approach allows estimating the dynamic response of a pile group by summing the individual responses of each pile with the interactions between pile pairs to account for pile-soil-pile effects (defined by the so-called interaction factors). The main advantage of this superposition approach in relation to more advanced models is its simplification, which makes it an interesting approach for the initial design stages or performing parametric studies. The effectiveness of the superposition methodology has been explored in the dynamic response of standard pile group configurations (typical arrangements for building foundations) [36, 39]. In these works, it has been demonstrated that the superposition method conducts to accurate dynamic estimations for medium and large pile spacing ratios. Lastly, another commonly used linear approach is the use of Beam on Dynamic Winkler foundation (BDWF) models [34, 38, 41], which consist of independent discrete springs and dashpots disposed in parallel between them and along the pile length, reproducing the dynamic response of the surrounding soil. In these linear BDWF models for pile groups, the pile-soil-pile effects are usually accounted through interaction factors [38, 41]. The main advantages of all the aforementioned linear models with respect to non-linear ones is their ease of definition and their computational efficiency. These facts make them suitable for conducting preliminary designs and parametric studies, where a large number of cases need to be computed. Regarding the study of the dynamic behaviour of OWTs, linear models are typically used in substructuring models in which SSI is represented through impedance functions and interaction factors [22, 23, 25, 29], or via LPMs [8, 24, 26].

On the other hand, non-linear SSI models capture the non-linear behaviour of soil-pile interaction, enabling to account for features such as: stiffness degradation, hysteresis behaviour, and plasticity. They usually involve hyperbolic soil resistance-deflection ($p-y$) relations and loading-unloading rules, which need iterative time-domain solutions. Due to all these characteristics, they are more complex models and considered more realistic than linear assumptions. Non-linear behaviours are simulated by means of BDWF models, whose springs along the pile length can be considered with an elastic or inelastic behaviour. For multiple pile foundations, the pile-soil-pile interaction effects are usually reproduced by soil resistance multipliers ($p-$multipliers), which are empirical reduction factors applied to the $p-y$ curves of a single (isolated) pile to account for group effects [46–48]. Lateral soil–pile interaction for OWT foundations is commonly represented through $p-y$ curves, which define the non-linear relationship between the lateral soil resistance (p) and deflection (y) at a given depth. Among the various formulations proposed in the literature, the empirical curves recommended by the American Petroleum Institute [49] have become the most widely adopted, since its application is recommended by the offshore standard DNV-OS-J101 [50]. For all these reasons, the implementation of non-linear SSI models for assessing the dynamic response of these structures has become increasingly significant in recent years, as reflected in the growing number of studies utilising such models [9–19, 21, 31].

Both SSI considerations (linear and non-linear) have been widely employed and studied for analysing the dynamic response of OWTs supported by monopiles and jacket substructures [8–19, 21–26, 29, 31]. Nevertheless, certain aspects concerning the

modelling of SSI and its associated effects on the seismic response of OWT pile foundations require further research. For instance, linear models have already been applied to assess the contribution of several parameters, such as wind turbine dimensions [8, 25], operational conditions [8, 26], seismic directionality [26], etc. However, the influence of the seabed profile typology on the seismic response of OWTs, and the analysis of SSI effects depending on the seabed profile definition have not been carried out yet. The understanding of all these aspects related to the seabed profile definition would be highly beneficial to address the dynamic analysis and design stages of these structures, especially in scenarios where accurately characterising the seabed profile presents significant challenges due to its inherent complexity. In addition, SSI is composed of two types of interactions: kinematic and inertial interaction. Kinematic one is influenced by soil motion and soil-pile interface, whereas inertial interaction is affected by the superstructure mass. The majority of studies addressing SSI effects tend to adopt a holistic approach [8–10, 21, 23–26], without examining the individual contributions of kinematic and inertial components that comprise it. A deeper understanding of how these two phenomena behave would enhance the understanding of the dynamic behaviour, as well as improving the SSI modelling of this type of structures. An additional unexplored aspect within SSI modelling for OWT pile foundations concerns the influence of accounting for non-linear and inelastic behaviour of SSI, in comparison to the linear elastic assumption. Although the non-linear effects in soil properties, such as plasticity and stiffness degradation, have been studied in the dynamic analysis of these structures (see, e.g., [51]), the non-linear effects in SSI modelling for the dynamic assessment of these devices have not yet been evaluated. Insight into the non-linear and inelastic effects in SSI modelling, in comparison with a linear elastic model, would help to define the applicability range of both assumptions, providing a valuable contribution to the dynamic analysis and design of such structures. Lastly, as commented before, the applicability of the superposition's method for traditional pile group setups of civil infrastructures has been widely evaluated (see, e.g., [36, 39]). Nevertheless, its feasibility for OWT pile group arrangements, which are composed of hollow cylindrical steel piles disposed in N-sided polygonal layouts, has not been addressed in the dynamic study of these structures. Therefore, assessing its applicability for OWT pile groups becomes necessary in order to determine whether this method may represent a valuable alternative for SSI modelling in such structures. Given all these factors, although a great number of dynamic analyses incorporating SSI effects have been performed for OWTs in the present century, significant uncertainties still remain regarding on: how the definition of the seabed profile influences the dynamic response of OWTs and SSI effects; a better understanding of the kinematic and inertial interaction contributions within the overall SSI; how the consideration of a non-linear and inelastic behaviour in SSI affects the dynamic response of these structures, in comparison to a linear elastic approach; and the applicability of the superposition method to determine the pile group impedance functions for OWTs.

1.3 Aims and objectives

This PhD thesis aims to advance the SSI modelling for the seismic analysis of OWT pile foundations. Investigating the influence of several aspects such as: soil heterogeneity, non-linear SSI behaviour, and pile group effects, through a series of parametric studies. Therefore, to achieve this, three partial objectives are established:

1. To examine the influence of the seabed profile definition on the seismic response of various monopile-supported OWTs, assessing the effects of SSI and its kinematic and inertial components.

2. To investigate the impact of non-linear and inelastic behaviour of soil-pile interaction on the seismic response of OWT pile foundations and monopile-supported OWTs.

3. To assess the suitability of the superposition method in the computation of impedance functions for OWT pile groups, analysing a wide range of realistic configurations and the influence of the main variables involved in the problem.

The objectives outlined not only enhance the modelling and understanding of the SSI phenomena on the seismic response of OWT pile foundations, but also provide a valuable contribution to the structural design and dynamic analysis of these systems. Based on the conclusions reached, it becomes possible to identify the most appropriate SSI models and considerations to be applied in each specific scenario.

1.4 Research group

This dissertation has been carried out within a research group with extensive experience in the formulation and implementation of numerical models for elastic wave propagation and structural dynamics problems. The primary methodology employed in the development of these models is the Boundary Element Method (BEM). To support this approach, increasingly sophisticated and efficient integral formulations have been devised, enabling a rigorous and computationally economical treatment of complex dynamic problems, such as soil-structure and pile-soil-pile problems [45, 52, 53]. All these models developed by the research group share a common hypothesis: the linear behaviour of all the media involved in the problem. One of the objectives of this PhD thesis is to initiate the incorporation of non-linear effects into the developed models conducted by the research group. The inclusion of these non-linear and inelastic effects would allow to expand the capabilities and application range of the linear models developed so far within the research group, as well as to establish a reliable applicability domain for these linear models.

In recent years, the research group has focused particularly on studying the dynamic response of bottom-fixed OWTs, along with the structural design of these systems. The

present dissertation is aligned with the latter field and has been conducted within the framework of the research project PID2020-120102RB-I00.

1.4.1 Research Project PID2020-120102RB-I00

The Research Project PID2020-120102RB-I00 was titled "ANN-based design of the support structures of offshore wind turbines including advanced models of soil-structure interaction and seismic actions". It was supported by the Ministerio de Ciencia e Innovación (MCI) and the Agencia Estatal de Investigación (AEI) of Spain. The project ran from September 1, 2021, to February 28, 2025, including an approved extension until the latter date. This research project focused on two main objectives:

1. To develop a methodology based on artificial neural networks for designing the support structures of bottom-fixed OWTs.

2. To continue the development of the numerical models created in the framework of previous projects (BIA2014-57640-R and BIA2017-88770-R) and apply them to studies aimed at advancing the understanding of the factors that influence the seismic response of these structures, in addition to generate practically applicable knowledge based on the findings.

This PhD thesis focuses on the second objective, aiming to advance in the modelling of SSI for the seismic analysis of OWT pile foundations, exploring the influence of some factors over this complex phenomenon.

1.5 Published works derived from the PhD Thesis

This PhD dissertation is composed of three publications published in scientific journals indexed in the Journal Citation Reports (JCR), which are listed in Section 1.5.1. In addition, a conference communication derived from this work is also mentioned in Section 1.5.2.

1.5.1 Contributions in JCR journals

- E. Rodríguez-Galván, G. M. Álamo, C. Medina and O. Maeso. Influence of seabed profile on the seismic response of monopile-supported offshore wind turbines including dynamic soil-structure interaction. Marine Structures, 92:103500, 2023.

- E. Rodríguez-Galván, G. M. Álamo, J. J. Aznárez and O. Maeso. Non-linear behaviour of soil–pile interaction phenomena and its effect on the seismic response of OWT pile foundations. Validity range of a linear approach through non-degraded soil properties. Computers and Geotechnics, 168:106188, 2024.

- E. Rodríguez-Galván, G. M. Álamo, J. J. Aznárez and O. Maeso. An accurate and ready-to-use approach for the estimation of impedance functions of regular pile groups for offshore wind turbine foundations. Vertical and rocking components. Engineering Structures, 323:119288, 2025.

1.5.2 Conference contribution

- E. Rodríguez-Galván, G. M. Álamo, C. Medina, L. A. Padrón, J. J. Aznárez and O. Maeso. Seismic response of monopile-supported offshore wind turbines embedded in different seabed profiles including dynamic soil-structure interaction. 9th International Conference on Computational Methods in Structural Dynamics and Earthquake Engineering (COMPDYN), 2023.

1.6 Justification of the thematic unity and coherence of the PhD Thesis

The dynamic response of OWTs is a complex problem which must be evaluated considering the interaction between all existing components: tower, substructure, foundation and soil. To perform these dynamic analyses, analytical and numerical models are needed. Incorporating SSI and its associated effects has been demonstrated to be crucial for correctly reproducing the dynamic response and performing the design of these structures. However, although SSI has been widely studied in recent years, there are still various unresolved questions regarding its modelling and its associated effects. For these reasons, this PhD thesis focuses on examining the influence of certain aspects related to the SSI modelling (soil heterogeneity, non-linear soil-pile interaction, and group effects), aiming to contribute to a better understanding of this phenomenon and to the dynamic assessment and design of pile-supported OWT structures. In pursuit of this objective, multiple SSI numerical models are developed and employed throughout this dissertation to analyse the effects of the different parameters that govern the problem. To this end, three parametric studies are conducted:

Firstly, the influence of the seabed profile on the seismic response of monopile-supported OWTs from 5 to 15 MW is studied, analysing the influence of SSI, as well as the inertial and kinematic interaction contributions within it [54]. For this purpose, a substructuring model is used. In order to examine the SSI effects, along with the kinematic and inertial contributions, different submodels are defined. In addition to enhancing the understanding of SSI effects on the seismic response of monopile-supported wind turbines founded on different soil profiles, this study also provides a valuable contribution to the design of such structures, where defining the soil profile often presents a significant challenge, due to the uncertainty involved in its definition when no geotechnical studies are available.

Secondly, the contribution of the non-linear and inelastic behaviour of soil-pile interaction on the seismic response of OWT pile foundations and monopile-supported

OWTs is analysed [55]. For this purpose, three SSI models based on Beam on Dynamic Winkler Foundation approach are developed: a plastic non-linear, an elastic non-linear and an equivalent non-degraded linear model. The seismic response of several single pile foundations embedded in two seabed typologies is studied, analysing the contributions of the kinematic and inertial interaction within SSI. Finally, the seismic response of several monopile-supported OWTs from 5 to 15 MW is examined for each model. The quantification of the non-linear and inelastic effects in the SSI modelling, together with the comparison of these models against an equivalent elastic one, suppose an significant advance in the understanding of SSI modelling for this type of structures, providing guidance in selecting the most suitable SSI model for design processes and seismic analysis.

Finally, the application of the superposition method for the estimation of the vertical and rocking impedance functions for OWT pile group foundations is evaluated [56]. The analysis of the rocking impedance term has been selected due to the key role of this component on the seismic response of this type of structures, as it was concluded in the first work of this PhD thesis [54]. This analysis is performed for a wide range of pile group foundations, analysing the influence of the main parameters involved within the problem. Some expressions dependent on these parameters are proposed in order to estimate the single pile response and the pile-soil-pile interaction. These expressions together with the superposition method allow to estimate the pile group impedance functions without the need of disposing any other model. Therefore, the proposed expressions along with the superposition method constitutes a useful approach to quickly determine the SSI impedance functions, which could be particularly effective to perform the initial design stages of these structures, or other parametric studies.

Although this PhD thesis addresses a wide range of SSI models and related aspects associated with them, the methodological framework adopted throughout the work remains consistent: the comparison and analysis of several SSI models, each specifically designed or selected to study the key phenomena under investigation. This comparison is carried out by performing parametric studies in which a wide range of configurations and variables involved in the problem are assessed, in order to obtain general conclusions that contribute to advance in the SSI modelling of these structures.

Concerning the organization of this dissertation, it is divided into three chapters: the first one contains the present introduction; the second one comprises the three contributions published in JCR-indexed journals, that compose the compendium thesis; and the third one includes a summary, the main conclusions, and future research directions resulting from this research work.

2. Publications

2.1 First publication: Rodríguez-Galván et al., 2023, Marine Structures

2.2 Second publication: Rodríguez-Galván et al., 2024, Computers and Geotechnics

2.3 Third publication: Rodríguez-Galván et al., 2025, Engineering Structures

2.1 First publication: Rodríguez-Galván et al., 2023, Marine Structures

Table 2.1. First publication data.

Title	Influence of seabed profile on the seismic response of monopile-supported offshore wind turbines including dynamic soil-structure interaction
Authors	E. Rodríguez-Galván, G.M Álamo, C. Medina and O. Maeso
Journal	Marine Structures
DOI	10.1016/j.marstruc.2023.103500
ISSN	0951-8339
Impact factor	4.0
CiteScore	8.7
Category	Engineering, Marine
Quartile	Q1 (11/105)
Publisher	ELSEVIER SCI LTD
Volume	92
Date	November 2023

Marine Structures 92 (2023) 103500

Contents lists available at ScienceDirect

Marine Structures

journal homepage: www.elsevier.com/locate/marstruc

Influence of seabed profile on the seismic response of monopile-supported offshore wind turbines including dynamic soil-structure interaction

Eduardo Rodríguez-Galván *, Guillermo M. Álamo, Cristina Medina, Orlando Maeso

Instituto Universitario de Sistemas Inteligentes y Aplicaciones Numéricas en Ingeniería, Universidad de Las Palmas de Gran Canaria, 35017 Las Palmas de Gran Canaria, Spain

ARTICLE INFO

Keywords:
Offshore wind turbines
Seabed profile
Soil-structure interaction
Kinematic interaction
Monopile
Seismic response

ABSTRACT

In this article, the seismic response of four different Offshore Wind Turbines (OWTs) from 5 to 15 MW, founded on monopiles embedded in homogeneous and non-homogeneous soil profiles with equivalent shear-wave velocities from 100 to 300 m/s is analysed. Two types of variable soil profiles with a semi-parabolic variation of the shear-wave velocity as depth increases are considered. The system seismic response under ten different accelerograms is computed through a finite element substructuring model in frequency domain. The foundation behaviour is obtained by a continuum model including kinematic and inertial interaction. Several models, in addition to that of rigid base condition, are considered to determine the influence of soil-structure interaction (SSI), as well as the contribution of each kinematic interaction (KI) factor. The seismic response of the OWTs is obtained in terms of maximum shear forces and bending moments at mudline level, as well as the acceleration amplification factor at hub level. It is found that the maximum response is produced when SSI is considered, including both the inertial and kinematic interaction. The differences arising due to the soil profile definition are shown to be mainly related to the rotational KI factor, which significantly affects the second vibration mode of the system. The largest responses are obtained for the homogeneous equivalent profile.

1. Introduction

The broad growth experienced by offshore wind energy in recent years has led to considering the installation of offshore wind farms in seismically active regions. As a consequence, the seismic analysis of this type of structures has gone from being a secondary hypothesis to becoming a relevant consideration. In fact, recommended practices are already emerging to reduce seismic risk in wind power plants (such as DNV-RP-0585 "Seismic design of wind power plants" [1], recently published in 2021). In addition, the growing size of wind turbines in search of increasing powers also implies additional uncertainty. Although the influence of the size of wind turbines on their seismic responses has been analysed in previous articles [2,3], such as the one by Medina et al. [2], concluding that the larger the wind turbine, the seismic loads increase to a lesser extent than the environmental loads, the seismic action should not be neglected, since even low or moderate intensity earthquakes can produce significant increases in the structural demands of the Offshore Wind Turbines (OWTs), and a possible combined action (environmental load together with the seismic load) could affect the design of this type of structures, as it is shown by recent works [3–9].

* Corresponding author.
E-mail addresses: eduardo.rodriguezgalvan@ulpgc.es (E. Rodríguez-Galván), guillermo.alamo@ulpgc.es (G.M. Álamo), cristina.medina@ulpgc.es (C. Medina), orlando.maeso@ulpgc.es (O. Maeso).

https://doi.org/10.1016/j.marstruc.2023.103500
Received 5 October 2022; Received in revised form 1 June 2023; Accepted 14 July 2023
Available online 26 July 2023

On the other hand, if wind turbines are founded on deformable soils, the inclusion of the Soil-Structure Interaction (SSI) plays a fundamental role in the dynamic response of the foundation-structure system. The influence of SSI on the dynamic characteristics of OWT has already been addressed in previous articles [10–12], finding all of them relevant variations in the natural frequency due to SSI inclusion, which is a critical factor in the design of this type of structures. Also, in other works [2,13,14] it is demonstrated that the response quantities such as displacements, rotations, accelerations, base shear forces and bending moments are significantly affected by SSI, where its inclusion can double the seismic response with respect to the rigid base assumption, as it is quantified by Medina et al. [2].

The dynamic response of OWTs under seismic loads have been carried out by employing different methodologies. Most of them are based on assuming either a non-linear or linear behaviour for modelling the soil–pile system, and the finite element method to reproduce the superstructure response. The non-linear SSI behaviour is commonly used [4,6–9,11,13,15–19], because it can simulate the plastic and cyclic behaviour of the SSI. In these models the pile–soil interaction is generally reproduced by using non-linear Winkler p-y, t-z and q-z springs, coupled with other finite element programs or codes (such as FAST, OpenSees or Abaqus). In these models, the expressions recommended by the API [20] are commonly used to define the non-linear soil–structure interaction. Nevertheless, these API expressions present significant limitations, since they can only accurately reproduce the pile–soil behaviour of small diameter piles. Besides, another disadvantage of the non-linear assumption is that it requires considerable computational effort. Regarding the linear assumption, it has also been used in numerous works [2,3,21]. Despite being simplified models, they are generally accepted as an initial approach, and they are useful when parametric studies involving a large number of simulations are made. In these linear models, the SSI is usually reduced to a set of impedance functions to reproduce the stiffness and damping of the foundation-soil system, and kinematic interaction factors to represent the filtering of the ground motion produced by the foundation. The linear assumption also allows to study the system response through the frequency domain method (like is made in [2,21]), useful to analyse systems with frequency-dependent and hysteretic damping properties.

Among all the existing types of foundations for offshore wind turbines, the vast majority of them (81.4% in Europe, according to Wind Europe [22]), consist of monopiles. This type of foundation is preferable mainly due to its wide range of installation depths, its low manufacturing cost and ease of installation compared with other foundation types. Monopiles consist of tubular steel sections of large diameters and lengths. Due to their geometric particularities, when monopiles are subjected to seismic excitations they undergo a remarkable rotation, which causes displacements and loads to be taken into account in the wind turbine design. The importance of considering kinematic interaction (KI) in SSI has already been studied by Kaynia [21], showing that such inclusion implies larger responses for a 5 MW wind turbine in different types of soil profiles.

All the works mentioned and those existing in the scientific literature are either carried out on the same type of soil profile or on a single OWT with small rated power (less than or equal to 5 MW). Furthermore, although many seismic SSI analyses can be found [2,3,11,13,14], very few have focused on analysing the KI effects within SSI. For these reasons, this paper aims to study the influence that the type of soil profile has on the seismic response of four OWTs supported by monopiles, analysing for each type of profile the relevance of the inclusion of the inertial and kinematic interaction in the seismic response. For that purpose, three different soil profiles are considered, one homogeneous and two non-homogeneous, the latter two with a semi-parabolic variation of the shear-wave velocity as depth increases. First, the dynamic behaviour of a foundation for a 10 MW OWT embedded in three types of soil profiles, with an equivalent time-average shear-wave velocity for the upper 30 m depth ($V_{S,30}$) of 200 m/s, is analysed in terms of impedances and KI factors. Then, the maximum seismic response of four OWTs from 5 to 15 MW founded on three types of soil profiles is computed. This maximum response is studied assuming various $V_{S,30}$ from 100 to 300 m/s, to consider different soil stiffnesses (soft-to-medium seabeds), and defining various models that allow quantifying the relevance of the inertial and kinematic interaction effects. Finally, to better quantify the relevance of considering the non-homogeneity of the seabed profile, results obtained in all the considered soil profiles and models are compared, addressing the relative differences with respect to the results corresponding to the equivalent homogeneous soil profile.

2. Methodology

The system seismic response is computed through a previously developed finite element substructuring model in the frequency domain [2], where the tower and the substructure are divided into Bernoulli's beam finite elements (see Fig. 1). The flexibility and damping of the foundation-soil are represented by impedances functions for the lateral (or horizontal), rocking and cross-coupled horizontal-rocking vibration modes (denoted as K_H, K_R and K_{HR} in Fig. 1). The filtering of the soil movement by the foundation is represented by lateral (or translational) and rotational KI factors (denoted as I_u and I_θ in Fig. 1). These impedances and KI factors are obtained through a continuum model [23] based on the integral expression of the reciprocity theorem, specially developed to efficiently analyse the harmonic behaviour of pile foundations in layered soils. The use of the substructuring approach allows to separately analyse the contribution of each component of the soil-interaction phenomena, i.e. foundation flexibility and lateral and rotational kinematic interaction, to the system seismic response.

Once the system response is computed in the frequency domain, the response in the time domain is obtained using the frequency domain method [24]. The seismic excitation is assumed to be a planar S wave vertically propagating through the soil, producing a free-field (without foundation) lateral displacement at ground level denoted as u_{ff} in Fig. 1. In order to isolate the seismic response, no environmental loads due to wind or waves are considered in this study.

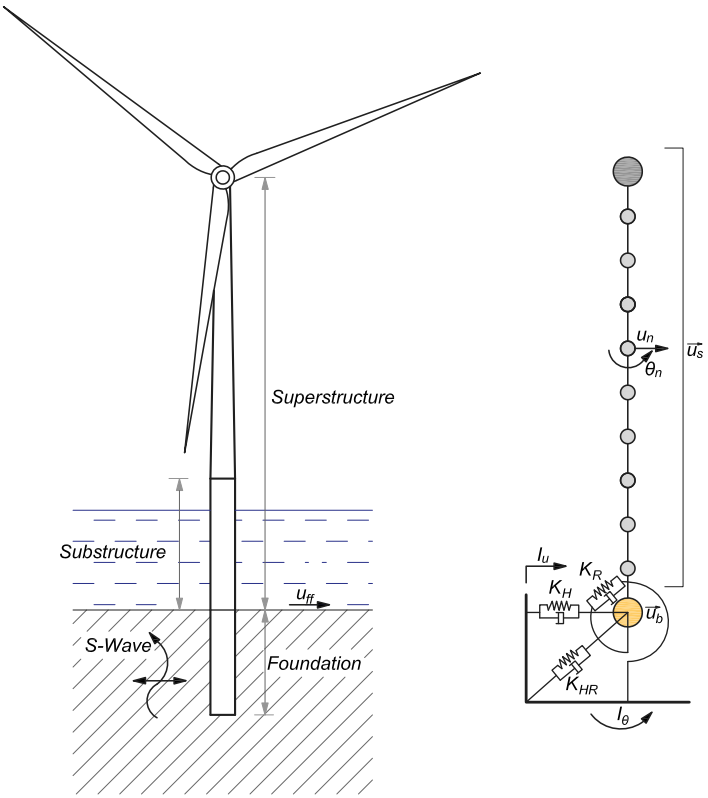

Fig. 1. Substructuring model used in this work.
Source: Adapted from: [2].

2.1. Superstructure modelling

Given the particularities of the problem, only the lateral behaviour of the structure is taken into account. The wind turbine hollow tower and the monopile are divided into finite elements of two nodes (Bernoulli's beams). Based on a convergence study, a sufficiently large number of elements is used, so that the conical shape of the tower is reproduced accurately enough. In this way, each node has two degrees of freedom: a lateral displacement (u_n) and a rotation (θ_n). Distributed inertial properties are assumed for each element. A hysteretic damping model is used for the steel of the monopile and the tower. The stiffness and elementary mass matrices used for each element are shown in Eqs. (1) and (2), being L_e the element length, A_e the cross-sectional area of the element, I_e the moment of inertia of the section area, ρ the material density and E^* the Young's Modulus of the material, including the hysteretic damping ($E^* = E(1+2i\xi)$, being ξ the hysteretic damping ratio and i the imaginary unit). These matrices are assembled to obtain the overall stiffness and mass matrix. The mass of the rotor-nacelle assembly is considered as a punctual mass at the top node. For simplification reasons, the transition piece between the monopile and the tower is not considered.

$$K_e^* = \frac{E^* I_e}{L_e^3}\begin{bmatrix} 12 & 6L_e & -12 & 6L_e \\ 6L_e & 4L_e^2 & -6L_e & 2L_e^2 \\ -12 & -6L_e & 12 & -6L_e \\ 6L_e & 2L_e^2 & -6L_e & 4{L_e}^2 \end{bmatrix} \tag{1}$$

$$M_e = \frac{\rho A_e L_e}{420}\begin{bmatrix} 156 & 22L_e & 54 & -13L_e \\ 22L_e & 4L_e^2 & 13L_e & -3L_e^2 \\ 54 & 13L_e & 156 & -22L_e \\ -13L_e & -3L_e^2 & -22L_e & 4{L_e}^2 \end{bmatrix} \tag{2}$$

2.2. Foundation modelling

The interaction of the structure with the foundation is modelled through the foundation impedance matrix (K_{SSI}), which represents the stiffness and damping of the monopile under the mudline level. As shown in Eq. (3), this matrix is made up of a

horizontal or lateral (K_H), a rocking (K_R) and a cross-coupled (K_{RH} and K_{HR}) impedance functions. All these terms represent the force or moment that should be applied at the monopile head to achieve an unitary displacement or rotation in each of its degrees of freedom, while restricting the rest. These are complex-valued, frequency dependent terms, whose real and imaginary parts represent, respectively, the soil-foundation stiffness and damping (energy dissipation).

$$K_{SSI}(\omega) = \begin{bmatrix} K_H(\omega) & K_{HR}(\omega) \\ K_{RH}(\omega) & K_R(\omega) \end{bmatrix} \tag{3}$$

The filtering effect due to the presence of the foundation is considered through the lateral (I_u) and rotational (I_θ) KI factors, which are grouped in a vector $\vec{I}_{SSI}$:

$$\vec{I}_{SSI}(\omega) = \begin{Bmatrix} I_u(\omega) \\ I_\theta(\omega) \end{Bmatrix} \tag{4}$$

both terms are also complex-valued, dependent on the excitation frequency and represent the offset with respect to the displacement that would occur at the mudline level if the foundation did not exist. Therefore, both terms are obtained as the ratio between the pile head displacement or rotation with respect to the free-field motion:

$$I_u(\omega) = \frac{u_p(\omega)}{u_{ff}} \tag{5}$$

$$I_\theta(\omega) = \frac{\theta_p(\omega)}{u_{ff}} \tag{6}$$

The foundation dynamic response in terms of impedances and KI factors is computed through a previously developed continuum numerical model [23]. This model is based on the integral expression of the reciprocity theorem in elastodynamics and the use of advanced fundamental solutions for reproducing the behaviour of the layered soil, which already satisfy the free-field and inter-layer boundary conditions. On the other hand, piles are treated as load lines in the soil formulation and their stiffness and inertial contribution is considered through their definition as beam finite elements. Pile–soil coupling is made by imposing equilibrium and compatibility conditions in terms of displacements and soil–pile interaction forces. Linear-elastic behaviour of soil and piles is assumed. The ability of this model to accurately reproduce the dynamic behaviour of OWT's foundation elements has been demonstrated in [25].

2.3. Coupled system response

Once the mass and stiffness matrices of the superstructure and the foundation behaviour have been obtained, the system of linear equations to be solved to obtain the response of the superstructure in the frequency domain, including the SSI, can be written as:

$$\left(\begin{bmatrix} K^*_{ss} & K^*_{sb} \\ K^*_{bs} & K^*_{bb} + K_{SSI}(\omega) \end{bmatrix} - \omega^2 \begin{bmatrix} M_{ss} & M_{sb} \\ M_{bs} & M_{bb} \end{bmatrix} \right) \begin{Bmatrix} \vec{u}_s(\omega) \\ \vec{u}_b(\omega) \end{Bmatrix} = \begin{Bmatrix} \vec{0} \\ \vec{f}_{SSI}(\omega) \end{Bmatrix} \tag{7}$$

where the subscript b refers to the submatrices corresponding to the base, while the subscript s refers to the rest of the structure. The vector $\vec{u}_s$ corresponds to the displacements and rotations of the active degrees of freedom of the system, while the vector $\vec{u}_b$ represents the displacement and rotation at the superstructure base and pile head connection (mudline level). The vector $\vec{f}_{SSI}$ contains the shear force and the bending moment at the superstructure base node due to soil-foundation interaction, which, in this case, would coincide with the shear force and the moment at the monopile head (see Fig. 1, where it can be seen that below this node there are no more contiguous elements). This vector $\vec{f}_{SSI}$ is calculated as:

$$\vec{f}_{SSI}(\omega) = K_{SSI}(\omega)\vec{I}_{SSI}(\omega) \tag{8}$$

In order to clarify the influence of including inertial and kinematic interaction, five models are defined:

- **Flexible base models: "with KI", "without KI", "I_u contribution" and "I_θ contribution"**
  Results corresponding to flexible base models are computed from Eq. (7), obtaining $\vec{I}_{SSI}$ from Eqs. (4), (9), (10), (11), to include KI factors, both and none of them, only lateral (I_u) or rotational (I_θ) KI factors, respectively. The models that only include the lateral or rotational KI factors (designated as "I_u contribution" and "I_θ contribution"), aim to quantify the contribution of each KI factor separately.

$$\vec{I}_{SSI}(\omega) = \begin{Bmatrix} 1 \\ 0 \end{Bmatrix} \tag{9}$$

$$\vec{I}_{SSI}(\omega) = \begin{Bmatrix} I_u(\omega) \\ 0 \end{Bmatrix} \tag{10}$$

$$\vec{I}_{SSI}(\omega) = \begin{Bmatrix} 0 \\ I_\theta(\omega) \end{Bmatrix} \tag{11}$$

Table 1
Main characteristics of the OWTs used in this work.
Source: [2].

OWT	5 MW [27]	8 MW [28]	10 MW [29]	15 MW [30]
Rotor-Nacelle-Assembly mass (t)	350	480	674	1017
Tower height (m)	90	110	119	135
Rotor diameter (m)	126	164	178.3	240
Rated wind speed (m/s)	11.4	12.5	11.4	10.59
Cut-out wind speed (m/s)	25	25	25	25
Rotor operational speed range (rpm)	6.9–12.1	6.3–10.5	6–9.6	5–7.56
Tower top diameter (m)	3.87	5	5.5	6.5
Tower bottom diameter (m)	6	7.7	8.3	10
Tower top thickness (m)	0.019	0.022	0.020	0.024
Tower bottom thickness (m)	0.027	0.036	0.038	0.041
Pile diameter (m)	6.04	7.70	8.30	10.00
Pile thickness (m)	0.067	0.084	0.090	0.107
Pile length over mudline (m)	32.6	32.6	32.6	32.6
Pile embedded length (m)	49.7	60.1	63.8	73.8

- **Rigid base model**
  The rigid base assumption implies neglecting SSI effects. Thus, the structure is subjected to the free-field motion directly at its base. Therefore, results for this scenario can be obtained as:

$$(K_{ss}^{*} - \omega^2 M_{ss})\vec{u}_s(\omega) = -(K_{sb}^{*} - \omega^2 M_{sb}) \begin{Bmatrix} 1 \\ 0 \end{Bmatrix} \tag{12}$$

Once the system displacements and rotations are obtained, the nodal values of the internal forces ($\vec{f}_e$, shear forces V and bending moments M) of each element e can be directly computed through:

$$\vec{f}_e = (K_e^{*} - \omega^2 M_e)\vec{u}_e \tag{13}$$

The calculated displacements, rotations and internal forces constitute the system's frequency response functions (FRFs) with respect to the free-field motion. Then, using the frequency domain method [24], the results in the time domain are obtained. Finally, the maximum value of the time history of internal forces and accelerations that take place in the entire system are computed. As shown in Medina et al. [2], the maximum shear forces and bending moments of the superstructure are reached at the mudline level, while the maximum accelerations occur at the nacelle height. Therefore, these are the variables studied in this article to quantify the system seismic response.

3. Problem definition

3.1. OWT properties

The four reference OWTs (see Table 1) as well as the corresponding monopiles (also shown in Table 1) considered in this study are extracted from Medina et al. [2], where monopiles sizing is addressed based on the procedure described by Arany et al. [26].

Both the wind turbine tower and the monopile are considered of S355 structural steel, whose main characteristics are: Young's modulus of 210 GPa, Poisson's ratio of 0.3 and density of 7850 kg/m^3. A hysteretic damping coefficient of 2% is considered for this steel.

3.2. Soil properties

Three types of soil profiles are studied in this article: a homogeneous profile and two non-homogeneous profiles (depth-dependent shear-wave velocity). Equivalent time-average shear-wave velocities for the upper 30 m depth ($V_{S,30}$) between 100 and 300 m/s (with steps of 25 m/s), representing different soft-to-medium seabeds, are used for each type of soil profile. The rest of seabed properties are considered constant with depth for all the soils. In this way, a Poisson's ratio of 0.49, a density of 2000 kg/m^3 and a hysteretic damping of 2.5% are adopted. These are typical values of moderately saturated sands.

To define the two variable profiles, one of the expressions treated by Wang and Wang [31], previously proposed by Hamilton [32], has been used. It defines a simple power law model, as shown in Eq. (14), where the parameter A represents the scale of the shear-wave velocity, and the exponent n indicates the increase in speed with depth.

$$V_S(z) = Az^n \tag{14}$$

Wang and Wang [31] compute A and n by fitting data from real soil wells from California and Japan, obtaining exponent values n between approximately 0.2 and 0.5. The boreholes treated by Wang and Wang include a wide variety of soils, being their results representative of other seismically active regions, e.g the Mediterranean area. In order to cover this range, non-homogeneous seabed

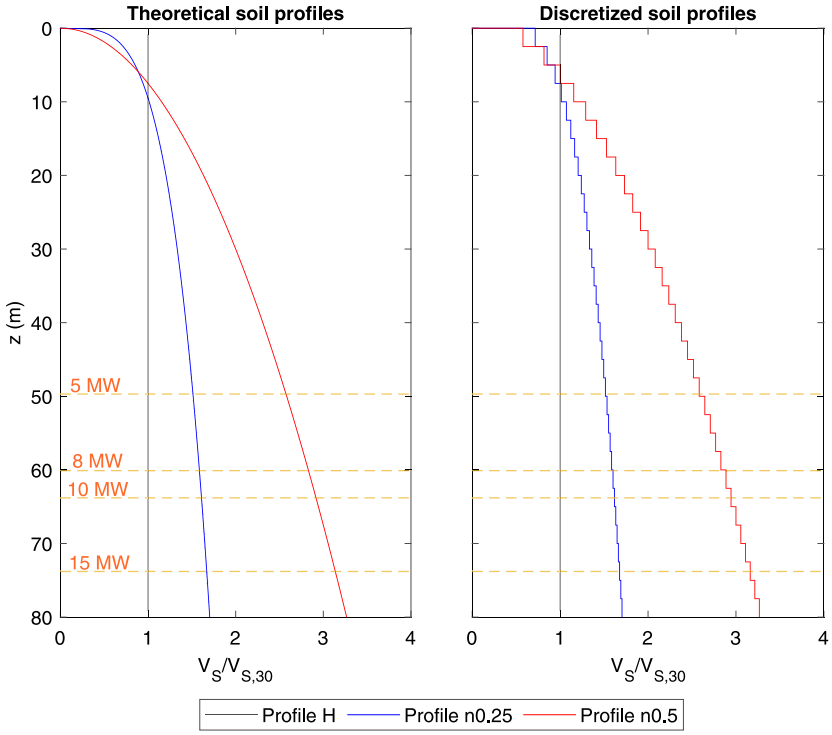

Fig. 2. Theoretical soil profiles studied (left) and discretized soil profiles (right).

Table 2
Information about the seismic signals (accelerograms) used in this work.
Source: [34].

RSN	Dir.(º)	Event Name	Year	Station Name	$V_{S,30}$ (m/s)	$a_{g,max}$ (g)
186	90	Imperial Valley-06	1979	Niland Fire Station	212	0.11
266	102	Victoria Mexico	1980	Chihuahua	242	0.15
729	0	Superstition Hills-02	1987	Imperial Valley W.L.A	179	0.21
1176	60	Kocaeli Turkey	1999	Yarimca	297	0.23
1498	59	Chi-Chi Taiwan	1999	TCU059	273	0.16
1792	90	Hector Mine	1999	Indio-Riverside C.F.G	282	0.12
2715	47	Chi-Chi Taiwan-04	1999	CHY047	170	0.13
3683	11	Taiwan SMART1(45)	1986	SMART1 O11	295	0.13
3965	8	Tottori Japan	2000	TTR008	139	0.32
5666	7	Iwate Japan	2008	MYG007	167	0.13

profiles with $n = 0.25$ and 0.5 are considered in this study. The scale parameter (A) is calculated by replacing Eq. (14) in Eq. (15), established in Eurocode 8 [33], in order to obtain different profiles with the same average shear-wave velocity.

$$V_{S,30} = \frac{30}{\int_0^{30} \frac{dz}{V_S(z)}} \tag{15}$$

Thus, the considered non-homogeneous soil profiles are defined by Eq. (16):

$$V_S(z) = \frac{V_{S,30}}{30^n(1-n)} z^n \tag{16}$$

Fig. 2 shows the variation with depth of shear-wave velocity for the homogeneous soil (named "Profile H" and represented by a black line) and variable soil profiles with $n = 0.25$ ("Profile n0.25", blue line) and $n = 0.5$ ("Profile n0.5", red line). Dashed horizontal lines represent the monopile embedded length for each OWT. To model the non-homogeneous profiles, the soil is discretized into homogeneous layers of 2.5 m deep. The resulting profile of shear-wave velocities throughout the entire depth of the soil is displayed in Fig. 2 right graph.

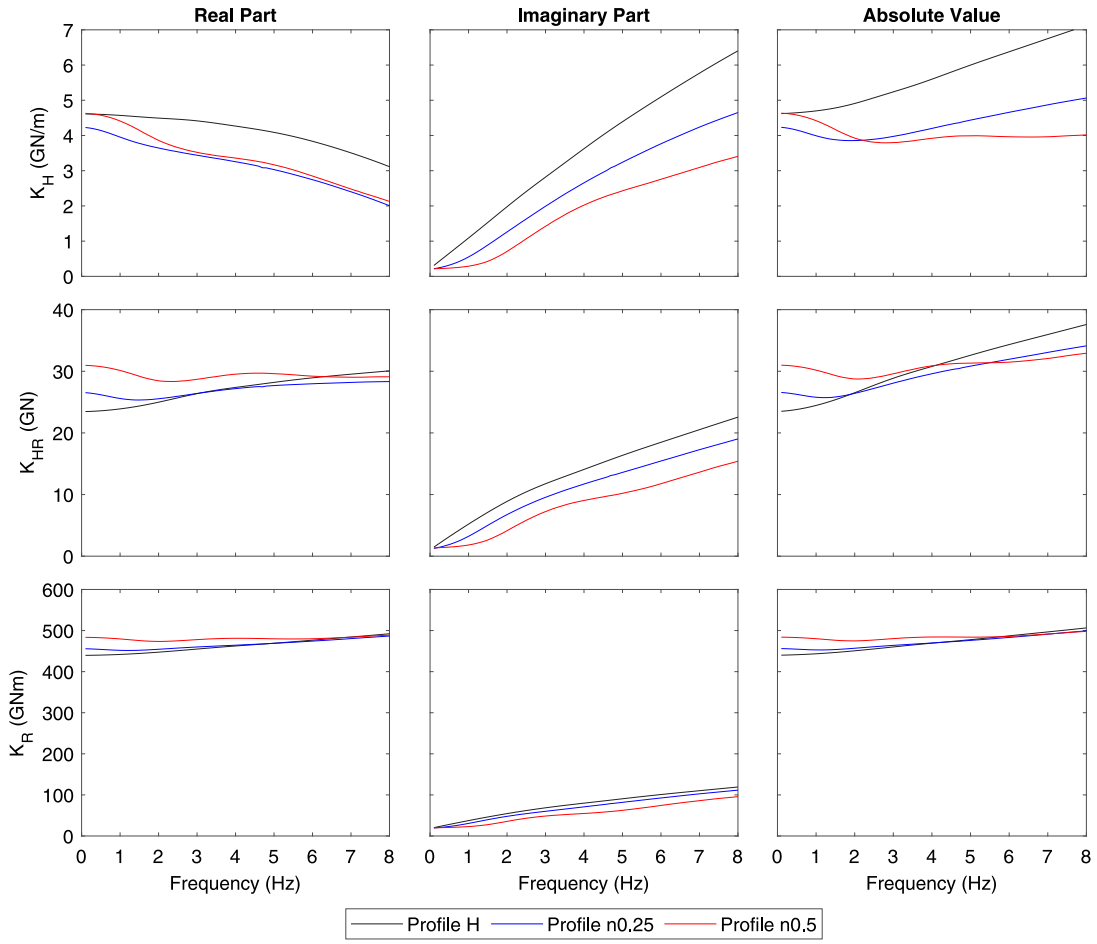

Fig. 3. Impedances functions for the three soil profiles with $V_{S,30} = 200$ m/s and the 10 MW OWT.

Table 3
Modal frequencies of the 10 MW OWT in all soils.

	$V_{S,30}$ (m/s)	100	125	150	175	200	225	250	275	300
Profile H	1st **mode (Hz)**	0.205	0.207	0.209	0.210	0.211	0.212	0.213	0.213	0.213
	2nd **mode (Hz)**	1.420	1.470	1.507	1.535	1.557	1.574	1.587	1.598	1.607
Profile n0.25	1st **mode (Hz)**	0.203	0.206	0.207	0.209	0.210	0.210	0.211	0.212	0.212
	2nd **mode (Hz)**	1.370	1.424	1.465	1.496	1.520	1.539	1.555	1.568	1.579
Profile n0.5	1st **mode (Hz)**	0.203	0.205	0.207	0.208	0.209	0.210	0.210	0.211	0.211
	2nd **mode (Hz)**	1.364	1.415	1.454	1.483	1.505	1.523	1.538	1.551	1.561

3.3. Seismic signals

The ten accelerograms used in Medina et al. [2], all of them obtained from the PEER Ground Motion Database [34] are also considered in this work. These earthquakes have been measured in soils with $V_{S,30}$ values between 100 and 300 m/s, covering the same range of $V_{S,30}$ established for the soil profiles used in this study. Table 2 provides the main information of each earthquake: the record sequence number (RSN) of the database, the direction with respect to the north of the horizontal component used, name and year of the earthquake event, name of the measuring station, the $V_{S,30}$ of the soils in which they were measured and the maximum ground acceleration ($a_{g,max}$) of the signal.

In order to make the results obtained for each earthquake comparable to each other, once the system response for each seismic signal is calculated, it is divided by the maximum ground acceleration of each signal. Finally, the average response of the ten

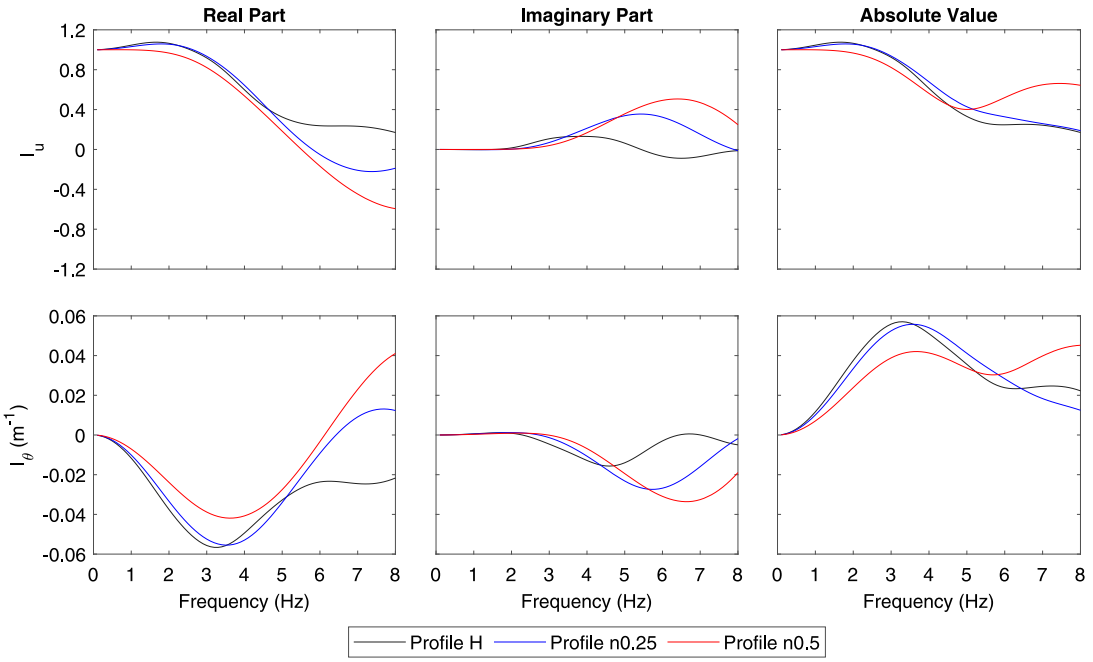

Fig. 4. KI factors for the three soil profiles with $V_{S,30} = 200$ m/s and the 10 MW OWT.

accelerograms is analysed, following the guidelines of DNV-RP-0585 [1], where it is recommended to use the mean response of, at least, seven earthquakes.

4. Results

This section is organized as follows: first, the foundation behaviour of the 10 MW OWT founded on the three types of soil profiles with a $V_{S,30} = 200$ m/s is studied as a representative configuration. The frequency dependence and the influence of the soil profile on the foundation-soil impedances (Fig. 3) and KI factors (Fig. 4) is analysed. Secondly, the first two modal frequencies of this OWT in all soils considered are studied (Table 3), in order to quantify the variation of the natural frequencies of the system depending on the soil profile on which it is founded. Then, the foundation behaviour for the first and second vibration mode of the system is studied, also in terms of impedances and KI factors (Figs. 5 and 6 respectively). After the analysis of the foundation behaviour, the maximum scaled seismic response in terms of amplification factors (Fig. 7), shear forces (Fig. 8) and bending moments (Fig. 9) is presented, comparing the contribution of the inertial and kinematic interaction. Finally, the effect of considering a homogeneous or non-homogeneous soil profile is examined. This influence is quantified in terms of relative differences between the maximum results computed in the two variable with depth soil profiles with respect to those of the homogeneous profile, also in terms of amplification factors, shear forces and bending moments (Figs. 10, 11 and 12 respectively).

4.1. Foundation behaviour

Fig. 3 shows the lateral K_H (first row), cross-coupled K_{HR} (second row) and rocking K_R (third row) impedances computed for the monopile of the 10 MW OWT founded on the three types of soil profiles with $V_{S,30} = 200$ m/s. The different columns present the real part (stiffness component), imaginary part (damping component) and absolute value of the impedance functions. Frequency is represented in the horizontal axis, where a frequency range from 0 to 8 Hz is considered, as a result of a convergence study. Results for homogeneous (black line), and variable profiles with $n = 0.25$ (blue line) and 0.5 (red line) are presented in a superimposed manner. Comparing the stiffness components, i.e. real parts, it can be seen that lateral impedances for the homogeneous profile are greater than those obtained for non-homogeneous profiles throughout the considered frequency range. The opposite occurs with cross-coupled and rocking impedances, which reach higher values for variable soil profiles, at least up to a frequency of 4–5 Hz. Note also that the highest rocking and cross-coupled impedances are obtained for the soil profile with the more pronounced variation of shear-wave velocity with depth. This trend (agreeing with the findings of previous works [35–37]) is due to the fact that the cross-coupled and rocking impedances are more affected by ground stiffness in the deeper layers, while the lateral impedance is more influenced by the layers near to the mudline level or seabed surface. Notice how in Fig. 2 this is appreciable, the two variable soils are stiffer in deep layers, while the homogeneous soil is stiffer in upper layers. Furthermore, it can also be seen that the rocking

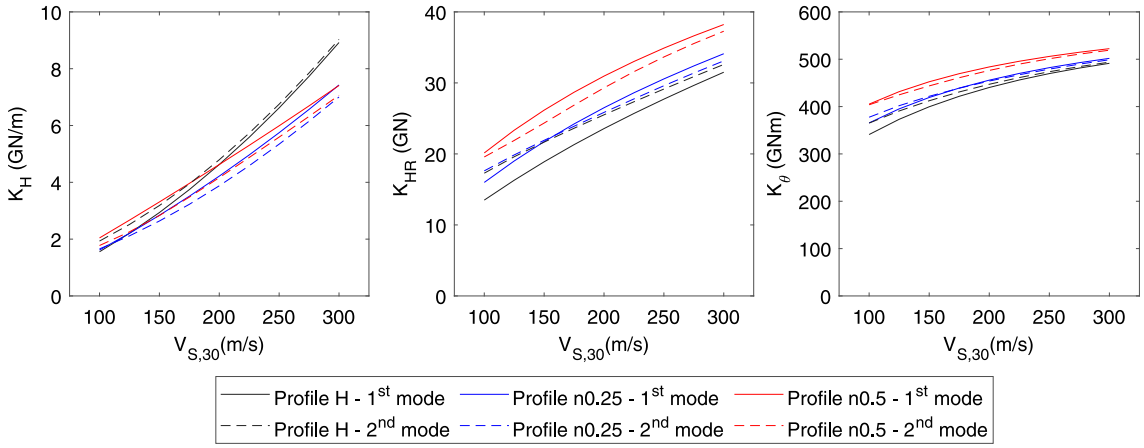

Fig. 5. Impedances vs $V_{S,30}$ in the first and second vibration mode for the 10 MW OWT.

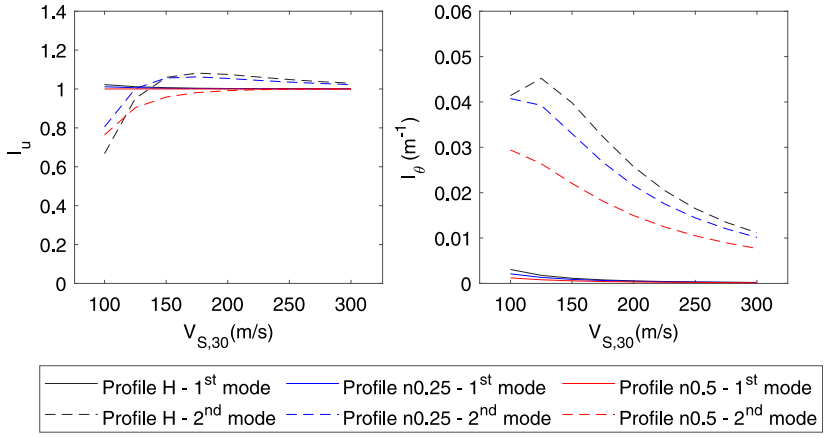

Fig. 6. KI factors vs $V_{S,30}$ in the first and second vibration mode for the 10 MW OWT.

impedances for the homogeneous and non-homogeneous with $n = 0.25$ profiles are quite similar to each other in comparison with those of the non-homogeneous profile with $n = 0.5$, which is much stiffer in the deeper layers than the other two profiles (see Fig. 2). Regarding the imaginary parts, the foundation damping increases with higher frequencies for the three soil profiles, which is typical of the radiation effects. In all vibration modes, the imaginary parts of the homogeneous profile are the greatest, followed by those of the non-homogeneous profile with $n = 0.25$. The absolute value of the impedance functions presents a similar trend that the one of stiffness component, slightly increasing its value at higher frequency due to the contribution of the damping.

In the same way, following the same graphic distribution as the one used in Figs. 3, 4 shows the results obtained in terms of KI factors in the frequency range considered, also for the 10 MW OWT and for a $V_{S,30} = 200$ m/s. The lateral KI factor (I_u) is shown in the first row and the rotational KI factor (I_θ) in the second one. The absolute value of the KI factors represents the filtering effect of the foundation. It shows that the lateral KI factors are quite similar for the three types of soil profiles (at least up to a frequency between 4 and 5 Hz). Regarding the rotational KI factor, a greater difference is observed between the three types of seabed profiles considered. Generally, the rotational KI factor for the homogeneous soil and for the non-homogeneous soil with $n = 0.25$ are similar, unlike those obtained for the variable soil with $n = 0.5$, which show considerable differences with respect to the other two soil profiles, obtaining a lower rotation in this latter profile (at least up to a frequency of 5 Hz). Analysing the real and imaginary parts of the KI factors, it can be observed that, for frequencies smaller than 2 Hz, the foundation and soil movement are both in phase (for these frequencies the rotational and lateral kinematic interaction factors are real valued). For frequencies larger than 2 Hz, foundation and soil movements become out of phase.

In order to study the influence of $V_{S,30}$ on the foundation behaviour for each type of seabed profile, the impedances and KI factors corresponding to the first two modes of vibration of the 10 MW OWT are analysed. To do this, the first two vibration modes are identified in each seabed considering the SSI. Table 3 shows these natural frequencies for each $V_{S,30}$. As can be seen, the more

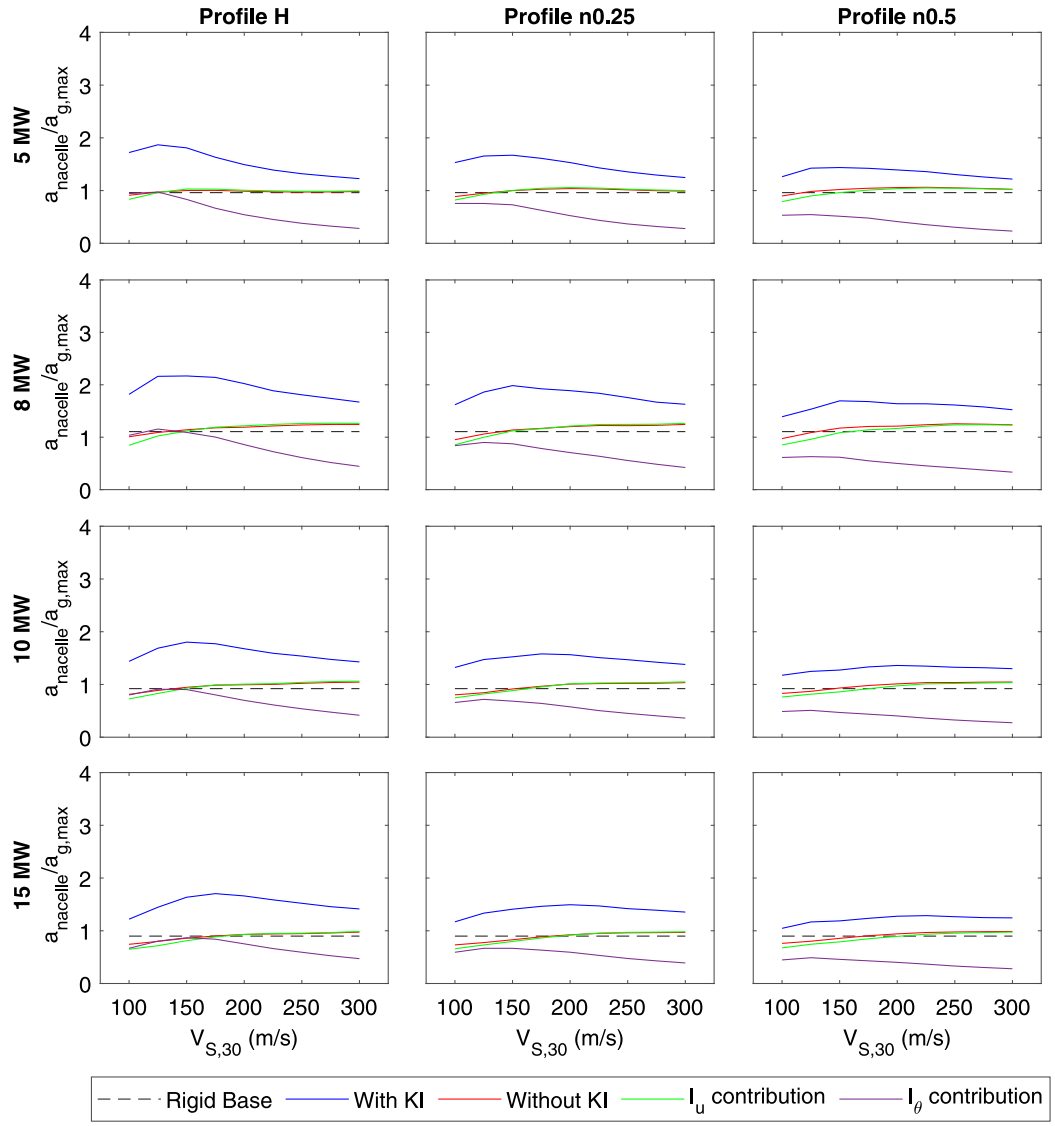

Fig. 7. Amplification factors at the nacelle height vs $V_{S,30}$ for all the study cases.

pronounced the variation of shear-wave velocity with depth, the lower the natural frequency. So, the system natural frequencies are also highly influenced by the layers closest to the mudline level. Note that when considering homogeneous soil (stiffer in upper layers), the largest natural frequencies are obtained. On the other hand, the modal shapes are not significantly affected by the soil profile.

Fig. 5 shows the impedances obtained for the first and second modes against $V_{S,30}$. The lateral, cross-coupled and rocking impedances are represented in the first, second and third column respectively. Results corresponding to the first mode are indicated by continuous lines, while those corresponding to the second mode are represented by dashed lines. For simplification reasons, only the absolute value is shown. Results for different seabed profiles are displayed with the same colours used in previous figures. It can be seen that as ground stiffness increases (crescent $V_{S,30}$), higher impedances are obtained both for the first and the second mode. In addition, in the homogeneous soil, larger impedances are obtained for the second mode in comparison with those corresponding to the first mode. The opposite occurs in the non-homogeneous profile with more pronounced variation of V_S ($n = 0.5$), where impedances corresponding to the second mode are slightly smaller than those for the first mode. While in the non-homogeneous profile with less pronounced variation of V_S ($n = 0.25$), similar impedances are reached for the two vibration modes. In general, the trend of the results in the two vibration modes is quite similar to what has been previously commented: the more pronounced is the

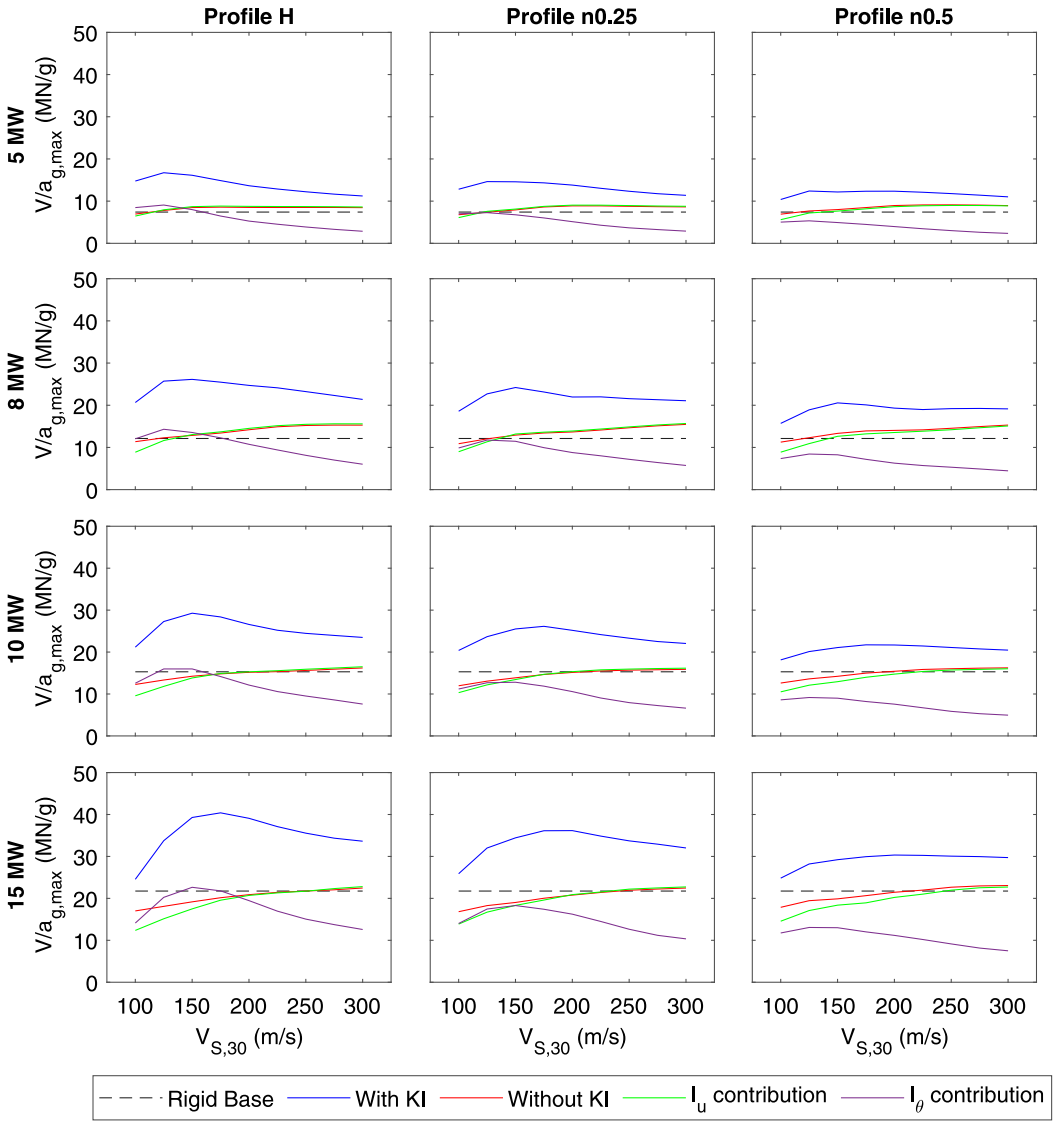

Fig. 8. Shear forces at the mudline level vs $V_{S,30}$ for all the study cases.

variation of V_S with depth in the soil profile, the greater the rocking and cross-coupled impedances are for all the values considered for $V_{S,30}$; while in the homogeneous soil the lateral impedances are bigger for $V_{S,30}$ greater than 200 m/s in the first mode, and for all the $V_{S,30}$ range in the second mode. Also, in the second mode and for all the $V_{S,30}$ range, it can be seen that the rocking and cross-coupled impedances obtained in the homogeneous and non-homogeneous profile with $n = 0.25$ are very similar to each other.

The KI factors (absolute values) for the first two modes against the different $V_{S,30}$ considered are shown in Fig. 6. The same layout as that presented in Fig. 5 is used. The left plot shows the results corresponding to the lateral KI factor and the right one those corresponding to the rotational KI factor. It can be observed that in the first mode and for the three types of soil profiles considered, the two KI factors remain practically constant as the $V_{S,30}$ of the soil increases. However, in the second mode, these two factors significantly change: the trend of the lateral KI factor is upward until a $V_{S,30}$ of approximately 150 m/s, then, from this speed, this factor remains practically constant; the trend of the rotational KI factor is generally decreasing as stiffness increases in all seabed profiles. Furthermore, if results are compared based on the types of soil profiles considered, it is observed that the rotational KI factors corresponding to the homogeneous soil profiles are the largest, followed by those obtained for the non-homogeneous with $n = 0.25$, revealing the influence that the non-homogeneity of the soil has on the pile head rotation, since the greater the stiffness in the deep layers, the smaller the rotation obtained. Besides, a common trend can be observed in the two KI factors for both modes,

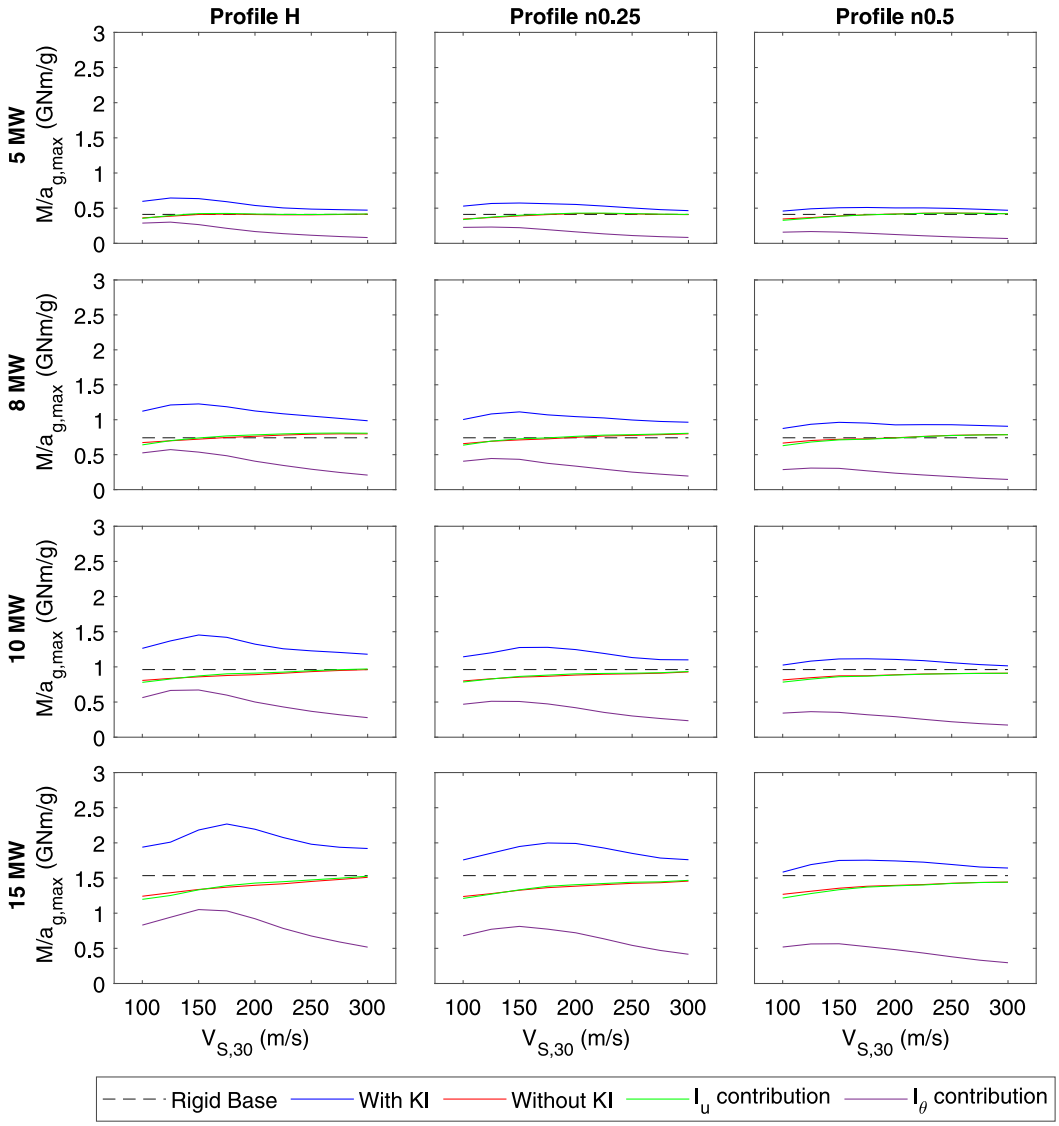

Fig. 9. Bending moments at the mudline level vs $V_{S,30}$ for all the study cases.

the KI factors computed for the three different profiles tend to each other as the value of $V_{S,30}$ increases, notice how the curves tend to approach each other. On the other hand, comparing the results that are obtained in the first mode with those of the second mode, it is observed that in the second mode the lateral KI factors corresponding to the homogeneous and those for the variable soil with $n = 0.25$ are slightly higher than those for the first mode, except for soil profiles with $V_{S,30}$ less than 150 m/s. The opposite occurs for the non-homogeneous profile with $n = 0.5$, where the lateral KI factors are greater in the first mode than in the second one. Finally, considering the rotational KI factor, higher results are reached in the second mode than in the first one for all soils.

4.2. Maximum seismic response

In order to quantify the influence of SSI and within this, the repercussion of each KI factor in the three types of soil profiles considered, the system maximum seismic response is studied for the four OWTs (shown in Table 1) and the different models considered (described in Section 2.3). This maximum response refers to the average obtained by taking into account all the seismic excitations (shown in Table 2). The system maximum response is studied in terms of maximum seismic bending moments and shear

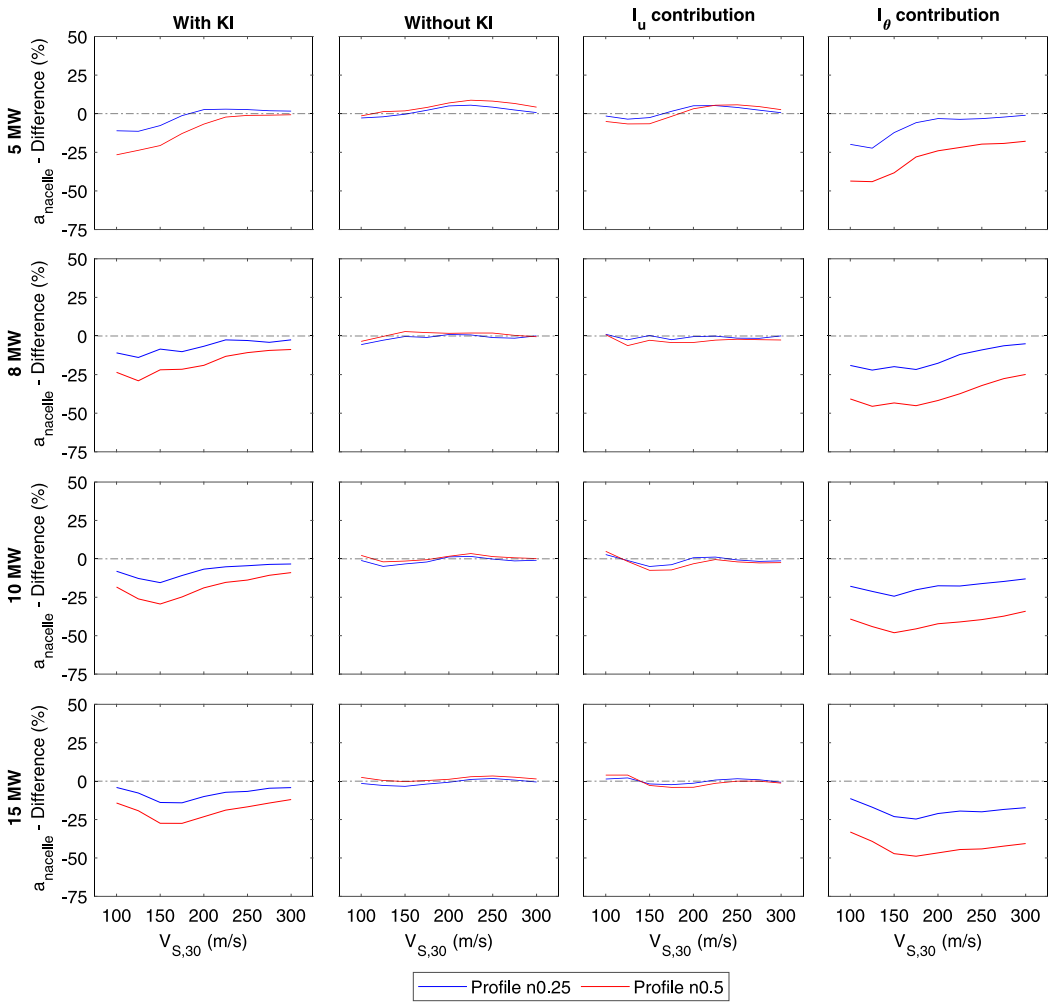

Fig. 10. Relative differences of the maximum amplification factors with respect to those of the homogeneous soil profile.

forces, which are computed at the mudline level, and in terms of relevant acceleration amplification factors at the nacelle height. The amplification factor is computed as the relation between the maximum acceleration of the nacelle and the maximum ground acceleration. Thus, this term quantifies how much the movement of the nacelle increases with respect to the free-field motion. Fig. 7 shows the amplification factors, while Figs. 8 and 9 display maximum shear forces and bending moments, respectively. These three figures show the results arranged in the same way, each figure is made up of different subgraphs, where the maximum scaled seismic response is represented against the different $V_{S,30}$ considered. The results of each wind turbine are arranged by rows while those corresponding to the different soil profiles are arranged by columns. Moreover, the results of each model considered are represented with different colours as indicated in the figure legend.

In all these representations, it is observed that the system greatest responses are obtained for the homogeneous soil profile. Note that this is mainly due to the influence of the rotational KI factor in the second mode of vibration, which is greater in the homogeneous soil profile (see Fig. 6). It can also be seen that as soil stiffness increases (crescent $V_{S,30}$), the results computed for the homogeneous and non-homogeneous with $n = 0.25$ profiles tend to coincide with each other (generally for $V_{S,30} \geq 200$ m/s). Note that this trend has also been obtained for the rotational KI factors around the second mode. In addition, it is observed that as the size of the wind turbine increases, greater shear forces and bending moments are reached in all seabed profiles. Nevertheless, in the amplification factors, the maximum values are obtained for the two smallest wind turbines. Also, analysing the results of the complete SSI model ("with KI"), in which the highest seismic responses are reached, it can be observed that as the size of the OWT increases, the system maximum response occurs for increasingly rigid soils (note how the highest value of the blue curve in Figs. 7–9 tends to move to the right).

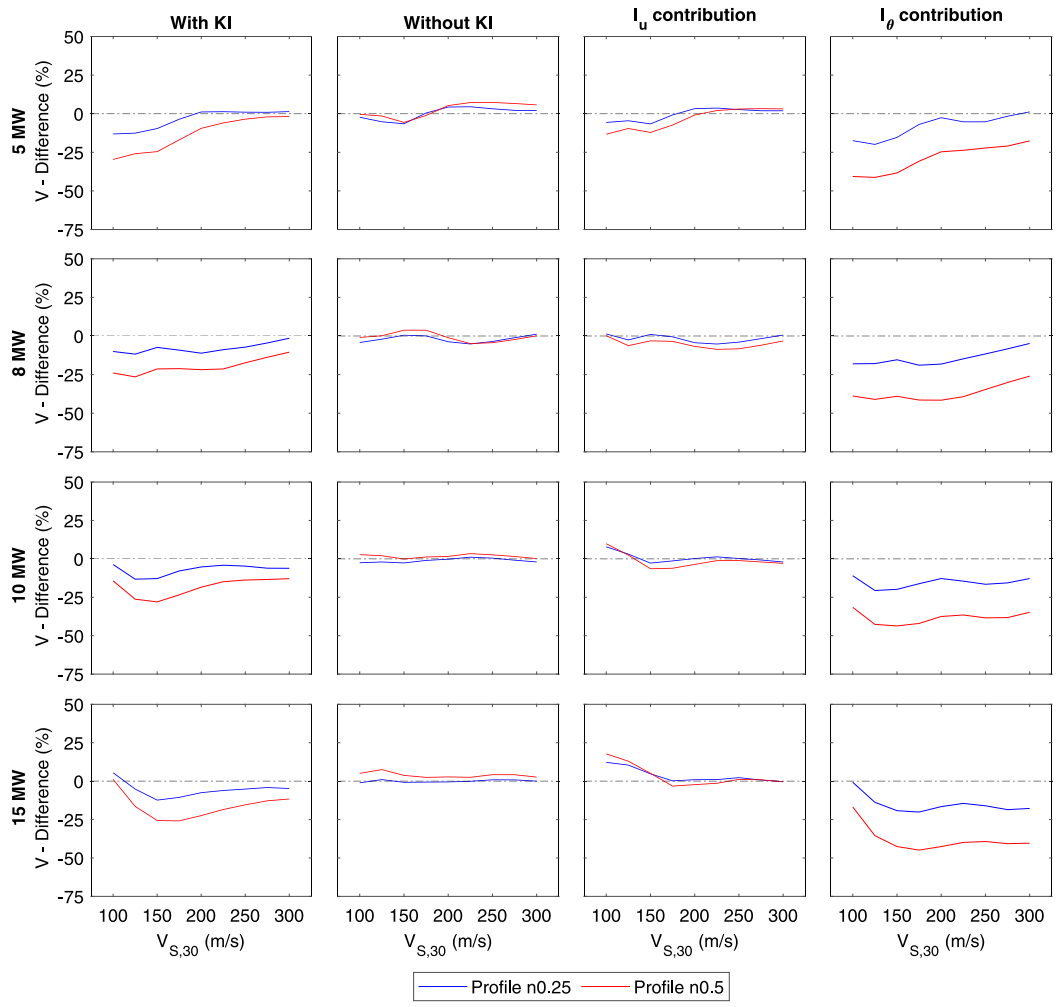

Fig. 11. Relative differences of the maximum shear forces with respect to those of the homogeneous soil profile.

On the other hand, when the influence of SSI is analysed, that is, comparing the blue curve (flexible base "with KI") with the black curve ("rigid base"), it can be observed that the system seismic response reached in the "with KI" model is greater than the response of the "rigid base" assumption, which reveals the influence that the consideration of SSI has on the seismic analysis.

Regarding the influence of KI, comparing the results corresponding to the "with KI" and "without KI" models (blue and red curve respectively), it can be seen the importance of considering the KI in the SSI, since remarkable greater responses are obtained in the "with KI" model. Moreover, it can be observed in all cases that results computed for the "without KI" and "I_u contribution" models are similar to each other, note the closeness between the green and red curves. This highlights the remarkable influence of the rotational KI factor on the seismic response of this type of structures, since the difference between considering or not the KI is marked by the "I_θ contribution" model. Note also the similarity in the shape of the curves in the "with KI" and "I_θ contribution" models. In addition, these two curves are quite similar to the curves of the rotational KI factors for the second vibration mode (previously shown in Fig. 6). This similarity is due to the fact that the effect of KI largely depends on the monopile rotation, which is greater in the second mode than in the first one (as confirmed by Kaynia [21]). Besides, it should be noticed that in the "with KI" and "I_θ contribution" models, the less pronounced the variation of the soil shear-wave velocity with depth and the larger the OWT, the greater the shear forces and bending moments.

4.3. Influence of the soil profile

With the aim of quantifying the relevance of considering a non-homogeneous profile with respect to a homogeneous one in the system seismic response, the results corresponding to the two variable profiles are compared against those computed for their

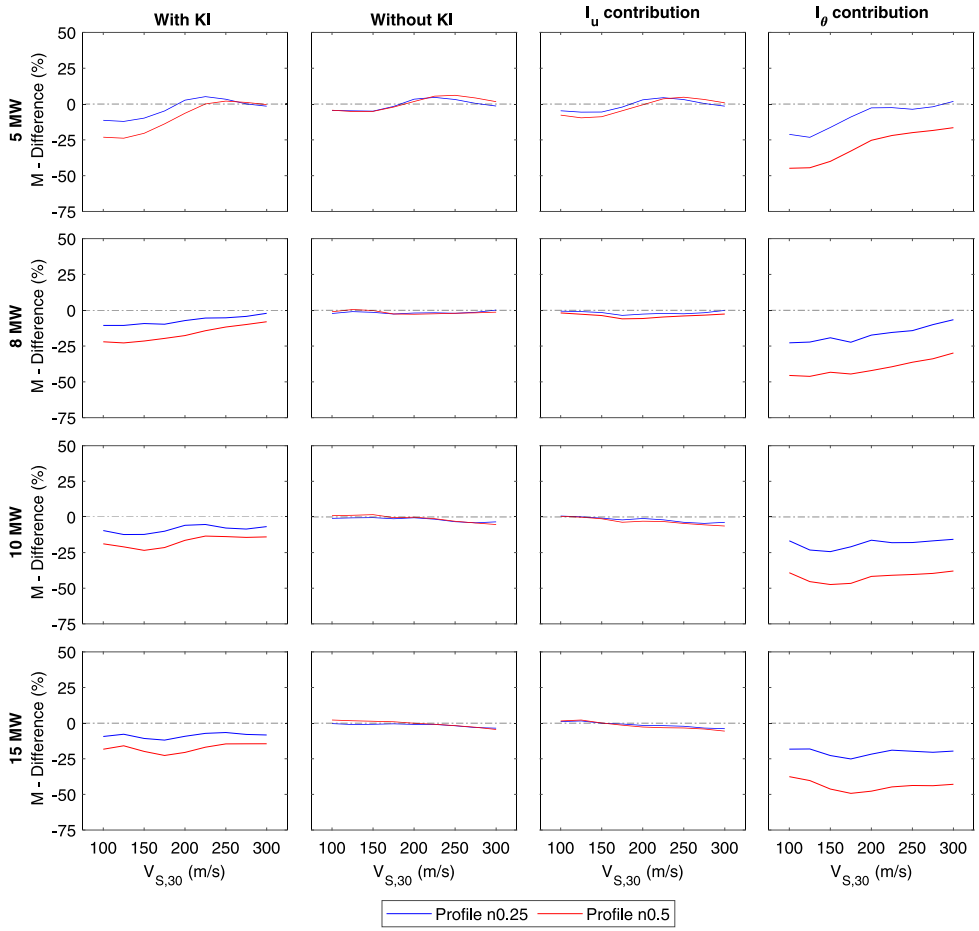

Fig. 12. Relative differences of the maximum bending moments with respect to those of the homogeneous soil profile.

equivalent homogeneous profile. For this purpose, the relative differences between the maximum results obtained in the two non-homogeneous profiles with respect to those corresponding to the homogeneous profile are studied. These relative differences in terms of maximum amplification factors, shear forces and bending moments for the different shear-wave velocities considered, are shown in Figs. 10, 11 and 12, respectively. Results for each OWT are arranged by rows, while results corresponding to different models are shown by columns. The two non-homogeneous profiles considered are depicted with a blue ($n = 0.25$) and a red ($n = 0.5$) curve respectively.

In all these representations it can be seen that the greatest differences arising from the soil profile occur when the rotational KI factor is considered ("with KI" and "I_θ contribution" models). Furthermore, these greater differences are obtained in soft soils ($V_{S,30}$ from 100 to 150 m/s), then, as soil stiffness increases, the differences tend to decrease. The greatest relative differences are found in the non-homogeneous profile with $n = 0.5$, doubling and even tripling those obtained for the non-homogeneous profile with $n = 0.25$. Note that the maximum differences in the "with KI" model are approximately 10% for the soil profile with $n = 0.25$, while in the profile with $n = 0.5$ they are between 25%–30%.

On the other hand, it is noteworthy that the differences arising from considering the non-homogeneity of the soil are due to the rotational KI factor. Note how the largest relative differences are those obtained with this model. While in the "without KI" and "I_u contribution" models, generally, the consideration of the non-homogeneity of the soil seems to be irrelevant, since the resulting differences in these two models are quite small. Nevertheless, for the two largest OWTs, remarkable differences are found in the "I_u contribution" model for soft soils, where differences reach approximately 20%, obtaining greater shear forces in the non-homogeneous profiles. Despite this fact, generally, for all the models, OWTs and $V_{S,30}$ considered, results corresponding to the $V_{S,30}$-equivalent homogeneous profile are greater than those corresponding to the variable profiles.

5. Conclusions

This paper studies the influence that the type of soil profile has on the seismic response of monopile-supported OWTs, including and analysing the inertial and kinematic interaction. For this purpose, three types of soil profiles are analysed, one homogeneous and two non-homogeneous (depth-dependent shear-wave velocity with semi-parabolic variation). Different values of time-average shear-wave velocity for the upper 30 m depth ($V_{S,30}$) are used for each of these three types of profiles, in order to analyse different soft-to-medium seabeds. Four references OWTs of different rated powers, with their corresponding monopiles, are considered. The system seismic response, in terms of maximum shear forces and bending moments at mudline level and acceleration amplification factors at hub level, is calculated using a finite element substructuring procedure. Several models that allow quantifying the influence of the inclusion of the inertial and kinematic interaction are used. The main conclusions drawn from the results are:

- Greater lateral impedances (K_H) are obtained for equivalent homogeneous soil profiles, but higher cross-coupled (K_{HR}) and rocking (K_R) impedances are reached for non-homogeneous seabed profiles. This effect is explained as the rotational motion is more affected by deeper ground properties than the lateral soil–pile motion.
- Related to the previous point, lower natural frequencies are reached for soils in which the variation of the shear-wave velocity with depth is more pronounced, indicating a major contribution of the lateral stiffness of the foundation.
- Regarding the KI factors, similar lateral KI factors (I_u) are obtained for the three soil profiles, while the rotational KI factor (I_θ) is more sensitive to soil profile type, obtaining higher rotational KI factors in the equivalent homogeneous profile.
- The highest seismic responses are obtained when both the inertial and kinematic soil–structure interaction are considered. Using a rigid base model or only incorporating the flexibility of the foundation leads to significantly smaller results than those obtained by the complete SSI model.
- However, the kinematic interaction only has a significant influence on the seismic response if the rotational KI factor is considered. This is directly related to the contribution of the second mode in the system response, as for the first mode the filtering effect of the foundation is negligible due to its low frequency.
- This influence of the rotational KI factor produces that, in general, greater seismic responses are obtained in the homogeneous seabed profile.
- Furthermore, the differences in the system seismic response owing to the definition of the soil profile are mainly explained by the rotational KI factor. These differences may be significant for soft soil profiles with pronounced variation of the shear-wave velocity with depth.

Declaration of competing interest

The authors declare that they have no known competing financial interests or personal relationships that could have appeared to influence the work reported in this paper.

Data availability

Data will be made available on request.

Acknowledgements

This research has been funded by Ministerio de Ciencia e Innovación and Agencia Estatal de Investigación (MCIN/AEI/10.13039/501100011033) of Spain and FEDER through research project PID2020-120102RBI00 and predoctoral research scholarship PRE2021-099200 (E. Rodríguez-Galván). This research was partially supported by ACIISI, Spain-Gobierno de Canarias and European FEDER Funds Grant EIS 2021 04.

References

[1] DNVSeismic Design of Wind Power Plants DNV-RP-0585; 2021. Det-Norske Veritas AS. 2022, Available online: https://www.dnv.com/energy/standards-guidelines/dnv-rp-0585-seismic-design-of-wind-power-plants.html. [Accessed on 24 august 2022].
[2] Medina C, Álamo GM, Quevedo-Reina R. Evolution of the seismic response of monopile-supported offshore wind turbines of increasing size from 5 to 15 MW including dynamic soil-structure interaction. J Mar Sci Eng 2021;9(11):1285.
[3] Padrón LA, Carbonari S, Dezi F, Morici M, Bordón JDR, Leoni G. Seismic response of large offshore wind turbines on monopile foundations including dynamic soil–structure interaction. Ocean Eng 2022;257:111653.
[4] Ju SH, Huang YC. Analyses of offshore wind turbine structures with soil-structure interaction under earthquakes. Ocean Eng 2019;187:106190.
[5] Wang W, Gao Z, Li X, Moan T. Model test and numerical analysis of a multi-pile offshore wind turbine under seismic, wind, wave, and current loads. J Offshore Mech Arct Eng 2017;139(3).
[6] Liang F, Yuan Z, Liang X, Zhang H. Seismic response of monopile-supported offshore wind turbines under combined wind, wave and hydrodynamic loads at scoured sites. Comput Geotech 2022;144:104640.
[7] Wang P, Zhao M, Du X, Liu J, Xu C. Wind, wave and earthquake responses of offshore wind turbine on monopile foundation in clay. Soil Dyn Earthq Eng 2018;113:47–57.
[8] Xi R, Xu C, Du X, El Naggar MH, Wang P, Liu L, et al. Framework for dynamic response analysis of monopile supported offshore wind turbine excited by combined wind-wave-earthquake loading. Ocean Eng 2022;247:110743.
[9] Patra SK, Haldar S. Seismic response of monopile supported offshore wind turbine in liquefiable soil. In: Structures, vol. 31. Elsevier; 2021, p. 248–65.

[10] Álamo GM, Aznárez JJ, Padrón LA, Martínez-Castro AE, Gallego R, Maeso O. Dynamic soil-structure interaction in offshore wind turbines on monopiles in layered seabed based on real data. Ocean Eng 2018;156:14–24.
[11] Shi S, Zhai E, Xu C, Iqbal K, Sun Y, Wang S. Influence of pile-soil interaction on dynamic properties and response of offshore wind turbine with monopile foundation in sand site. Appl Ocean Res 2022;126:103279.
[12] Arany L, Bhattacharya S, Macdonald JHG, Hogan SJ. Closed form solution of Eigen frequency of monopile supported offshore wind turbines in deeper waters incorporating stiffness of substructure and SSI. Soil Dyn Earthq Eng 2016;83:18–32.
[13] Yang Y, Bashir M, Li C, Wang J. Analysis of seismic behaviour of an offshore wind turbine with a flexible foundation. Ocean Eng 2019;178:215–28.
[14] Ghaemmaghami AR, Mercan O, Kianoush R. Seismic soil–structure interaction analysis of wind turbines in frequency domain. Wind Energy 2017;20(1):125–42.
[15] Mo R, Cao R, Liu M, Li M. Effect of ground motion directionality on seismic dynamic responses of monopile offshore wind turbines. Renew Energy 2021;175:179–99.
[16] Jiang W, Lin C. Lateral responses of monopile-supported offshore wind turbines in sands under combined effects of scour and earthquakes. Soil Dyn Earthq Eng 2022;155:107193.
[17] Jiang W, Lin C, Sun M. Seismic responses of monopile-supported offshore wind turbines in soft clays under scoured conditions. Soil Dyn Earthq Eng 2021;142:106549.
[18] De Risi R, Bhattacharya S, Goda K. Seismic performance assessment of monopile-supported offshore wind turbines using unscaled natural earthquake records. Soil Dyn Earthq Eng 2018;109:154–72.
[19] Bisoi S, Haldar S. Dynamic analysis of offshore wind turbine in clay considering soil-monopile-tower interaction. Soil Dyn Earthq Eng 2014;63:19–35.
[20] API RP 2A-WSDRecommended Practice for Planning, Designing and Constructing Fixed Offshore Plaftorms - Working Stress Design. American Petroleum Institute.
[21] Kaynia AM. Effect of kinematic interaction on seismic response of offshore wind turbines on monopiles. Earthq Eng Struct Dyn 2021;50(3):777–90.
[22] Wind Europe. Offshore wind in Europe – Key trends and statistics 2020. Technical report, Brussels, Belgium: WindEurope asbl/vzw; 2021.
[23] Álamo GM, Martínez-Castro AE, Padrón LA, Aznárez JJ, Gallego R, Maeso O. Efficient numerical model for the computation of impedance functions of inclined pile groups in layered soils. Eng Struct 2016;126:379–90.
[24] Chopra AK. Dynamics of structures. Theory and applications to earthquake engineering. Seventh ed. NJ, USA: Pearson/Prentice Hall, Englewood Cliffs; 2017.
[25] Álamo GM, Bordón JDR, Aznárez JJ. On the application of the beam model for linear dynamic analysis of pile and suction caisson foundations for offshore wind turbines. Comput Geotech 2021;134:104107.
[26] Arany L, Bhattacharya S, Macdonald J, Hogan SJ. Design of monopiles for offshore wind turbines in 10 steps. Soil Dyn Earthq Eng 2017;92:126–52.
[27] Jonkman J, Butterfield S, Musial W, Scott G. Definition of a 5-MW reference wind turbine for offshore system development. Technical report, Golden, CO (United States): National Renewable Energy Lab.(NREL); 2009.
[28] Desmond C, Murphy J, Blonk L, Haans W. Description of an 8 MW reference wind turbine. In: Journal of physics: Conference series, vol. 753, no. 9. IOP Publishing; 2016, 092013.
[29] Bak C, Zahle F, Bitsche R, Kim T, Yde A, Henriksen LC, et al. The DTU 10-MW reference wind turbine. In: Danish wind power research 2013. 2013.
[30] Gaertner E, Rinker J, Sethuraman L, Zahle F, Anderson B, Barter G, et al. Definition of the IEA 15-Megawatt offshore reference wind turbine. National Renewable Energy Laboratory (NREL); 2020.
[31] Wang SY, Wang HY. Site-dependent shear-wave velocity equations versus depth in California and Japan. Soil Dyn Earthq Eng 2016;88:8–14.
[32] Hamilton EL. Shear-wave velocity versus depth in marine sediments: A review. Log Anal 1977;18(01).
[33] European Committee for Standardization. Eurocode 8: Design of structures for earthquake resistance. Part 5: Foundations, Retaining Structures and Geotechnical Aspects. 2004, Brussels.
[34] Pacific Earthquake Engineering Research Center (PEER). NGA-West2 Ground Motion Database. 2022, Available online: . [Accessed on 20 august 2022].
[35] Kaynia AM, Kausel E. Dynamics of piles and pile groups in layered soil media. Soil Dyn Earthq Eng 1991;10(8):386–401.
[36] Miura K, Kaynia AM, Masuda K, Kitamura E, Seto Y. Dynamic behaviour of pile foundations in homogeneous and non-homogeneous media. Earthq Eng Struct Dyn 1994;23(2):183–92.
[37] Álamo GM, Martínez-Castro AE, Padrón LA, Aznárez JJ, Gallego R, Maeso O. A proposal for normalized impedance functions of inclined piles in non-homogeneous media. Procedia Eng 2017;199:86–91.

2.2 Second publication: Rodríguez-Galván et al., 2024, Computers and Geotechnics

Table 2.2. Second publication data.

Title	Non-linear behaviour of soil–pile interaction phenomena and its effect on the seismic response of OWT pile foundations. Validity range of a linear approach through non-degraded soil properties
Authors	E. Rodríguez-Galván, G.M Álamo, J.J. Aznárez and O. Maeso
Journal	Computers and Geotechnics
DOI	10.1016/j.compgeo.2024.106188
ISSN	0266-352X
Impact factor	6.2
CiteScore	9.0
Category	Engineering, Geological
Quartile	Q1 (26/239)
Publisher	ELSEVIER SCI LTD
Volume	168
Date	April 2024

Computers and Geotechnics 168 (2024) 106188

Contents lists available at ScienceDirect

Computers and Geotechnics

journal homepage: www.elsevier.com/locate/compgeo

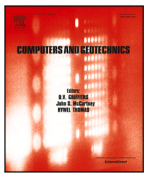

Research paper

Non-linear behaviour of soil–pile interaction phenomena and its effect on the seismic response of OWT pile foundations. Validity range of a linear approach through non-degraded soil properties

Eduardo Rodríguez-Galván, Guillermo M. Álamo *, Juan J. Aznárez, Orlando Maeso

Instituto Universitario de Sistemas Inteligentes y Aplicaciones Numéricas en Ingeniería, Universidad de Las Palmas de Gran Canaria, 35017 Las Palmas de Gran Canaria, Spain

ARTICLE INFO

Keywords:
Soil–pile interaction
Non-linear analysis
Inelastic behaviour
Offshore wind turbines
Beam on dynamic Winkler foundation
Seismic response

ABSTRACT

The effect of non-linear and inelastic behaviour of the soil–pile interaction on the seismic response of offshore wind turbine pile foundations embedded in sandy soils is analysed. For this purpose, the responses obtained assuming three different Beam on Dynamic Winkler Foundation (BDWF) models are compared: a Plastic Non-Linear Model (PNLM), an Elastic Non-Linear Model (ENLM) and a simple elastic linear model with non-degraded properties of soil (NDLM). The influence of non-linearity and plasticity assumption is studied by evaluating the effects of the kinematic and inertial interaction within soil–pile interaction. Two soil stiffness levels are analysed: very loose and medium dense sand. The seismic response under ten earthquakes is computed in terms of mean envelopes of internal forces along the pile length. The non-linearity and inelastic influence of soil–pile interaction is quantified by means of relative differences with respect to the linear elastic model. Results show that the non-linear and inelastic models acquire relevance when the contribution of the inertial interaction dominates, leading to lower maximum responses than the linear elastic model. If the inertial interaction is not significantly activated, similar results between the three models are obtained, being the linear elastic model enough to reproduce the soil–pile dynamic interaction.

1. Introduction

One of the most relevant applications of piled foundations is its use in offshore wind turbine (OWT) structures. Monopiles are the dominant OWT foundation, representing 64.4% of the total OWTs foundation market for installed projects in 2021 (Musial et al., 2022). This type of foundation predominates due to its ease of installation and manufacturing, which make it a very economically competitive solution. Monopiles with larger dimensions are evolving to increase its range of application, both in seabed depths and in supporting high-powered wind turbines. The new generation of OWTs (≥ 15 MW) requires monopiles with more than 10 meters in diameter and 100 meters in length. For smaller OWTs, monopiles acquire diameters of up to 8 m and lengths of up to 90 m (BOSLAN Engineering and Consulting, 2022). In addition, piles are also very present in the rest of the OWT bottom-fixed foundations. Jackets, tripods and tripiles substructures are founded on suction caissons or on smaller sized piles, which generally have diameters between 1 and 4 m and lengths from 25 to 80 m. In this way, piles can acquire a great variety of sizes depending on the type of OWT foundation.

The wide expansion of the offshore wind technology has led to considering its installation in seismically active regions with more aggressive environmental conditions. For this reason, with the aim of analysing the dynamic-structural response of bottom-fixed OWTs, numerous dynamic studies have been carried out in recent years (Shi et al., 2022; Liang et al., 2022; Wang et al., 2018; Yang et al., 2019; Xi et al., 2022; Mo et al., 2021; Patra and Haldar, 2021; Padrón et al., 2022; Medina et al., 2021; Kaynia, 2021; Álamo et al., 2018; Jiang and Lin, 2022; Jiang et al., 2021; Bisoi and Haldar, 2014; Ju and Huang, 2019; Yan et al., 2022; Alati et al., 2015; Hassan, 2018; Carswell et al., 2016; Bisoi and Haldar, 2015; Wang et al., 2023). In many of these studies (Shi et al., 2022; Yang et al., 2019; Padrón et al., 2022; Medina et al., 2021; Kaynia, 2021; Álamo et al., 2018), especially those that focus on monopiles, the relevance of soil–structure interaction in the structural behaviour is demonstrated, both in the dynamic properties of the systems (natural frequencies, damping, etc.) and its responses. The dynamic soil–structure interaction essentially includes kinematic and inertial interaction. Kinematic interaction is mainly affected by

* Corresponding author.
E-mail addresses: eduardo.rodriguezgalvan@ulpgc.es (E. Rodríguez-Galván), guillermo.alamo@ulpgc.es (G.M. Álamo), juanjose.aznarez@ulpgc.es (J.J. Aznárez), orlando.maeso@ulpgc.es (O. Maeso).

https://doi.org/10.1016/j.compgeo.2024.106188
Received 17 November 2023; Received in revised form 2 February 2024; Accepted 22 February 2024
Available online 24 February 2024

soil motion and soil–pile interface, while inertial interaction is mainly associated to the mass of the superstructure.

The seismic and dynamic analysis of OWTs can be carried out assuming a linear or non-linear soil–structure interaction. Although it is more complex, the non-linear behaviour is commonly used (Shi et al., 2022; Liang et al., 2022; Wang et al., 2018; Yang et al., 2019; Xi et al., 2022; Mo et al., 2021; Jiang and Lin, 2022; Jiang et al., 2021; Bisoi and Haldar, 2014; Hassan, 2018; Patra and Haldar, 2021; Carswell et al., 2016; Bisoi and Haldar, 2015; Wang et al., 2023), because it is considered a more realistic approach than the linear one. In these type of numerical simulations, the soil–pile dynamic interaction is usually represented by a non-linear Beam on Dynamic Winkler Foundation (BDWF) model with springs in parallel with dashpots, that can be considered elastic or plastic. In these BDWF models the soil resistance - deflection (p-y) relationship is usually modelled by using the API (Designing API RP 2A-WSD, 2002) expressions (Hassan, 2018; Carswell et al., 2016; Bisoi and Haldar, 2015; Wang et al., 2023; Bisoi and Haldar, 2014; Wang et al., 2018; Mo et al., 2021; Shi et al., 2022). Although this API method has not been designed to simulate the p-y curves for large diameter piles, its application has been recommended by several design guidelines, as the DNV-OS-J101 (DNV, 2014a), and it has been widely employed in the dynamic study of monopile-supported OWTs, as well as in prominent works such as the OC3 project (Jonkman and Musial, 2010), where the soil–pile dynamic interaction of the NREL 5MW OWT (6 m diameter pile) is reproduced by employing the API method.

On the other hand, linear models have also been used in numerous studies (Padrón et al., 2022; Medina et al., 2021; Kaynia, 2021; Álamo et al., 2018; Arany et al., 2016), and they may be a necessary and sufficient approximation depending on the case and phenomenon to be addressed. In these linear approaches, the soil–pile dynamic interaction is usually modelled by a set of impedance functions and kinematic interaction factors. Despite being simplified models, they are useful when a large number of simulations have to be addressed, and they are generally accepted as a initial approach. Regardless of the fact that both approaches have been studied in detail, many few works have focused on comparing them: Firoj and Maheshwari (2022) compares two linear soil behaviours with two non-linear ones, for combined piled raft foundation of a Nuclear Power Plant structure; Cheng et al. (2023) employs an elastoplastic and a elastic soil to analyse the dynamic response of a monopile-supported OWT in clay; and Tabesh and Poulos (2001) analyses the effects of soil yielding on the seismic response of small piles (up to 1.5 m diameter) embedded in clay and sandy soils, comparing an elastic and an elastoplastic soil–pile interaction.

For this reason, in the absence of an exhaustive comparison between these considerations, this paper aims to compare the structural-seismic response of OWT pile foundations embedded in sandy soils considering three different soil–pile interaction models: a Plastic Non-Linear Model (PNLM), an Elastic Non-Linear Model (ENLM) and a simple elastic linear model with non-degraded properties of soil (Non-Degraded Linear Model, NDLM). These three models have been specifically designed for isolating the influence of the soil–pile interaction. Thus, all the differences obtained in the results can be directly explained by the assumptions made for the soil–pile interaction phenomena. This fact allows to focus on the main scope of this work: the analysis of the effects of assuming a linear or non-linear (either inelastic or elastic) behaviour in the soil–pile interaction for evaluating seismic loads, and how this influence depends on the contribution of the inertial properties of the structure. In order to obtain general trends and useful conclusions that can help to choose the appropriate model depending on the interest problem, an exhaustive parametric study for a wide range of excitations and OWT pile foundations is carried out.

In the three models under analysis, the soil–pile interaction is represented by a BDWF approach based on the p-y curves recommended by the API RP 2A-WSD (Designing API RP 2A-WSD, 2002). Vertically incident S waves that propagates through an elastic medium with linear variation of soil properties with depth is considered in each model. In this way, the effect of non-linear and inelastic behaviour of soil–pile interaction is isolated and analysed. Besides, the relevance of the soil properties is also studied by considering two stiffness levels: a very loose and a medium dense sandy soil (following the API sandy soil classification (Designing API RP 2A-WSD, 2002)). In order to examine the role of the kinematic and inertial effects on the non-linear and inelastic soil–pile behaviour, different single piles with several cap masses values from 0 to the mass equivalent to its ultimate axial bearing capacity are studied. Results are presented in terms of envelopes of maximum internal forces, accelerations and soil resistances. To better quantify the relevance of the non-linear and plastic behaviour of soil–pile interaction, the relative differences of the maximum seismic responses with respect to those corresponding to the linear elastic model are computed. Finally, the conclusions drawn of this analysis are tested with three reference monopiled OWTs of different rated powers (5, 10 and 15 MW), comparing the envelopes of the three OWTs with those of its corresponding monopiles with a pile cap mass equivalent to its supported superstructure weight.

2. Methodology

The seismic response of the soil-monopile system is obtained through a BDWF model, the pile is discretized by beam finite elements, and the soil–pile interaction is reproduced through independent springs attached to each node of pile elements (Fig. 1). To study the effects of non-linearity and the consideration of the plastic-cyclic behaviour of soil–pile interaction, the three different models studied are (Fig. 1(a)): a Plastic Non-Linear Model (PNLM), an Elastic Non-Linear Model (ENLM) and a Non-Degraded Linear Model (NDLM). In order to limit the study to the relevance of the plastic and non-linear behaviour of soil–pile interaction, the gap formation between the soil–pile is not considered. In these three models, the seismic excitation is assumed to be a planar and harmonic S-wave vertically propagating through an elastic non-homogeneous halfspace with linear variation of soil properties with depth. Only the system seismic response is analysed (no environmental loads due to wind or waves are considered).

First, in order to study the kinematic and inertial effects in soil–pile interaction, several values of translational cap masses (m) are studied in a soil–pile subsystem (see Fig. 1(b)) by considering the three soil–pile models previously introduced. On this manner, the influence of the non-linear and inelastic behaviour of soil–pile interaction is analysed. These translational masses (m) are defined as a fraction (δ) of the ultimate axial bearing capacity of piles (Q_u). Finally, the application of the main conclusions drawn of this study are verified by using an integrated system that includes different reference monopiled OWTs (see Fig. 1(c)). In this section, the methodology followed to define the different systems and models is explained.

2.1. System modelling

The pile and wind turbine are discretized into finite elements of two nodes (Bernoulli's beams). Therefore, the soil–pile interface is concentrated into the beam axis, and consequently the local effects produced at the soil-shell interface are not captured. This simplification has been verified in previous works, such as in Álamo et al. (2021), which concludes that a soil-beam model accurately reproduces the global foundation response for not excessively high frequencies, even for foundations with small aspect ratios (L/D). Given the particularities of the problem, only the lateral behaviour of the system is considered. Thus, each node n has two degrees of freedom: a lateral displacement (u_n) and a rotation (θ_n). Distributed inertial properties are assumed for each element. Based on a convergence study, an element length (L_e) of 0.5 m and 1 m have been chosen to discretize the foundation (embedded pile) and the supestructure respectively, so that the soil–pile interaction and the conical shape of the tower are reproduced

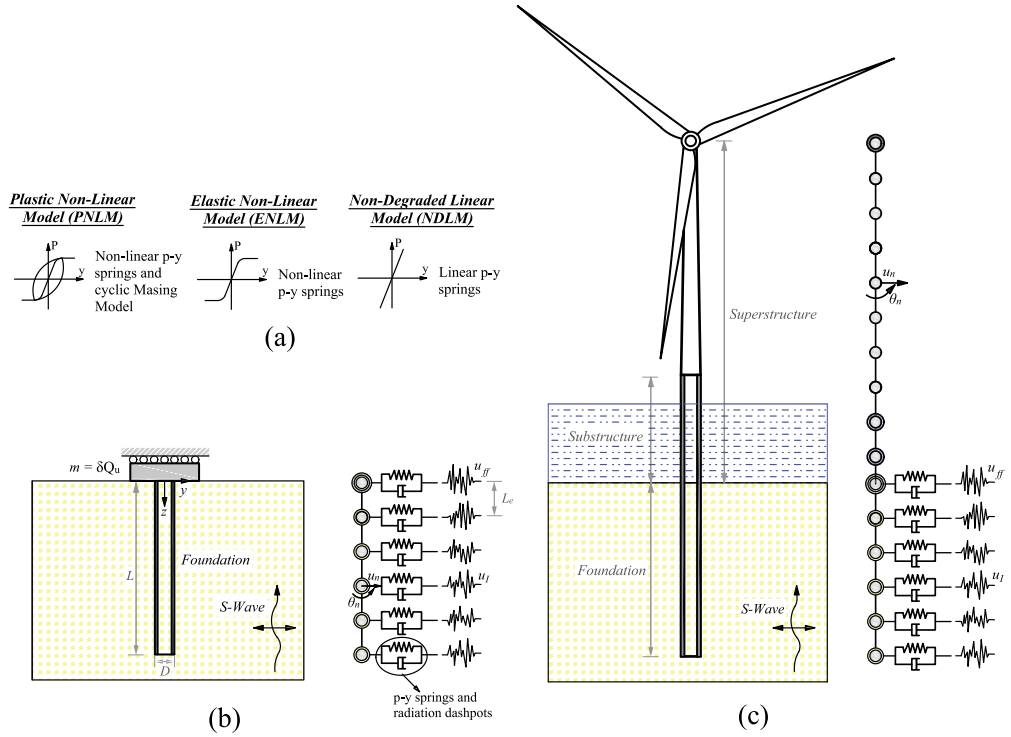

Fig. 1. (a) Soil–pile interaction models studied in this work. (b) Soil–pile subsystem for kinematic and inertial effects parametric analysis. (c) Integrated model including OWT superstructure.

accurately enough. For the soil–pile subsystem the pile cap mass (m) is modelled as a punctual and translational mass at the top node (pile head rotation is assumed to be restricted, as depicted in Fig. 1(b)). In the integrated system with the OWT superstructure the mass of the rotor-nacelle assembly is also considered as a punctual mass at the highest node. In this last model, the transition piece between the monopile and the tower is not taken into account for simplification reasons (see Fig. 1(c)).

The classic Bernoulli's stiffness and elementary mass matrices ($\mathbf{K_e}$ and $\mathbf{M_e}$) used for each element are shown in (1) and (2), being L_e the element length, A_e the cross-sectional area of the element, I_e the moment of inertia of the cross-section, ρ the material density and E the Young's Modulus of the material. For the soil–pile subsystem and for the integrated system including OWT superstructure, the equivalent soil mass inside the foundation is considered as an added distributed elementary mass. For the integrated model with OWT superstructure the interaction between the monopile and the water is modelled as two added distributed elementary masses: one for the water inside the pile and another for the mobilized water outside the substructure, as it is described in (3), being ρ_w the water density, A_{in} and A_{out} the circle areas corresponding to the inner and outside diameters of the pile section, and C_a an added mass coefficient that, for long cylinders in infinite fluid, takes a value of 1 following the DNV-RP-C205 (DNV, 2014b). It is important to consider these two water added masses, since they can significantly affect the first natural system frequency, as it is demonstrated in Chen et al. (2022). All these elemental matrices are assembled to obtain the global stiffness and mass matrices of the system.

$$\mathbf{K_e} = \frac{EI_e}{L_e^3}\begin{bmatrix} 12 & 6L_e & -12 & 6L_e \\ 6L_e & 4L_e^2 & -6L_e & 2L_e^2 \\ -12 & -6L_e & 12 & -6L_e \\ 6L_e & 2L_e^2 & -6L_e & 4{L_e}^2 \end{bmatrix} \tag{1}$$

$$\mathbf{M_e} = \frac{\rho A_e L_e}{420}\begin{bmatrix} 156 & 22L_e & 54 & -13L_e \\ 22L_e & 4L_e^2 & 13L_e & -3L_e^2 \\ 54 & 13L_e & 156 & -22L_e \\ -13L_e & -3L_e^2 & -22L_e & 4{L_e}^2 \end{bmatrix} \tag{2}$$

$$\mathbf{M_{ew}} = \frac{\rho_w L_e(A_{in} + C_a A_{out})}{420}\begin{bmatrix} 156 & 22L_e & 54 & -13L_e \\ 22L_e & 4L_e^2 & 13L_e & -3L_e^2 \\ 54 & 13L_e & 156 & -22L_e \\ -13L_e & -3L_e^2 & -22L_e & 4{L_e}^2 \end{bmatrix} \tag{3}$$

2.2. Dynamic soil–pile interaction models

In this work, in order to study the effects of non-linear and inelastic behaviour of soil–pile interaction, three different models are studied: a Plastic Non-Linear Model (PNLM), an Elastic Non-Linear Model (ENLM) and a Non-Degraded Linear Model (NDLM).

2.2.1. Plastic Non-Linear Model (PNLM)

In this model, the lateral soil resistance-deflection is modelled using the non-linear p-y relationship for sands, established and recommended by the API (Designing API RP 2A-WSD, 2002):

$$P = Ap_u \tanh\left[\frac{kz}{Ap_u}\bar{y}\right] \tag{4}$$

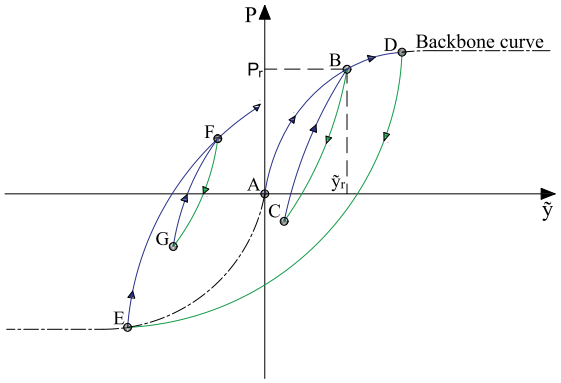

Fig. 2. Extended masing rules, example of the evolution of soil resistance (P) versus soil–pile relative displacement ($\tilde{y}$).

where P is the reaction force of soil per unit length; $\tilde{y}$ is the soil–pile relative displacement ($\tilde{y} = u - u_I$), defined as the difference between the lateral displacement of the pile (u) and that of the soil due to the incident field (u_I); A is a dimensionless coefficient which depends on the type of loading, in this case, A is taken as 0.9 (cyclic loading); k is the initial modulus of subgrade reaction, that can be graphically calculated as function of angle of internal friction (Φ_s) with Figure 6.8.7-1 of API RP 2A-WSD (Designing API RP 2A-WSD, 2002); and p_u is the ultimate bearing capacity at depth z, which is computed according to:

$$p_u = \min(p_{us}, p_{ud}) \tag{5}$$

where:

$$p_{us} = (C_1 z + C_2 D)\gamma_s z \tag{6}$$

and

$$p_{ud} = C_3 D \gamma_s z \tag{7}$$

being γ_s the effective soil weight; D the pile diameter; and C_1, C_2, C_3 dimensionless coefficients which are functions of Φ_s and can be determined with Figure 6.8.6-1 of API RP 2A-WSD (Designing API RP 2A-WSD, 2002).

To model the plastic-cyclic behaviour of soil–pile interaction, the non-linear p-y relationship of soil is modelled by using a cyclic extended Masing model, in which the backbone curve is described by (4). These types of cyclic non-linear models are very common to simulate the stress–strain hysteretic behaviour of soil, since they can reproduce the unloading-reloading behaviour, stiffness degradation and other effects (Gerolymos and Gazetas, 2005b,a). The four Masing rules that define the cyclic model are (see e.g. Kramer (1996)):

1. For initial loading, the p-y curve follows the backbone curve (from A to B in Fig. 2).
2. If a deflection reversal occurs at a point defined by (P_r, $\tilde{y}_r$) (point B in Fig. 2), the p-y curve follows a path given by:

$$P = P_r + 2Ap_u \tanh\left[\frac{kz}{Ap_u}\frac{\tilde{y} - \tilde{y}_r}{2}\right] \tag{8}$$

3. If the unloading or reloading curve exceeds the maximum past deflection and intersects the backbone curve, it follows the backbone curve until the next deflection reversal (from C to D in Fig. 2).
4. If an unloading or reloading curve crosses an unloading or reloading curve from the previous cycle, the p-y curve follows that of the previous cycle (from G to F in Fig. 2).

In this way, in each time step, using the Newmark non-linear method (Section 2.6.2) with the correct p-y curve ((4) or (8) depending on the path given by the Masing Rules), displacements, velocities and accelerations of the system are computed.

2.2.2. Elastic Non-Linear Model (ENLM)

In this model, as in the previous one, the non-linear relationship between the lateral soil resistance-deflection is computed by means of the API p-y curve for sands. However, an elastic soil behaviour is considered. Thus, Masing rules are not applied and the p-y relationship is limited to the original backbone curve (dashed line in Fig. 2). Therefore, in each time step, applying Newmark non-linear method (Section 2.6.2) with the p-y curve (4), displacements, velocities and accelerations of the system are calculated.

2.2.3. Non-Degraded Linear Model (NDLM)

A linear relationship between the lateral soil resistance-deflection is considered in this model. This linear relationship is defined as the initial slope of the p-y curve (4) at $\tilde{y} = 0$ m. Thus, the linear relation between the soil reaction per unit length (P) and lateral soil–pile relative displacement ($\tilde{y}$) is:

$$P = kz\tilde{y} \tag{9}$$

2.3. System damping

System material damping is considered following the Rayleigh approach, so the damping matrix $\mathbf{C_M}$ can be computed by (see e.g. Chopra (2011)):

$$\mathbf{C_M} = A\mathbf{M_m} + B\mathbf{K_m} \tag{10}$$

where $\mathbf{M_m}$ and $\mathbf{K_m}$ are the global stiffness and mass matrices of the system (without considering the interaction with the soil and the water). Parameters A and B are calculated as:

$$A = \zeta\frac{2\omega_i\omega_j}{\omega_i + \omega_j} \tag{11}$$

$$B = \zeta\frac{2}{\omega_i + \omega_j} \tag{12}$$

being ω_i and ω_j the natural frequencies, and ζ the damping fraction for the i^{th} and j^{th} modes. In this work, the first and last modes are chosen and a damping value of 2% is considered.

In order to model the loss of the energy transmitted from the foundation to the soil, a radiation damping in parallel with lateral soil–pile spring is contemplated. Considering that the soil is nearly incompressible, this radiation damping per unit length can be calculated following (Gazetas and Dobry, 1984):

$$c_r = 4D\rho_s V_s \tag{13}$$

being D the pile diameter; ρ_s and V_s the density and shear wave velocity of soil respectively. With these radiation and material dampings, the global damping matrix of the system is determined.

2.4. Seismic input incident field

The system is excited by planar shear waves that propagate vertically through the soil acting in the y direction, producing a free-field (without foundation) lateral displacement at ground level that is denoted as u_{ff}. The harmonic incident field is assumed to propagate through a non-homogeneous medium with continuous variation of soil properties with depth and linear behaviour.

For a continuously non-homogeneous soil with a single layer, the horizontal displacements (u_I) in frequency domain due to the incident field can be computed following the expressions proposed by

Rovithis et al. (2011), where the shear wave propagation velocity (V_s) is determined according to the generalized power-law function:

$$V_s(z) = V_r \left(b + q \frac{z}{z_r} \right)^n \tag{14}$$

being z the depth from ground surface; V_r and z_r the reference shear wave velocity and depth respectively (established at 15 m); $b = (V_0/V_s)^{1/n}$ and $q = 1 - b$ the parameters that determine the shear wave velocity at surface level (V_0); and n the parameter that determines the evolution of the shear wave with depth. In this work, in order to follow the same profile represented by the API curves (linear variation with depth of the soil shear modulus), the values $V_0 = 0$ m/s and $n = 0.5$ are considered.

The lateral displacements at a certain level and frequency ($u_I(z,\omega)$) due to an incident field propagating in a non-homogeneous medium with these characteristics is determined by the following equation established in Rovithis et al. (2011):

$$u_I(z,\omega) = \frac{C_1 (b + qz/z_r)^{\mu}}{N_{\nu+1}(\lambda b^{\ell/2})} \left\{ J_\nu \left[\lambda \left(b + q \frac{z}{z_r} \right)^{\ell/2} \right] N_{\nu+1} \left(\lambda b^{\ell/2} \right) - J_{\nu+1} \left(\lambda b^{\ell/2} \right) N_\nu \left[\lambda \left(b + q \frac{z}{z_r} \right)^{\ell/2} \right] \right\} \tag{15}$$

where C_1 is a boundary constant; J_ν and N_ν are the Bessel functions of the first and second kind and order ν respectively; ℓ, μ and ν are dimensionless parameters defined as $\ell = 2(1-n)$, $\mu = (1-2n)/2$ and $\nu = (2n-1)/(2(1-n))$; and $\lambda = 2k_I z_r/(\ell q)$ is the wave length corresponding to the wave number $k_I = \omega/V_r$.

With the displacements $u_I(z,\omega)$ calculated, the velocities $v_I(z,\omega)$ due to the seismic excitation in the frequency domain are determined:

$$v_I(z,\omega) = \mathrm{i}\omega u_I(z,\omega) \tag{16}$$

once the horizontal displacements and velocities are computed in frequency domain, they are obtained in time domain employing the frequency domain method. For this purpose, the frequency response functions of displacements and velocities at the desired depths with respect to the free field displacement are computed by using (15).

2.5. Ultimate axial bearing capacity

In this section, the methodology followed to compute the different cap translational masses (m) studied for the soil–pile subsystem (Fig. 1(b)) is explained. As it has been mentioned, the values adopted for these cap masses are a fraction (δ) of the ultimate axial bearing capacity (Q_u) of the piles, that is computed following the API (Designing API RP 2A-WSD, 2002):

$$Q_u = Q_f + Q_p = f A_s + q A_p \tag{17}$$

being Q_f the skin friction resistance, Q_p the total end bearing, f the unit skin friction capacity, A_s the side surface area of pile, q the unit end bearing capacity and A_p the gross end area of pile.

If the pile is unplugged, the shaft friction f acts on both inside and outside the pile, for plugged piles this shaft friction only acts on outside the pile. On this manner, the ultimate axial bearing capacity for unplugged piles is computed as the sum of the outside and inside skin friction resistance and the total end bearing corresponding to the annular section of the pile; while for plugged piles this ultimate bearing capacity is calculated as the sum of the external skin friction resistance and the total end bearing of the entire cross section of the pile. To determine if the pile is plugged or unplugged, the minimal value of the Q_u for unplugged and plugged pile is selected, as it is established in the API.

The shaft friction f, for piles in cohesionless soils, can be computed as:

$$f = K p_o \tan \delta_s \tag{18}$$

where K is the coefficient of lateral earth pressure, that takes a value of 0.8 and 1 for unplugged and plugged piles, respectively; p_o is the effective overburden pressure at the point in question, that is the product of the soil density and depth; and δ_s the friction angle between the soil and pile wall (whose values are described in the Table 6.4.3-1 of the API (Designing API RP 2A-WSD, 2002)). This shaft friction f is assumed to linearly increase with the overburden pressure until a limiting skin friction value is reached (f_{lim}, whose value is also established in Table 6.4.3-1 of API).

The unit end bearing q for cohesionless soils can be computed as:

$$q = p_o N_q \tag{19}$$

being N_q a dimensionless bearing capacity factor. The value of q is also limited by a unit end bearing value (q_{lim}, Table 6.4.3-1 of API).

2.6. Dynamic analysis

The time response of the system under variable loads can be computed by using the dynamic equation of motion in finite elements:

$$\mathbf{M}\ddot{\vec{u}}(t) + \mathbf{C}\dot{\vec{u}}(t) + \mathbf{K}\vec{u}(t) = \vec{F}(t) \tag{20}$$

where $\vec{u}$, $\dot{\vec{u}}$, $\ddot{\vec{u}}$ are the nodal displacements, velocities and accelerations, respectively; $\mathbf{M}$, $\mathbf{C}$, $\mathbf{K}$ are the mass, damping and stiffness matrices of the system; $\vec{F}$ is the nodal force vector; and t is the time. To solve (20) the Newmark Method is employed (see e.g. Chopra (2011)). In this study, the average acceleration method is considered. The nodal force vector ($\vec{F}$) is composed of the elastic and damping linear forces that the soil–pile interaction exerts on the pile due to the incident field.

Once displacements, velocities and accelerations of the system have been computed, with the stiffness, mass, damping matrices of each element, and by using (20), internal forces of each element are determined (shear forces $\vec{V}$ and bending moments $\vec{M}$).

2.6.1. Linear system resolution

Newmark Method for linear systems is used to compute displacements, velocities and accelerations for the NDLM. According to this method, the displacement in the time step ($\vec{u}_{t+1}$) can be calculated by:

$$\left(\mathbf{K} + \frac{\gamma}{\beta \Delta t}\mathbf{C} + \frac{1}{\beta(\Delta t)^2}\mathbf{M} \right) \vec{u}_{t+1} = \hat{\vec{F}}_{t+1} \tag{21}$$

where Δt is the time step and $\hat{\vec{F}}_{t+1}$ is the equivalent force vector at time $t+1$, which can be computed from the response of the previous time instant as:

$$\hat{\vec{F}}_{t+1} = \vec{F}_{t+1} + \left[\frac{1}{\beta(\Delta t)^2}\mathbf{M} + \frac{\gamma}{\beta \Delta t}\mathbf{C} \right] \vec{u}_t + \left[\frac{1}{\beta(\Delta t)}\mathbf{M} + \left(\frac{\gamma}{\beta} - 1 \right)\mathbf{C} \right] \dot{\vec{u}}_t + \left[\left(\frac{1}{2\beta} - 1 \right)\mathbf{M} + \Delta t \left(\frac{\gamma}{2\beta} - 1 \right)\mathbf{C} \right] \ddot{\vec{u}}_t \tag{22}$$

once $\vec{u}_{t+1}$ is computed, the velocities and accelerations in the next time step ($\dot{\vec{u}}_{t+1}$ and $\ddot{\vec{u}}_{t+1}$ respectively) are determined using:

$$\dot{\vec{u}}_{t+1} = \frac{\gamma}{\beta \Delta t}(\vec{u}_{t+1} - \vec{u}_t) + \left(1 - \frac{\gamma}{\beta} \right)\dot{\vec{u}}_t + \Delta t \left(1 - \frac{\gamma}{2\beta} \right)\ddot{\vec{u}}_t \tag{23}$$

$$\ddot{\vec{u}}_{t+1} = \frac{1}{\beta(\Delta t)^2}(\vec{u}_{t+1} - \vec{u}_t) - \frac{1}{\beta \Delta t}\dot{\vec{u}}_t - \left(\frac{1}{2\beta} - 1 \right)\ddot{\vec{u}}_t \tag{24}$$

2.6.2. Non-linear system resolution

Newmark Method for non-linear system is used to solve (20) in non-linear models (PNLM and ENLM). This method is based on iterating the value of the displacement until a solution of the non-linear equilibrium equation is achieved. The main equation governing this method is (see e.g. Chopra (2011)):

$$(\hat{\mathbf{K}}_T)^{(j)}_{t+1} \vec{\Delta u}^{(j)} \equiv \hat{\vec{R}}^{(j)}_{t+1} \tag{25}$$

Table 1
Main characteristics of soils considered in this work.

	Very loose sand (Loose)	Medium dense sand (Dense)
Poisson's ratio [ν_s]	0.49	0.49
Density [ρ_s] (kg/m^3)	2000	2000
Shear wave velocity [V_s] (m/s)	92.41	232.56
Angle of internal friction [Φ] (°)	28	36
Initial modulus of subgrade reaction [k] (MN/m^3)	4.07	25.79
C_1	1.60	3.30
C_2	2.40	3.60
C_3	22	60
Soil-pile friction angle [δ_s] (°)	15	25
Limiting skin friction value [f_{lim}] (kN/m^2)	47.8	81.3
N_q	8	20
Limiting unit end bearing value [q_{lim}] (MN/m^2)	1.9	4.8

being $(\hat{\mathbf{K}}_T)^{(j)}_{t+1}$ the tangent stiffness for the j^{th} iteration in the next time step $t+1$; $\vec{\Delta u}^{(j)}$ the variation of displacement; and $\hat{\vec{R}}^{(j)}_{t+1}$ the residual force. All these terms must be updated in each iteration and time step following:

$$(\hat{\mathbf{K}}_T)^{(j)}_{t+1} \equiv (\hat{\mathbf{K}}_T)^{(j)}_{t+1} + \frac{\gamma}{\beta \Delta t}\mathbf{C} + \frac{1}{\beta(\Delta t)^2}\mathbf{M} \tag{26}$$

$$\vec{\Delta u}^{(j)} = \vec{u}^{(j+1)}_{t+1} - \vec{u}^{(j)}_{t+1} \tag{27}$$

$$\begin{aligned}\hat{\vec{R}}^{(j)}_{t+1} = {} & \vec{F}_{t+1} - (\vec{F}_S)^{(j)}_{t+1} - \left[\frac{1}{\beta(\Delta t)^2}\mathbf{M} + \frac{\gamma}{\beta \Delta t}\mathbf{C}\right]\left(\vec{u}^{(j)}_{t+1} - \vec{u}_t\right) \\ & + \left[\frac{1}{\beta \Delta t}\mathbf{M} + \left(\frac{\gamma}{\beta} - 1\right)\mathbf{C}\right]\dot{\vec{u}}_t + \left[\left(\frac{1}{2\beta} - 1\right)\mathbf{M} + \Delta t\left(\frac{\gamma}{2\beta} - 1\right)\mathbf{C}\right]\ddot{\vec{u}}_t\end{aligned} \tag{28}$$

where the term $(\vec{F}_S)^{(j)}_{t+1}$ is the restoration force, that is, the elastic force. The initialization of the iteration is carried out considering a displacement equal to that of the previous time instant.

After each iteration, the solution is verified and the iterative process ends when a measure of error is less than a specified tolerance. In this work, the convergence criterion is established in terms of the norm of the difference of the displacement vectors between iterations:

$$|\vec{\Delta u}^{(j)}| \leq \varepsilon_u \tag{29}$$

being ε_u the tolerance, fixed as 10^{-10} m. Once the tolerance criterion is fulfilled, the velocities and accelerations are computed following (23) and (24).

3. Problem definition

3.1. Soil properties

A very loose (Loose) and a medium dense (Dense) sandy soils are considered in this study. Each soil is assumed to be a halfspace, where the lateral bearing capacity and the soil resistance deflection relationship varies with depth following the API expressions. The main characteristics of each soil type are shown in Table 1, together with the values assumed for the definition of the API *p-y* curves and the Q_u calculation.

3.2. Pile properties

In order to analyse typical piles of OWT foundations, three different piles with diameters $D = 0.5, 1$ and 5 m are studied. For all piles, a length $L = 30$ m is considered. In this way, small piles (typical of jackets) and larger piles (typical of monopiles) are included. Two more lengths ($L = 15$ and 60 m) are considered for the pile with $D = 1$ m. The thickness of each pile (t_p) is determined by the expression proposed by the API RP 2A-WSD (Designing API RP 2A-WSD, 2002):

$$t_p \geq 6.35 + \frac{D}{100}\ [\text{mm}] \tag{30}$$

Table 2
Main characteristics of the piles studied in this work.

D (m)	L (m)	t_p (mm)	Q_u (t) - Loose	Q_u (t) - Dense	Plugged/Unplugged
0.5	30	11.35	232.8	428.8	Plugged
1	15	16.35	290.4	508.6	Unplugged
	30	16.35	541.8	1050	Plugged
	60	16.35	1001	1831	Plugged
5	30	56.35	3850	6721	Unplugged

The cap masses (m) analysed in the soil–pile subsystem (see Fig. 1(b)) are defined as a fraction (δ) of the ultimate bearing capacity (Q_u), ranging from $\delta = 0$ to 1, with steps of 0.125. The main information about the piles analysed in this work, along with the ultimate axial bearing capacity (Q_u) of each pile and soil is presented in Table 2.

3.3. OWT properties

Three reference OWTs with rated powers of 5, 10 and 15 MW and its corresponding monopiles are analysed in this study. The main characteristics of these OWTs and monopiles are summarized in Table 3. The monopile dimensions have been extracted from Medina et al. (2021), where its sizing has been addressed based on the procedure described by Arany et al. (2016).

Finally, the necessary inertial characteristics to reproduce the equivalent weight of the superstructure of these OWTs are indicated in Table 4. In this table, the masses of the different components of the system (Fig. 1(c)), the total mass of the superstructure (m), and the ultimate axial bearing capacity of the OWT monopiles (Q_u) are listed. Besides, to quantify this total mass with respect to the Q_u of each monopile and soil, the relation between these two parameters (δ) is also presented. Piles and the wind turbine are considered of S355 structural steel, whose main characteristics are: Young's modulus of 210 GPa, Poisson's ratio of 0.3 and density of 7850 kg/m^3. To determine the additional mass due to the interaction between pile and water, a density of sea water of 1030 kg/m^3 and a maximum water depth of 25 m have been considered.

3.4. Seismic signals

Ten accelerograms are used in this study, all of them obtained from the PEER Ground Motion Database (Pacific Earthquake Engineering Research Center (PEER), 2022). Table 5 provides the main information of each earthquake: the record sequence number (RSN) of the database, the direction with respect to the north of the horizontal component used, name and year of the earthquake event, name of the measuring station, the time-average shear-wave velocity for the upper 30 m depth ($V_{s,30}$) of the soils in which they have been measured, the maximum ground acceleration ($a_{g,max}$) and the time step (ΔT) of each signal.

Table 3
Main characteristics of the OWTs used in this work.
Source: Medina et al. (2021).

OWT	5 MW (Jonkman et al., 2009)	10 MW (Bak et al., 2013)	15 MW (Gaertner et al., 2020)
Tower height (m)	90	119	135
Rotor diameter (m)	126	178	240
Rated wind speed (m/s)	11.4	11.4	10.6
Cut-out wind speed (m/s)	25	25	25
Rotor operational speed range (rpm)	6.9–12.1	6–9.6	5–7.6
Tower top diameter (m)	3.9	5.5	6.5
Tower bottom diameter (m)	6	8.3	10
Tower top thickness (m)	0.019	0.020	0.024
Tower bottom thickness (m)	0.027	0.038	0.041
Pile diameter (m)	6.04	8.30	10.00
Pile thickness (m)	0.067	0.090	0.107
Pile length over mudline (m)	32.6	32.6	32.6
Pile embedded length (m)	49.7	63.8	73.8

Table 4
Inertial characteristics of the OWTs and its corresponding monopiles in the two soils studied in this work.

Mass (t)	5 MW	10 MW	15 MW
Rotor-nacelle assembly	350	674	1017
Tower	347.46	605	860
Substructure	321.74	594.05	851.04
Water inside substructure	703.38	1329.6	1931.1
Total weight [m]	1722.6	3202.7	4659.1
Loose			
Q_u (t) - Unplugged	8292.7	15 057	21 275
δ $[m/Q_u]$	0.208	0.213	0.219
Dense			
Q_u (t) - Unplugged	14 346	26 037	36 784
δ $[m/Q_u]$	0.120	0.123	0.127

Based on a convergence analysis, these time steps are the ones used to compute the system kinematic variables with the Newmark Method.

These acceleration signals are assumed to correspond to the free-field acceleration at surface level for all soil profiles. In order to make the structural response of all these seismic signals comparable to each other, the accelerograms are scaled to a maximum ground acceleration of 0.6 g. The system seismic response is computed as the average response of the ten accelerograms, following the DNV-RP-0585 guidelines (DNV, 2021), which recommends to evaluate the seismic design of wind power plants by computing the mean response of, at least, seven earthquakes.

4. Results and discussion

This section presents the comparative analysis carried out for the soil–pile subsystem (Fig. 1(b)) and its applicability to understand the behaviour of the complete OWT-monopile system (Fig. 1(c)).

Regarding the parametric analysis conducted using the soil–pile subsystem, the results are organized as follows:

- First, the mean envelopes of maximum seismic responses for three different piles without pile cap (soil–pile subsystem with $\delta = 0$) are studied (Fig. 3) with the aim of quantifying the non-linear and inelastic behaviour in the kinematic soil–pile interaction problem.
- Secondly, these same envelopes are analysed for the same piles with a cap mass equivalent to its ultimate axial bearing capacities ($\delta = 1$, Fig. 4) in order to study the inertial interaction effect within soil–pile non-linear and plastic behaviour.
- Next, the soil resistance temporal evolution in each model at two different depths is presented in Figs. 5 and 6 for the two previous configurations in order to illustrate the activation of the non-linear an plastic behaviours.
- After that, the contribution of the inertial effect within soil–pile interaction is analysed for several piles and δ values, computing the relative differences of the maximum seismic responses of each model with respect to those of the linear one (Figs. 7–9).

Finally, the mean envelopes of maximum seismic responses of three different monopiled OWTs are studied and compared with the envelopes of its corresponding monopiles with a pile cap mass equivalent to the weight of each supported OWT (Fig. 10) in order to verify the conclusions of the parametric analysis.

4.1. Envelopes of maximum seismic responses

Fig. 3 shows the mean envelopes of maximum bending moments (M), shear forces (V), accelerations (a) and soil resistances (P) for the three diameters (D) considered. These results correspond to the soil–pile subsystem (Fig. 1(b)) without pile cap mass ($\delta = 0$) and with a pile length of 30 m. Results of each response variable are disposed by columns, while those corresponding to the diameters are arranged by rows. Each subgraph is divided into two parts separated by a line of points and dashes: the envelopes corresponding to the medium dense sandy soil (Dense) and the very loose one (Loose) are shown on left and right sides, respectively. The depth and the envelopes values are represented on y-axis and x-axis accordingly. The envelopes obtained in the different considered models (NDLM, ENLM, PNLM) are distinguished with different colours. In the envelopes corresponding to the soil resistance (fourth column), an additional green curve is included to represent the ultimate lateral resistance of the soil (P_u).

In Fig. 3 it can be observed that virtually the same results between the three models are obtained for all diameters and response variables studied. Thus, in this case without pile cap mass, where the kinematic effects governs the soil–pile interaction, the consideration of a non-linear and inelastic soil–pile interaction model seems to be irrelevant, so a linear elastic model is enough to reproduce the soil–pile kinematic response.

Regarding the influence of the soil type, it can be appreciated that greater bending moments and shear forces are reached in the Loose soil, while higher accelerations are obtained in the Dense one. As the diameter increases, greater internal forces and lower acceleration envelopes are found. The maximum bending moments and accelerations are obtained at pile head, however, the maximum shear forces are reached at shallow levels, increasing this depth when the pile diameter grows. With respect to the soil resistance envelopes (fourth column of Fig. 3), it can be seen that the ultimate lateral bearing capacity of soil (p_u) is not reached in any case. In fact, the soil resistance is quite smaller than the value of the ultimate resistance at the different depths, approaching the limit only near the free surface level. This fact, will be further studied in Section 4.2.

To analyse the effect of the inertial interaction within soil–pile dynamic interaction, the same envelopes than those presented in Fig. 3

Table 5
Information about the seismic signals (accelerograms) used in this work.
Source: Pacific Earthquake Engineering Research Center (PEER) (2022).

RSN	Dir. (°)	Event name	Year	Station name	$V_{S,30}$ (m/s)	$a_{g,max}$ (g)	Δt (s)
186	90	Imperial Valley-06	1979	Niland Fire Station	212	0.11	0.005
266	102	Victoria Mexico	1980	Chihuahua	242	0.15	0.010
729	0	Superstition Hills-02	1987	Imperial Valley W.L.A	179	0.21	0.005
1176	60	Kocaeli Turkey	1999	Yarimca	297	0.23	0.005
1498	59	Chi-Chi Taiwan	1999	TCU059	273	0.16	0.005
1792	90	Hector Mine	1999	Indio-Riverside C.F.G	282	0.12	0.010
2715	47	Chi-Chi Taiwan-04	1999	CHY047	170	0.13	0.004
3683	11	Taiwan SMART1(45)	1986	SMART1 O11	295	0.13	0.010
3965	8	Tottori Japan	2000	TTR008	139	0.32	0.010
5666	7	Iwate Japan	2008	MYG007	167	0.13	0.010

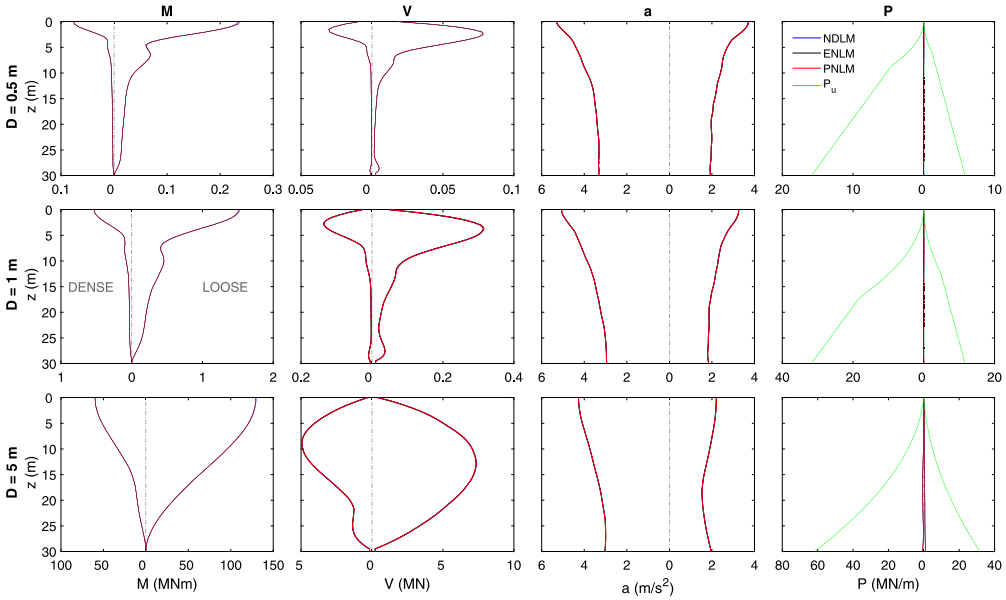

Fig. 3. Mean envelopes of maximum seismic responses for the soil–pile subsystem without a cap mass ($\delta = 0$).

but with a pile cap mass equivalent to the ultimate axial bearing capacity of each pile ($\delta = 1$) are shown in Fig. 4. The same graph distribution that the one previously used for Fig. 3 is also employed in Fig. 4.

In Fig. 4 remarkable differences between the envelopes obtained in the three different models are seen. So, the non-linear and inelastic behaviour of soil–pile dynamic interaction becomes relevant when the inertial interaction is activated by the dynamic excitation. For lower diameters (0.5 and 1 m), greater differences between the envelopes of the three models can be distinguished; while for the diameter of 5 m, the envelopes are very similar between the three models. The highest maximum value of the seismic responses (that are obtained at pile head for bending moments, shear forces and accelerations) are found for the linear model (NDLM) in the pile diameters of 0.5 and 1 m. Thus, in terms of maximum seismic responses, the NDLM is a conservative assumption for lower diameters.

Comparing the responses corresponding to the plastic and elastic non-linear models (PNLM and ENLM), very similar envelopes are obtained. Only in the acceleration envelopes of the diameters 0.5 and 1 m, and for the Dense soil, a relevant difference between these two models can be observed. Higher envelopes are reached in the ENLM for the two soils and the three diameters. Thus, although the consideration of an elastic and plastic non-linear model leads to similar structural-seismic responses, the elastic non-linear approach seems to be the most conservative between these two.

Regarding the highest responses values, these are generally computed at pile head for the internal forces and accelerations. Furthermore, greater internal forces, accelerations and soil resistances are obtained when a Dense soil is defined, a contrary trend to what has been obtained when the pile cap mass is not considered (Fig. 3), where greater internal forces are computed in the Loose soil.

According to the soil resistance envelopes, for the shallower depths, the soil resistance corresponding to the Non-Degraded Linear Model overpasses the ultimate lateral bearing capacity of soil (p_u), while in the non-linear plastic and elastic models the soil ultimate lateral bearing capacity is reached in these same depths (note that the soil resistance in these two models are limited to the p_u value). Furthermore, it can be observed that the soil resistance of the linear model exceeds p_u to a greater extent as the diameter becomes smaller. This fact justifies the remarkable differences between the linear and the two non-linear models for the diameters of 0.5 and 1 m. Finally, it is important to highlight that the differences between the three models are obtained in the shallower depths, that is, in the same soil levels where the ultimate lateral bearing capacity is exceeded by the linear model.

4.2. Evolution of soil resistance

To better understand the differences between the two non-linear models and the linear one in the soil–pile subsystem without and with

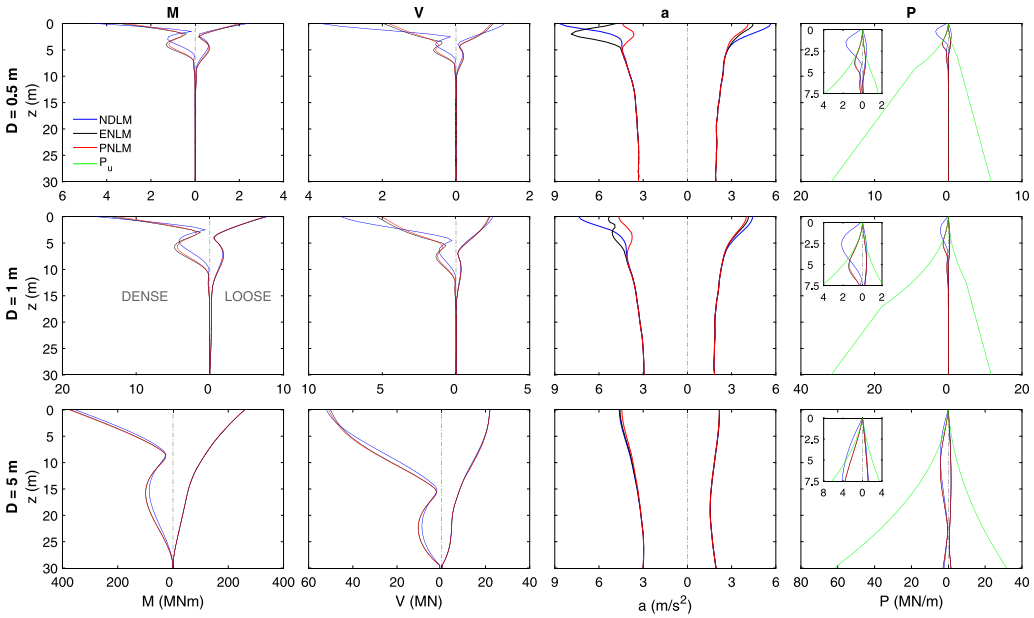

Fig. 4. Mean envelopes of maximum seismic responses considering a mass equal to the ultimate axial bearing capacity ($\delta = 1$).

pile cap mass previously studied in Section 4.1, the evolution of soil resistance (P, y-axis) with respect to the soil–pile deflection ($\tilde{y}$, x-axis) at pile head and at depth equal to a diameter are represented in Figs. 5 and 6. These results correspond to the same earthquake event: the Imperial Valley signal (see Table 5). Fig. 5 shows the temporal evolutions for the subsystem without pile cap mass ($\delta = 0$), while Fig. 6 those corresponding to the subsystem with pile cap mass equal to the ultimate axial pile bearing capacity ($\delta = 1$). In both figures, results of the three diameters are presented by columns, and those corresponding to the two depths and soils are shown by rows: the two upper rows presents the results of the Loose soil and the two bottom ones, those of the Dense soil. The soil resistance evolution at pile head and at a depth equal to the pile diameter are disposed in the first and second row of each soil, accordingly. By using different colours the three models are distinguished.

The temporal evolutions of the *p-y* relation clearly show the non-linear behaviour of the plastic (red curve) and elastic non-linear models (black curve). When only the kinematic interaction effect is analysed (Fig. 5), the three models reach similar values of maximum soil resistances and soil–pile deflections, except for the soil resistances at pile head for the diameters of 0.5 and 1 m, where the maximum values correspond to the Non-Degraded Linear Model. When the diameter and depth increases, the evolution of soil resistance of non-linear models tend to assimilate to the evolution obtained in the linear model, indicating that the ultimate lateral bearing capacity is far from being reached. Higher soil resistances and soil–pile deflections are found for the Loose soil, in agreement with the previous results in terms of envelopes (Fig. 3). When a Dense soil is considered, for a depth equivalent to the pile diameter, the evolution of soil resistance for the non-linear models is practically linear.

When a pile cap mass equivalent to the ultimate axial bearing capacity of pile is considered ($\delta = 1$, Fig. 6), high differences are obtained between the soil resistances of the two non-linear models with respect to the linear one. For the small diameters (0.5 and 1 m), the soil resistances of the linear model greatly exceed the ultimate lateral soil resistance. Furthermore, contrary to what has been stated for Fig. 5, the maximum soil resistance values are obtained for the Dense soil, where a remarkable difference between the maximum values of the linear and non-linear models can be appreciated. Note that these trends coincide with the ones for the envelopes with $\delta = 1$ (Fig. 4).

4.3. Relative differences with respect to the non-degraded linear model

With the aim of comparing the three models for different δ values, the relative differences between the maximum results of the non-linear models (ENLM and PNLM) with respect to those obtained in the non-degraded linear model (NDLM) are depicted in Figs. 7–9. The differences of maximum mean bending moments (M), shear forces (V), accelerations (a) and soil resistances (P) are arranged by columns; while the different two soil profiles are placed in rows. In all these representations, the relative differences (y-axis) with respect to the different value of δ (x-axis) are shown. The results corresponding to the PNLM and ENLM are presented in different colours.

In Fig. 7, the relative differences of the maximum responses for the subsystem with a pile diameter of 1 m and a length of 30 m are shown. The relative differences corresponding to the ten seismic signals are depicted with points, while the relative differences of the maximum mean responses of the ten seismic signals are presented with a continuous line. Analysing the relative differences of the maximum mean responses, it can be appreciated that in the Loose soil similar results between the non-linear models and the linear one are obtained for δ values lower or equal than 0.5. When δ increases, relevant relative differences are obtained, reaching values between 5 and 10% for the internal forces, accelerations and soil resistances in the highest values of δ. Regarding the Dense soil, important relative differences can be observed from δ values higher than 0.25. The differences computed in the Dense soil are approximately three and four times greater than those of the Loose one, reaching values over a 30%. In both soils, once the inertial interaction effect acquires relevance, the relative differences of the Plastic Non-Linear Model (PNLM) are higher than those of the Elastic Non-Linear Model (ENLM). However, these relative differences are, in general, negative, indicating that the Non-Degraded Linear Model (NDLM) is the most conservative in terms of maximum seismic responses.

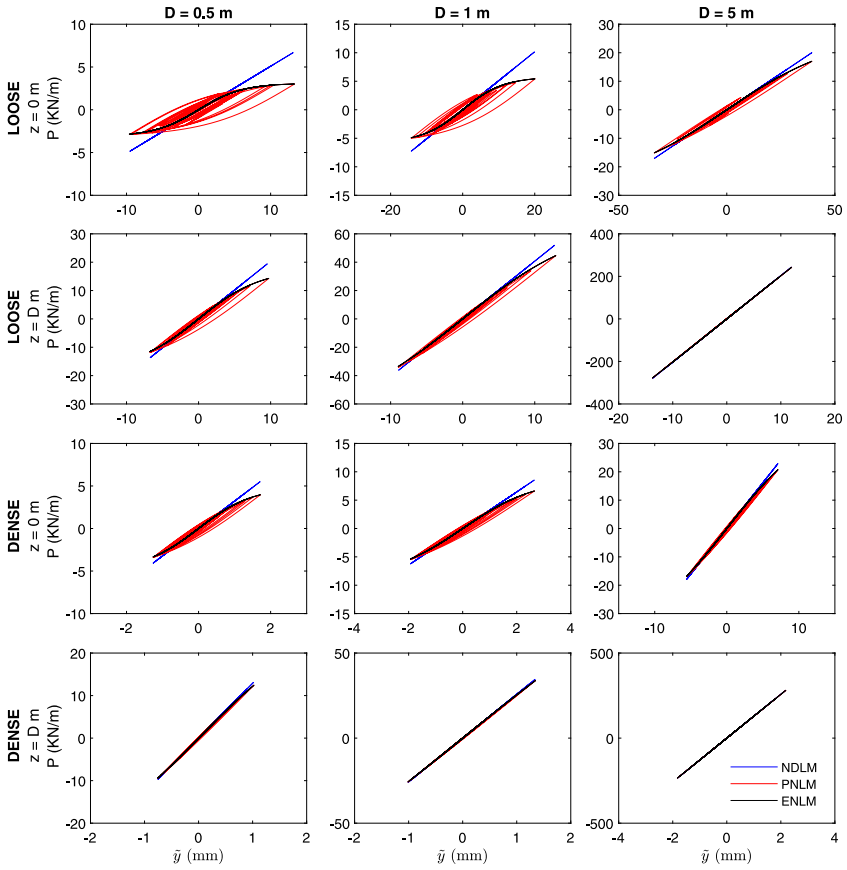

Fig. 5. Evolution of soil resistance (P) versus soil–pile relative displacement ($\bar{y}$), for $\delta = 0$. Results for the Imperial Valley signal.

Attending to the relative differences of each earthquake, it can be observed that some differences are positive for a few seismic signals in the bending moments and soil resistances. Furthermore, it can be seen that several seismic excitations leads to remarkable higher and lower differences than the ones obtained for the maximum mean responses, justifying the importance of considering the mean response of at least seven earthquakes (as it is recommended in the DNV-RP-0585 guideline DNV, 2021). Also, it can be observed that for large values of δ the dispersion of the results tends to increase.

Fig. 8 shows the relative differences for the three pile diameters studied, all of them with a pile length of 30 m. By using different types of lines the results of each diameter are distinguished. The highest relative differences are reached for the lowest pile diameters, following a similar trend to what Tabesh and Poulos (2001) exposes. Besides, for small pile diameters, lower δ values are required to obtain relevant differences between the linear and non-linear models. Note how for a pile diameter of 0.5 m and δ values greater than 0.25, significant relative differences appear. The relative differences in the three diameters are mostly negative, excepting the bending moments and soil resistances of the 5 m pile diameter. For this pile diameter, negligible relative differences (lower than 5%) are generally obtained in the entire δ interval, excepting the bending moment and soil resistance differences for the highest δ values. For all diameters and δ values, greater relative differences are reached in the Plastic Non-Linear Model. As it has been previously commented, in the Dense soil higher differences are generally reached compared to the Loose one.

The relative differences corresponding to the soil–pile subsystem with a diameter of 1 m and three different pile lengths (15, 30 and 60 m) are represented in Fig. 9. Different line plots are used to distinguish the three lengths studied. The highest differences are reached for large pile lengths. A similar trend in the results than the ones previously commented is generally obtained: the differences are mostly negative and the Plastic Non-Linear Model leads to the highest relative differences; the bending moment and soil resistance relative differences are sometimes positive for a length of 15 m, a similar trend to those it has been obtained for the differences of the 5 m pile diameter (previously shown in Fig. 8). In conclusion, for non-slender piles, the non-linear models lead to a greater response than the linear one in terms of bending moments and soil resistances if the inertial effects are activated.

4.4. Envelopes of monopiled OWTs and its corresponding monopiles

Fig. 10 shows the mean envelopes of maximum bending moments (M), shear forces (V) and accelerations (a), for three monopiled OWTs with rated powers of 5, 10 and 15 MW obtained by the integrated model including OWT superstructure, (Fig. 1(c)) and its corresponding monopiles subsystems, with a pile cap mass equivalent to its supported superstructure weight (see Table 4). The different response variables are arranged by columns, while the envelopes corresponding to each OWT are disposed by rows. The same results disposal than the ones previously used for the envelopes of Figs. 3 and 4 is employed: the envelopes corresponding to the dense and the loose soil are shown on left and right side respectively (separated by a vertical line); the envelopes obtained in the different models considered (NDLM, ENLM,

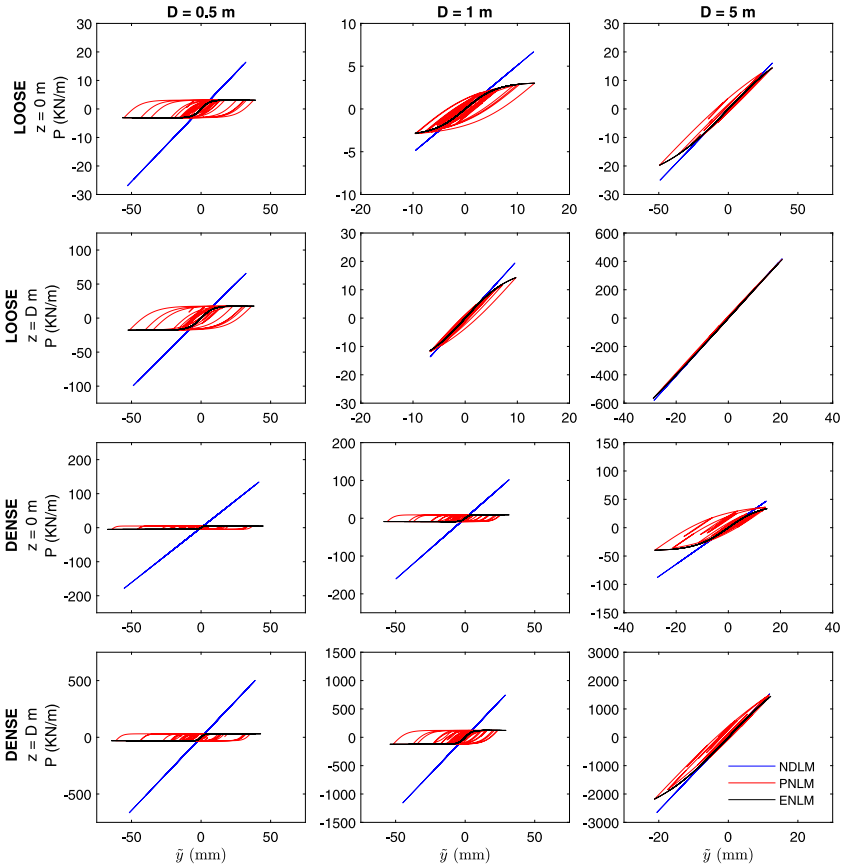

Fig. 6. Evolution of soil resistance (P) versus soil–pile relative displacement ($\bar{y}$), for $\delta = 1$. results for the Imperial Valley signal.

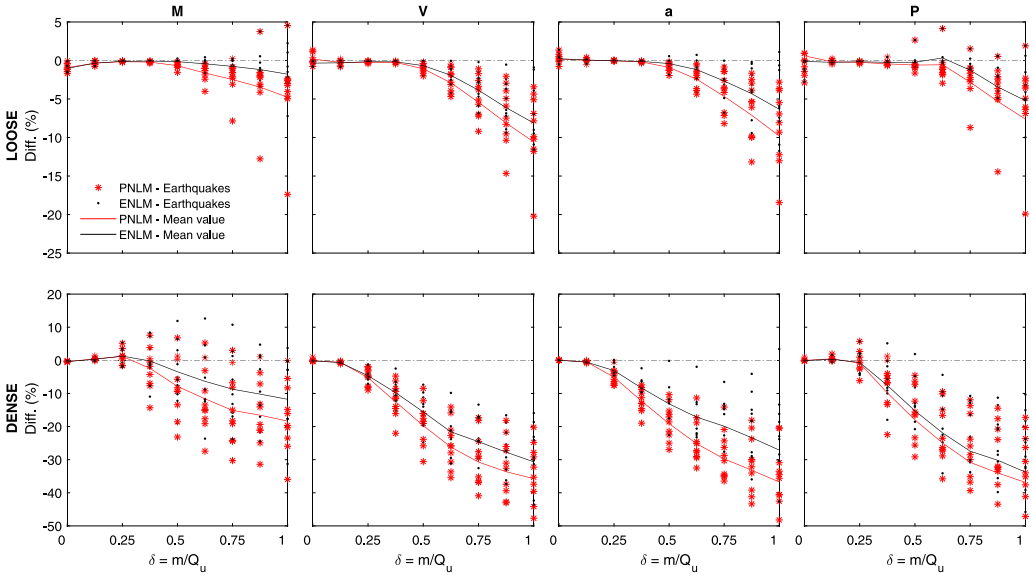

Fig. 7. Relative differences of maximum results of each earthquake with respect to those of the NDLM.

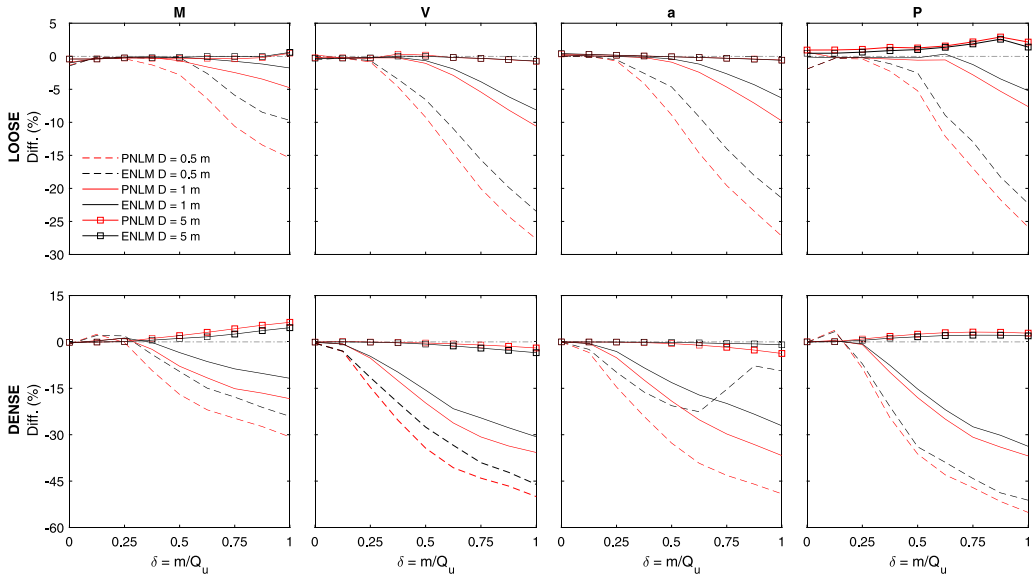

Fig. 8. Relative differences of mean maximum results with respect to those of the NDLM, for several pile diameters ($L = 30$ m).

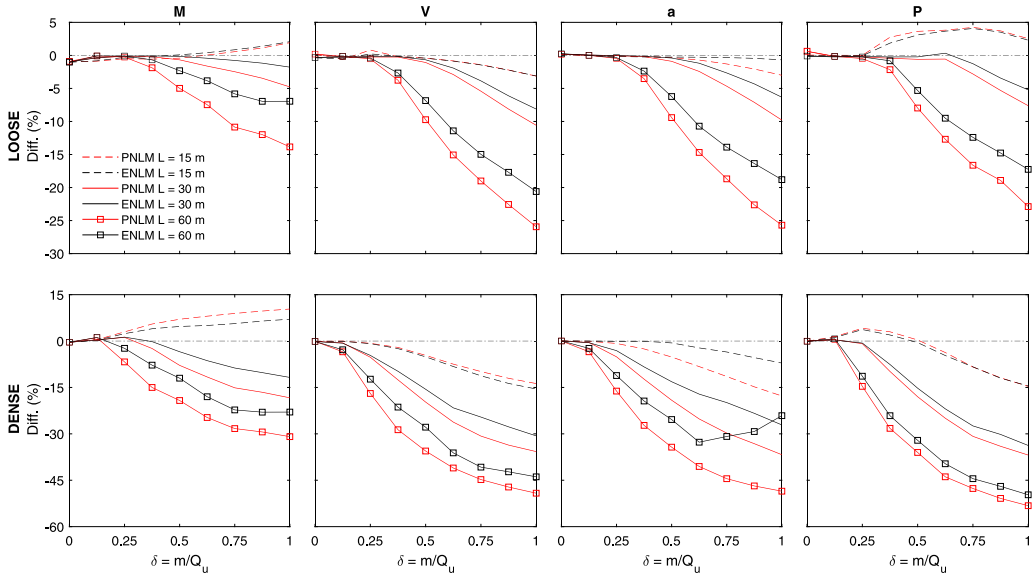

Fig. 9. Relative differences of mean maximum results with respect to those of the NDLM, for several pile lengths ($D = 1$ m).

PNLM) are distinguished with different colours. Two dashed horizontal lines are used to represent the seabed surface (yellow line) and the height of the substructure (blue line). The envelopes for the soil–pile subsystems are presented by dotted lines.

In Fig. 10 it can be observed that similar envelopes are obtained for the three models studied. Note that the equivalent δ value of these superstructures and its corresponding monopiles are around 0.2 and 0.12 for the Loose and Dense soil respectively (see Table 4). As presented in Section 4.3, these values correspond to the δ range for which the non-linearity of the soil–pile interaction has no relevance. Some small differences can be observed between the linear and non-linear models in the envelopes of the Dense soil, where the results of the Non-Degraded Linear Model are slightly larger than those of the non-linear models. In terms of the global foundation-structure-OWT system seismic response, the linear elastic model for soil–pile interaction is conservative, as it has been obtained throughout this study.

Comparing the envelopes of the entire system (OWT and monopiles) with those of the monopiles and the equivalent pile cap OWT masses, greater maximum internal forces are obtained for the Dense soil when the entire system is considered, while in the Loose soil higher internal forces values are reached in the single monopile configuration. With respect to the kinematic variables studied (displacements and accelerations), similar envelopes are computed in the two configurations. Note

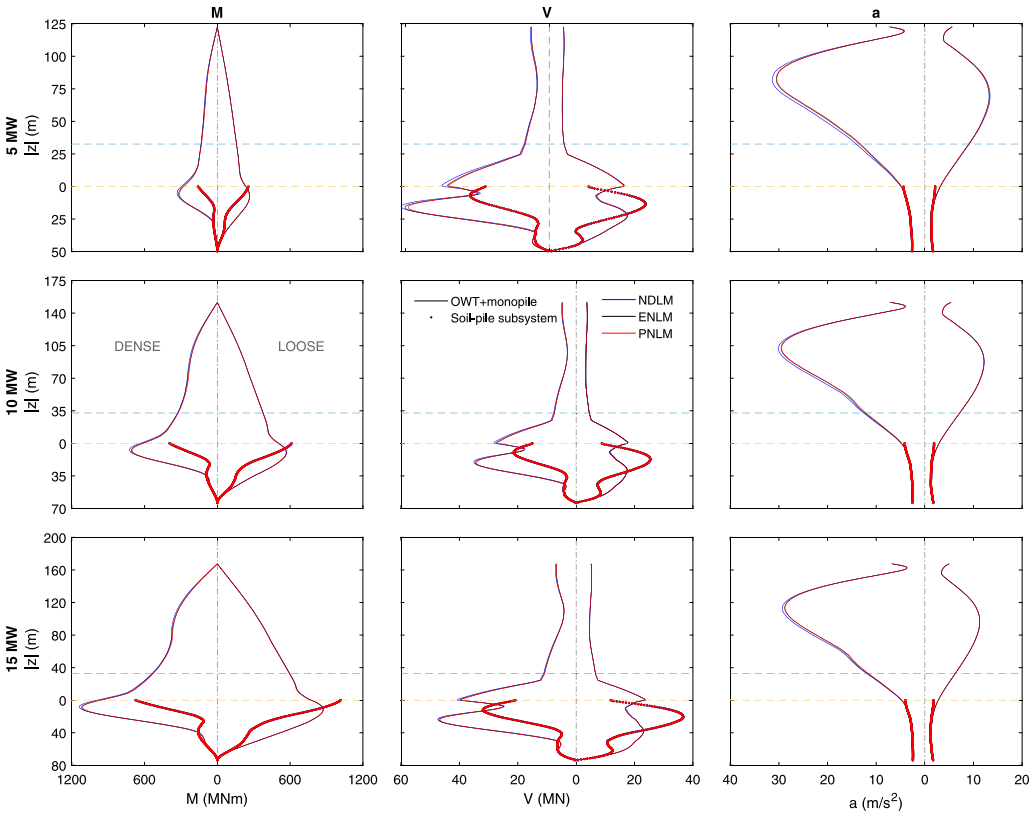

Fig. 10. Mean envelopes of maximum seismic responses for the monopiled OWTs and its corresponding soil–pile subsystems.

that the principal difference between the two models is the pile head rotation restriction that is imposed in the soil–pile subsystem.

5. Conclusions

This paper studies the influence of non-linearity and plasticity of soil–pile interaction on the seismic response of OWT pile foundations embedded in two different types of sandy soils. For this purpose, three different models: a Plastic Non-Linear, an Elastic Non-Linear and a Non-Degraded Linear Model are analysed and compared. These three models reproduce the soil–pile interaction by a Beam on Dynamic Winkler Foundation approach based on the *p-y* curves established by the API RP 2A-WSD. An incident field for non-homogeneous medium with linear variation of soil properties is contemplated in each soil–pile model. Characteristic pile geometries of jacket and monopile foundations embedded in very loose and medium dense sandy soils are studied. The effects of the non-linear and plastic assumptions are analysed by evaluating the kinematic and inertial effects within soil–pile interaction. For this purpose, different translational cap masses are studied in a soil–pile subsystem. From the analysis of the envelopes of maximum responses and its relative differences with respect to the linear model, the following conclusions are drawn:

- Similar results between models are obtained when the kinematic interaction effect predominates within soil–pile dynamic interaction. Thus, the consideration of a linear elastic model is enough to reproduce the soil–pile kinematic interaction.
- The non-linear and inelastic behaviour of soil–pile dynamic interaction acquires relevance when the inertial interaction is excited. Nevertheless, the consideration of a linear elastic model leads generally to higher maximum seismic responses.
- Similar seismic responses are obtained by considering a plastic or elastic non-linear model. Between these two models, greater responses are found in the elastic non-linear one. For this reason, if a non-linear model must be used, it is enough to consider an elastic soil–pile interaction, avoiding the complexity of the cyclic behaviour of soil–pile interaction.
- Greater internal forces are obtained in soft (Loose) soils when the kinematic interaction effect prevails, while when the inertial interaction predominates higher internal forces are computed in stiffer (Dense) soils.
- Higher differences between models are produced for small-diameter slender piles and in the Dense soil. These differences arise because the ultimate lateral resistance is greatly exceeded in the Non-Degraded Linear Model.

The main conclusions drawn of the analysis of the soil–pile subsystems are tested with three reference OWTs, comparing its envelopes of maximum responses with those of its corresponding monopiles with a pile cap mass equivalent to the superstructure mass.

- For these configurations, similar envelopes of maximum bending moments, shear forces and accelerations between models are obtained, as the mass of the superstructure is not enough to activate the inertial interaction effects.

Therefore, focusing on the soil–pile interaction phenomena, when the kinematic interaction dominates and a linear incident field is

considered, an elastic linear Winkler model formulated through non-degraded soil properties allows to reach accurate and conservative seismic responses. This is a general and interesting conclusion due to the simplicity of the proposed solution and it has been fully demonstrated with an extensive study of problems and excitations. By means of a simple model that reduces the complexity of the soil–pile interaction phenomena, it is possible to obtain accurate and conservative results. As a second phase of the two non-linear models and the work carried out, it is necessary to incorporate the non-linear behaviour of the incident field and to compare it with the linear assumption. On this manner, it can be evaluated to what extent a linear model is accurate enough to reproduce the system seismic response, or how it should be modified to adjust to that response. In this respect, there are very interesting recent works, see e.g Stacul et al. (2022), which, from a different approach and less specific analysis, obtain conclusions that follow a similar trend to what has been obtained in this study: the kinematic pile seismic response is mainly influenced by the model stiffness, rather than by the non-linear or inelastic behaviour of free field response and soil–pile interaction.

CRediT authorship contribution statement

Eduardo Rodríguez-Galván: Writing – original draft, Visualization, Software, Methodology, Conceptualization. **Guillermo M. Álamo:** Writing – review & editing, Software, Conceptualization. **Juan J. Aznárez:** Writing – review & editing, Supervision, Funding acquisition, Conceptualization. **Orlando Maeso:** Writing – review & editing, Supervision, Conceptualization.

Declaration of competing interest

The authors declare that they have no known competing financial interests or personal relationships that could have appeared to influence the work reported in this paper.

Data availability

Data will be made available on request.

Acknowledgements

This research has been funded by Ministerio de Ciencia e Innovación and Agencia Estatal de Investigación (MCIN/AEI/10.13039/501100011033) of Spain and FEDER through research project PID2020-120102RBI00 and predoctoral research scholarship PRE2021-099200 (E. Rodríguez-Galván), also funded by FSE+. This research has been partially supported by ACIISI, Spain-Gobierno de Canarias and European FEDER Funds Grant EIS 2021 04.

References

Álamo, G.M., Aznárez, J.J., Padrón, L.A., Martínez-Castro, A.E., Gallego, R., Maeso, O., 2018. Dynamic soil-structure interaction in offshore wind turbines on monopiles in layered seabed based on real data. Ocean Eng. 156, 14–24.

Álamo, G.M., Bordón, J.D.R., Aznárez, J.J., 2021. On the application of the beam model for linear dynamic analysis of pile and suction caisson foundations for offshore wind turbines. Comput. Geotech. 134, 104107.

Alati, N., Failla, G., Arena, F., 2015. Seismic analysis of offshore wind turbines on bottom-fixed support structures. Phil. Trans. R. Soc. A 373 (2035), 20140086.

Arany, L., Bhattacharya, S., Macdonald, J.H.G., Hogan, S.J., 2016. Closed form solution of eigen frequency of monopile supported offshore wind turbines in deeper waters incorporating stiffness of substructure and SSI. Soil Dyn. Earthq. Eng. 83, 18–32.

Bak, C., Zahle, F., Bitsche, R., Kim, T., Yde, A., Henriksen, L.C., Natarajan, A., Hansen, M., 2013. Description of the DTU 10 MW reference wind turbine. In: DTU Wind Energy Report-I-0092. Vol. 5, DTU Wind Energy.

Bisoi, S., Haldar, S., 2014. Dynamic analysis of offshore wind turbine in clay considering soil–monopile–tower interaction. Soil Dyn. Earthq. Eng. 63, 19–35.

Bisoi, S., Haldar, S., 2015. Design of monopile supported offshore wind turbine in clay considering dynamic soil–structure-interaction. Soil Dyn. Earthq. Eng. 73, 103–117.

BOSLAN Engineering and Consulting, 2022. The Next Generation Monopile Foundations for Offshore Wind Turbines - Manufacturing , Design and Handling Challenges. Technical report.

Carswell, W., Arwade, S.R., DeGroot, D.J., Myers, A.T., 2016. Natural frequency degradation and permanent accumulated rotation for offshore wind turbine monopiles in clay. Renew. Energy 97, 319–330.

Chen, L., Wu, W., Liu, H., Hu, A., Newson, T., El Naggar, M.H., Mei, G., Xu, M., 2022. Analytical solution for lateral vibration of offshore pipe piles considering hydrodynamic pressure. Comput. Geotech. 151, 104962.

Cheng, X., Wang, T., Zhang, J., Wang, P., Tu, W., Li, W., 2023. Dynamic response analysis of monopile offshore wind turbines to seismic and environmental loading considering the stiffness degradation of clay. Comput. Geotech. 155, 105210.

Chopra, A.K., 2011. Dynamics of Structures: Theory and Applications To Earthquake Engineering, Fourth Prentice-Hall International Series in Civil Engineering and Engineering Mechanics.

Designing API RP 2A-WSD, Recommended Practice for Planning and Constructing Fixed Offshore Plaftorms - Working Stress Design. American Petroleum Institute.

DNV, 2014a. Design of offshore wind turbine structures. Offshore Standard DNV-OS-J101. Det-Norske Veritas AS.

DNV, 2014b. Environmental conditions and environmental loads. Recommended Practice DNV-RP-C205. Det-Norske Veritas AS.

DNV, 2021. Seismic design of wind power plants. Recommended Practice DNV-RP-0585. Det-Norske Veritas AS.

Firoj, M., Maheshwari, B.K., 2022. A new nonlinear spring-dashpot model of CPRF of NPP structure based on coupled BEM-FEM approach. Earthq. Eng. Struct. Dyn..

Gaertner, E., Rinker, J., Sethuraman, L., Zahle, F., Anderson, B., Barter, G., Abbas, N., Meng, F., Bortolotti, P., Skrzypinski, W., et al., 2020. Definition of the IEA 15-megawatt offshore reference wind turbine.

Gazetas, G., Dobry, R., 1984. Simple radiation damping model for piles and footings. J. Eng. Mech. 110 (6), 937–956.

Gerolymos, N., Gazetas, G., 2005a. Constitutive model for 1-D cyclic soil behaviour applied to seismic analysis of layered deposits. Soils Found. 45 (3), 147–159.

Gerolymos, N., Gazetas, G., 2005b. Phenomenological model applied to inelastic response of soil-pile interaction systems. Soils Found. 45 (4), 119–132.

Hassan, A.M., 2018. Winkler model for pile seismic analysis considering end constraints effects. HBRC J. 14 (3), 316–320.

Jiang, W., Lin, C., 2022. Lateral responses of monopile-supported offshore wind turbines in sands under combined effects of scour and earthquakes. Soil Dyn. Earthq. Eng. 155, 107193.

Jiang, W., Lin, C., Sun, M., 2021. Seismic responses of monopile-supported offshore wind turbines in soft clays under scoured conditions. Soil Dyn. Earthq. Eng. 142, 106549.

Jonkman, J., Butterfield, S., Musial, W., Scott, G., 2009. Definition of a 5-MW Reference Wind Turbine for Offshore System Development. Technical report, National Renewable Energy Lab.(NREL), Golden, CO (United States).

Jonkman, J., Musial, W., 2010. Offshore Code Comparison Collaboration (OC3) for IEA Wind Task 23 Offshore Wind Technology and Deployment. Technical report, National Renewable Energy Lab.(NREL), Golden, CO (United States).

Ju, S.H., Huang, Y.C., 2019. Analyses of offshore wind turbine structures with soil-structure interaction under earthquakes. Ocean Eng. 187, 106190.

Kaynia, A.M., 2021. Effect of kinematic interaction on seismic response of offshore wind turbines on monopiles. Earthq. Eng. Struct. Dyn. 50 (3), 777–790.

Kramer, S.L., 1996. Geotechnical Earthquake Engineering. Prentice-Hall International Series in Civil Engineering and Engineering Mechanics, ISBN: 0-13-374943-6,

Liang, F., Yuan, Z., Liang, X., Zhang, H., 2022. Seismic response of monopile-supported offshore wind turbines under combined wind, wave and hydrodynamic loads at scoured sites. Comput. Geotech. 144, 104640.

Medina, C., Álamo, G.M., Quevedo-Reina, R., 2021. Evolution of the seismic response of monopile-supported offshore wind turbines of increasing size from 5 to 15 MW including dynamic soil-structure interaction. J. Mar. Sci. Eng. 9 (11), 1285.

Mo, R., Cao, R., Liu, M., Li, M., 2021. Effect of ground motion directionality on seismic dynamic responses of monopile offshore wind turbines. Renew. Energy 175, 179–199.

Musial, W., Spitsen, P., Duffy, P., Beiter, P., Marquis, M., Hammond, R., Shields, M., 2022. Offshore Wind Market Report: 2022 Edition. Technical report, National Renewable Energy Lab.(NREL), Golden, CO (United States).

Pacific Earthquake Engineering Research Center (PEER), 2022. NGA-West2 Ground Motion Database. Accessed on 20 August 2022. Available online: ngawest2.berkeley.edu/.

Padrón, L.A., Carbonari, S., Dezi, F., Morici, M., Bordón, J.D.R., Leoni, G., 2022. Seismic response of large offshore wind turbines on monopile foundations including dynamic soil–structure interaction. Ocean Eng. 257, 111653.

Patra, S., Haldar, S., 2021. Seismic response of monopile supported offshore wind turbine in liquefiable soil. In: Structures. Vol. 31, Elsevier, pp. 248–265.

Rovithis, E.N., Parashakis, H., Mylonakis, G.E., 2011. 1D harmonic response of layered inhomogeneous soil: Analytical investigation. Soil Dyn. Earthq. Eng. 31 (7), 879–890.

Shi, S., Zhai, E., Xu, C., Iqbal, K., Sun, Y., Wang, S., 2022. Influence of pile-soil interaction on dynamic properties and response of offshore wind turbine with monopile foundation in sand site. Appl. Ocean Res. 126, 103279.

Stacul, S., Rovithis, E., Di Laora, R., 2022. Kinematic soil–pile interaction under earthquake-induced nonlinear soil and pile behavior: An equivalent-linear approach. J. Geotech. Geoenviron. Eng. 148 (7), 04022055.
Tabesh, A., Poulos, H.G., 2001. The effects of soil yielding on seismic response of single piles. Soils Found. 41 (3), 1–16.
Wang, Y., Zhang, Z., Wu, X., Zhu, B., Chen, Y., 2023. The py model of single pile foundation for OWTs under combined lateral environment loading and earthquake in saturated sand. Ocean Eng. 268, 113406.
Wang, P., Zhao, M., Du, X., Liu, J., Xu, C., 2018. Wind, wave and earthquake responses of offshore wind turbine on monopile foundation in clay. Soil Dyn. Earthq. Eng. 113, 47–57.
Xi, R., Xu, C., Du, X., El Naggar, M.H., Wang, P., Liu, L., Zhai, E., 2022. Framework for dynamic response analysis of monopile supported offshore wind turbine excited by combined wind-wave-earthquake loading. Ocean Eng. 247, 110743.
Yan, Y., Yang, Y., Bashir, M., Li, C., Wang, J., 2022. Dynamic analysis of 10 MW offshore wind turbines with different support structures subjected to earthquake loadings. Renew. Energy 193, 758–777.
Yang, Y., Bashir, M., Li, C., Wang, J., 2019. Analysis of seismic behaviour of an offshore wind turbine with a flexible foundation. Ocean Eng. 178, 215–228.

2.3 Third publication: Rodríguez-Galván et al., 2025, Engineering Structures

Table 2.3. Third publication data.

Title	An accurate and ready-to-use approach for the estimation of impedance functions of regular pile groups for offshore wind turbine foundations. Vertical and rocking components
Authors	E. Rodríguez-Galván, G.M Álamo, J.J. Aznárez and O. Maeso
Journal	Engineering Structures
DOI	10.1016/j.engstruct.2024.119288
ISSN	0141-0296
Impact factor	6.4
CiteScore	11.2
Category	Engineering, Civil
Quartile	Q1 (29/407)
Publisher	ELSEVIER SCI LTD
Volume	323, Part B
Date	January 2025

Engineering Structures 323 (2025) 119288

Contents lists available at ScienceDirect

Engineering Structures

journal homepage: www.elsevier.com/locate/engstruct

An accurate and ready-to-use approach for the estimation of impedance functions of regular pile groups for offshore wind turbine foundations. Vertical and rocking components

Eduardo Rodríguez-Galván, Guillermo M. Álamo *, Juan J. Aznárez, Orlando Maeso

Instituto Universitario de Sistemas Inteligentes y Aplicaciones Numéricas en Ingeniería (SIANI), Universidad de Las Palmas de Gran Canaria, 35017, Las Palmas de Gran Canaria, Spain

ARTICLE INFO

Keywords:
Pile groups
Group impedances
Interaction factor
Pile-to-pile interaction
Dynamic analysis
Offshore Wind Turbines

ABSTRACT

The interaction factor superposition method in the determination of the vertical and rocking impedances of pile groups for jacket-supported Offshore Wind Turbines is studied. The vertical and rocking group dynamic impedances obtained by this method are compared with those computed by a previously developed continuum model. The influence of the main parameters that define the problem is also studied. In order to propose an alternative calculation solution, some expressions dependent of these parameters are fitted from an extensive selection of jacket pile group configurations. These expressions allow to estimate the vertical flexibility of the source pile and the interaction factor between a pair of piles. Subsequently, applying elastic superposition, the group impedance functions are determined. Results show that the interaction factor superposition method correctly reproduces the vertical and rocking group dynamic impedances. Therefore, for these regular pile groups with large spacing ratios, the assumption of only considering the direct interaction between pile pairs leads to accurate results. Results obtained with the proposed fitted expressions generally conduct to a good estimation, properly reproducing the variation produced by the influence of the different parameters. Thus, this superposition method and the proposed expressions can be employed to quickly and simply reproduce the vertical soil–structure interaction of this type of structures.

1. Introduction

Pile groups are commonly used in a large variety of structural foundations, such as buildings, bridges and offshore platforms. Within this last group, piles were originally used in oil extraction platforms, but, in recent years, with the search of a sustainable and low-carbon future, they are also employed as Offshore Wind Turbine (OWT) foundations. According to the recent 2023 Global Offshore Wind Report [1], 2021 and 2022 have been the highest years in offshore wind history installation, with 21.1 GW and 8.8 GW of new power installed projects in both years, respectively, representing the 23% and 11% of the total new installations in the last 16 years. The predictions show that this growth will continue and will also be overcome throughout the next ten years. Among all existing offshore wind energy installed projects, monopiles are the most common substructure typology (60.2%) followed by jackets (10.4%) [2]. Although monopiles are expected to keep heading the OWT substructures, it is predicted that jacket substructures will grow to represent 15% of the future market. This increase is assumed by the need of installing OWTs in deeper waters and further from the coast. These jacket substructures are founded on suction caissons or on slender piles. Both suction caissons and piles are located at vertices of a regular polygon, depending on the number of jacket legs. The choice between these two solutions depends on multiple factors such as soil conditions and project-specific requirements. Although suction caissons are faster, cheaper and quieter than piles in terms of installation and removal, pile foundations are more suitable in terms of soil conditions versatility, high load-bearing capacity and settlement control, due to their larger length and vertical and rotational stiffnesses [3].

In this sense, the study of the dynamic response of pile groups is a key problem in the structural design of these devices and the development of this technology. Thus, with other applications, it has already been a widely studied problem over the years. This is a complex problem that involves pile–soil and pile–pile phenomena. The dynamic response of pile groups can be addressed by directly modelling the complete system or by superimposing simple interaction problems. On

* Corresponding author.
E-mail addresses: eduardo.rodriguezgalvan@ulpgc.es (E. Rodríguez-Galván), guillermo.alamo@ulpgc.es (G.M. Álamo), juanjose.aznarez@ulpgc.es (J.J. Aznárez), orlando.maeso@ulpgc.es (O. Maeso).

https://doi.org/10.1016/j.engstruct.2024.119288
Received 3 August 2024; Received in revised form 17 October 2024; Accepted 5 November 2024
Available online 18 November 2024

the one hand, direct models can be carried out with several modelling approaches, such as, the finite element method (FEM), boundary element method (BEM), coupling of these two, or other procedures [4–9]. These direct models exhaustively reproduce pile–pile and pile–soil interactions, but they require a high computational cost. On the other hand, the superposition method is based on estimating the pile group response by superimposing interaction factors [10–15]. The simple nature of this superposition procedure makes it an interesting approach to be used in the design stages and for carrying out parametric studies.

The elastic superposition method (also known as the interaction factor superposition method) was firstly introduced by Poulos [10]. In this work he demonstrated that the static settlement of pile groups can be calculated from simple pile pair configurations, superimposing the source and receiver pile displacements. He also introduced the interaction factor concept as the relation between the receiver (unloaded) and source (loaded) pile displacements. Thereafter, Kaynia [4] studied the dynamic response of pile groups by introducing soil flexibility matrices and pile dynamic stiffness and compared his method with the superposition one, concluding that the Poulos's elastic superposition methodology gives reasonable results either statically and dynamically. Subsequently, Dobry and Gazetas [11] extended Poulos's superposition method to the dynamic analysis of pile groups. This work proposed some frequency dependent expressions to compute the vertical and horizontal displacement of one pile under its own load, as well as the interaction factor. With these expressions pile group dynamic impedances are obtained applying elastic principle of superposition effects. Interaction factors are also employed to simulate pile–soil–pile effects by Winkler models [13,14,16,17], in which Poulos's superposition procedure is then applied. These Winkler approaches can reproduce the interplay between the receiver pile and the soil subjected to the displacement field. Recent works, such as Zheng et al. [18], analysed the scattering and wave diffraction, proposing interaction factors that account these effects.

A large part of the performed works in this area [4,11,15,16,19,20] compared the superposition method with rigorous direct models. Nevertheless, all of them were focused on the analysis of standard pile configurations (square and rectangular arrangements), and not on pile configurations for jacket-supported OWTs, which are characterised by being formed by hollow cylindrical steel piles arranged in N-sided polygonal groups. For this reason, the main scope of this work is to study the interaction factor superposition method in the vertical dynamic response of pile groups for jacket-supported OWTs, considering a wide range of pile group configurations. Three different polygonal pile arrangements are studied, composed of 3, 4 and 5 hollow cylindrical piles embedded in an homogeneous halfspace. The influence of the main variables that intervene in the problem (frequency and pile and soil parameters) is studied. These parameters are considered in order to fit and propose some expressions that allow directly estimating the vertical flexibility of the source pile and the interaction factor of a pair of piles. Then, the dynamic vertical group response is computed applying elastic superposition. In order to carry out the superposition method and fitted expressions, the vertical flexibilities and interaction factors are obtained through a previously developed continuum model [8], which will also be used to verify the final result obtained from the proposed procedure. The proposed expressions allow to reproduce the vertical flexibility of the source pile and the interaction factor of a pair of piles, capturing the influence of the main pile and soil parameters that participate in the problem. These expressions together with the interaction factor superposition method could be useful to compute the vertical and rocking impedances for a wide range of pile groups for jacket-supported OWTs with different pile and soil characteristics. Thus, the overall methodology proposed in this work allows to obtain the vertical and rocking impedance functions in a fast and straightforward way, without the requirement to execute a complex model, with a good level of precision and accounting the influence of all relevant properties of the system. These impedances can be later used in substructuring models or in the design stages of these jacket-supported OWTs, in order to reproduce the soil–structure interaction (SSI). The relevance of considering this interaction has been highlighted in many works [21–25], in which it is emphasised that SSI inclusion plays an important role in the dynamic characteristics of jacket-supported OWTs, mainly in the determination of their natural frequencies, a critical factor in the design of this type of structures.

The present paper is organised in five sections. After the introduction presented in this Section 1, Section 2 describes the methodology followed to perform the work. Section 3 presents the problem definition, exposing the parameters studied and used to obtain the fitted expressions. Section 4 shows the main results and the proposed fitted expressions. Finally, the main conclusions drawn from this work are presented in Section 5.

2. Methodology

This section describes the methodology followed to compute the vertical and rocking group impedances and the procedure to obtain the fitted expressions. First, the interaction factor superposition method (or elastic superposition method) is explained (Section 2.1), then, the curve fitting procedure is described (Section 2.2).

2.1. The interaction factor superposition method

The vertical and rocking group impedances are obtained by superimposing the vertical interaction effects between all possible pile pairs of the group. Thus, it is possible to determine the dynamic stiffness of a pile group composed of N identical piles by knowing the dynamic stiffness or flexibility of a single and pair of piles at each frequency ω. This simplified method implies that the rest of piles are not influencing the interplay between pile pairs, a simplification very close to reality taking into account that jacket pile group configurations are composed of few piles with large separations.

Applying superposition of effects based on elastic theory, the flexibility and stiffness of a pile group (with identical piles) can be obtained through the sum of two simple submodels, as it is shown in Fig. 1. Submodel (a) corresponds to a single isolated pile subjected to a dynamic vertical load at its head (Q); whereas submodel (b) presents a pile pair separated by a distance S, in which the pile i is the active, source or loaded pile, while pile j is the passive, receiver or unloaded pile. From submodel (a) the vertical displacement of the isolated source pile subjected to its own axial load is calculated (w_{ii}). From submodel (b) the vertical displacement of the receiver pile due to the load acting over the active pile is obtained (w_{ji}). Thus, the vertical flexibility of the source pile (F_{ii}, subproblem (a)) and the flexibility of the receiver pile (F_{ji}, subproblem (b)) can be determined as the relation between the vertical displacement of the source and receiver piles and the axial load respectively (see Eqs. (1) and (2)). These displacements and flexibilities are frequency dependent and complex-valued terms.

$$F_{ii}(\omega) = \frac{w_{ii}(\omega)}{Q(\omega)} \tag{1}$$

$$F_{ji}(\omega) = \frac{w_{ji}(\omega)}{Q(\omega)} \tag{2}$$

The displacements of the source and receiver piles at their heads are computed through a previously developed continuum numerical model [8], particularly developed to efficiently analyse the harmonic behaviour of pile foundations in soils which can be stratified. The model is based on the integral expression of the reciprocity theorem in elastodynamics and the use of effective fundamental solutions to simulate the layered soil behaviour, which already satisfy the interlayer and free-field boundary conditions. This formulation allows to directly consider the radiation damping in the soil region without the need of including any artificial boundary condition. Piles are modelled

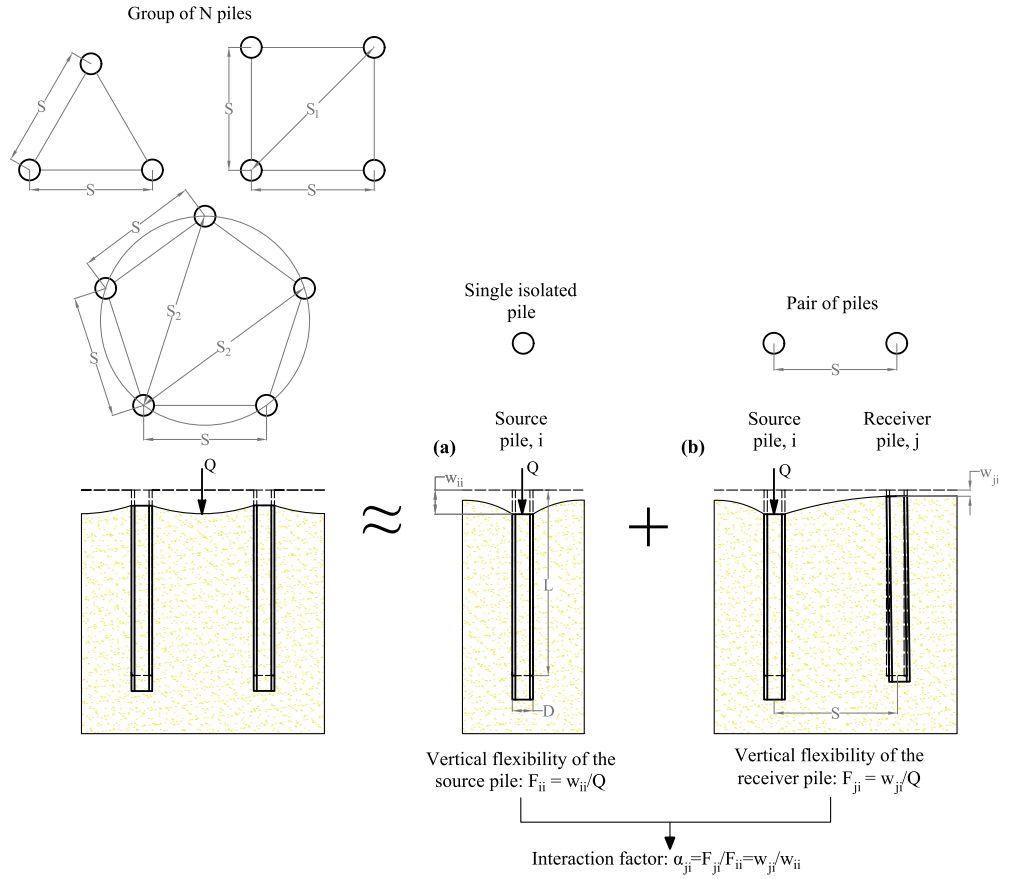

Fig. 1. Vertical modelling approach based on elastic superposition.

as load lines in the soil formulation and as beam finite elements to reproduce their stiffness and inertial contribution. Pile–soil coupling is made by imposing compatibility and equilibrium conditions in terms of displacements and soil–pile interaction forces. Linear-elastic behaviour of soil and piles is assumed. The capacity of this model to correctly reproduce the dynamic behaviour of OWT's foundation elements has been shown in [26].

Once the flexibilities of the source and receiver piles are obtained, the vertical dynamic interaction factor (α_{ji}) can be computed from:

$$\alpha_{ji}(\omega) = \frac{F_{ji}(\omega)}{F_{ii}(\omega)} = \frac{w_{ji}(\omega)}{w_{ii}(\omega)} \tag{3}$$

therefore, knowing this vertical dynamic interaction factor and the flexibility of the source pile, the flexibility of the receiver pile can be expressed in terms of this interaction factor ($F_{ji} = F_{ii}\alpha_{ji}$).

2.1.1. Vertical group impedances calculation

Once the flexibilities of the source pile and the interaction factors are obtained, the vertical flexibility of any pile i of the group (F_i) can be estimated by superimposing the vertical flexibility of the source pile (F_{ii}) with the interaction factors due to its all surrounding piles:

$$F_i = F_{ii}(1 + \sum_{j\neq i}^{j=N} \alpha_{ji}) \tag{4}$$

where N is the number of piles of the group, and α_{ji} is the interaction factor between pile j and i. In this case, as the pile groups are N-sided polygonal configurations, each pile of the group have the same vertical flexibility, so it is enough to determine the vertical flexibility of a unique pile. With this pile vertical flexibility, the pile vertical stiffness (K_i) can be calculated as its inverse:

$$K_i = F_i^{-1} \tag{5}$$

and the vertical group stiffness (K_G) is determined by multiplying it by the number of piles of the group:

$$K_G = N K_i \tag{6}$$

2.1.2. Rocking group impedances calculation due to the vertical component

If a group of piles is subjected at its centre of gravity to a rotation (θ) on the x-axis (as it is described in Fig. 2), it is possible to calculate the vertical displacement that each pile experiences due to this rocking motion as:

$$w_{\theta i} = \theta d_i \tag{7}$$

being d_i the distance between the centre of the pile and the centre of gravity of the group, measured in the y-axis (see Fig. 2). Thus, by using the flexibility definition, it is possible to determine the vertical force that appears at each pile head due to the rocking:

$$Q_{\theta i} = \frac{w_{\theta i}}{F_{\theta i}} \tag{8}$$

where $F_{\theta i}$ is the rocking flexibility due to the vertical component of pile i of the group. This flexibility can be computed with the vertical flexibility of the source pile and the vertical interaction factor:

$$F_{\theta i} = F_{ii}(1 + \sum_{j\neq i}^{j=N} \alpha_{ji} \frac{d_j}{d_i}) \tag{9}$$

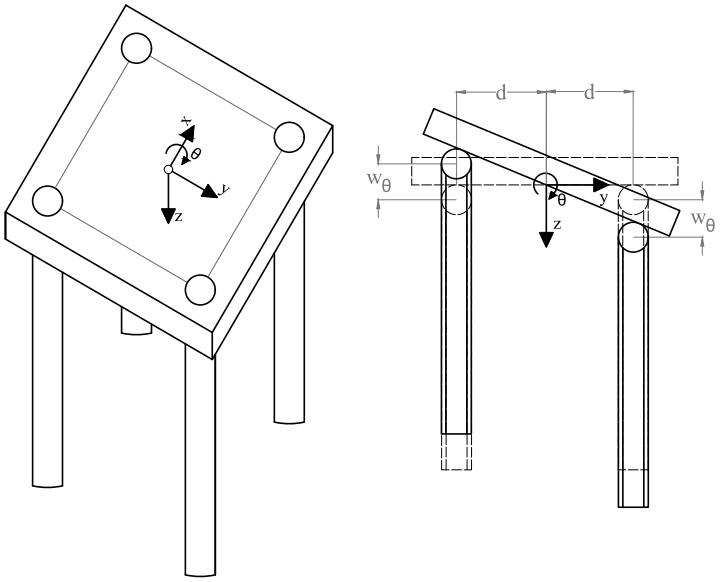

Fig. 2. Rocking problem definition.

being d_j the distance (either positive or negative) between the centre of the adjacent pile (j) and the centre of gravity of the group measured in the y-axis. Thus, for a unitary rotation, replacing Eq. (7) in Eq. (8), and multiplying this by the distance between the pile and the centre of gravity, the contribution of pile i to the group rocking stiffness is determined. In this way, by superimposing the contribution of each pile, the rocking impedance of the group is obtained as:

$$K_{\theta G} = \sum_{i=1}^{i=N} \frac{d_i^2}{F_{\theta i}} \tag{10}$$

This procedure is illustrated assuming a rotation around the x-axis. However, this type of regular polygonal pile arrangements presents an axisymmetric behaviour. Thus, the expressions can be applied to rotations around any axis contained in the xy-plane.

2.2. Proposed expressions for the estimation of the vertical flexibilities of the source pile and interaction factors

The dynamic problem under study depends on many parameters, such as the frequency and pile and soil properties. In this work the variables are defined in dimensionless form. These are: the dimensionless frequency (a_o), which is obtained from:

$$a_o = \frac{\omega D}{V_s} \tag{11}$$

where ω is the frequency, V_s the shear wave velocity of the soil and D the pile diameter; the ratio between the separation among two piles (S) and the diameter (pile spacing ratio: S/D); the relation between the pile length (L) and the pile diameter (pile slenderness ratio: L/D); the ratio between the pile and soil Young's Modulus (Young's Modulus pile–soil ratio: E_p/E_s); the relation between the pile and soil density (density pile–soil ratio: ρ_p/ρ_s); the pile and soil Poisson's ratios (ν_p and ν_s); and the soil hysteretic damping (ξ_s). Among these parameters, the dependency of the dimensionless frequency, pile spacing ratio, pile slenderness relationship, Young's Modulus pile–soil ratio, and soil hysteretic damping is studied on the vertical flexibilities of the source pile, interaction factors and the dynamic group impedances. From these parameters and for a wide and realistic range of them, simple expressions for the estimation of the flexibility of the source pile and interaction factor are fitted through the results computed with the continuum model [8].

In order to obtain expressions that collect the dependency of the main parameters studied, the fits are addressed in two steps. First, the flexibilities of the source pile and interaction factors are fitted for a reference case ($\hat{F}_{ii}$ and $\hat{\alpha}_{ji}$) with the same pile geometry and soil characteristics. For this case, the flexibility of the source pile is fitted as a function of the dimensionless frequency ($\hat{F}_{ii}(a_o)$), while the interaction factor is fitted as a function of the dimensionless frequency and pile spacing ratio ($\hat{\alpha}_{ji}(a_o, S/D)$).

Then, with the aim of introducing the dependency of the pile and soil characteristics in the expressions, different correction factors (β) are computed and fitted to adjust the reference case expressions. The correction factors for the flexibility of the source pile and interaction factor (β_F^P and β_α^P) are defined as a ratio between the flexibility of the source pile or interaction factor due to the change of the generic parameter P (F_{ii}^P and α_{ji}^P) and the reference flexibility of the source pile or interaction factor:

$$\beta_F^P(a_o, P) = \frac{F_{ii}^P(a_o, P)}{\hat{F}_{ii}(a_o)} \tag{12}$$

$$\beta_\alpha^P(a_o, P) = \frac{\alpha_{ji}^P(a_o, \frac{S}{D})}{\hat{\alpha}_{ji}(a_o, \frac{S}{D})} \tag{13}$$

These correction factors are fitted as a function of the dimensionless frequency, or the product of this one and the pile spacing ratio, and the parameter that they rectify. Therefore, the complete expressions of the flexibility of the source pile and interaction factor, are made up of as many correction factors as parameters are going to be rectified:

$$F_{ii}(a_o, \frac{L}{D}, \frac{E_p}{E_s}, \xi_s) = \beta_F^{\frac{L}{D}}(a_o, \frac{L}{D})\beta_F^{\frac{E_p}{E_s}}(a_o, \frac{E_p}{E_s})\beta_F^{\xi_s}(a_o, \xi_s)\hat{F}_{ii}(a_o) \tag{14}$$

$$\alpha_{ji}(a_o, \frac{S}{D}, \frac{L}{D}, \frac{E_p}{E_s}, \xi_s) = \beta_\alpha^{\frac{L}{D}}(a_o, \frac{L}{D})\beta_\alpha^{\frac{E_p}{E_s}}(a_o, \frac{E_p}{E_s})\beta_\alpha^{\xi_s}(a_o \frac{S}{D}, \xi_s)\hat{\alpha}_{ji}(a_o, \frac{S}{D}) \tag{15}$$

In this study, three correction factors are fitted to introduce in the expressions the pile slenderness, Young's Modulus ratios and soil damping dependency. Although the flexibility of the source pile can be easily

Table 1
Parameters studied in this work.

Parameter	Notation	Range/Value	Step
Pile spacing ratio	$\frac{S}{D}$	**[3 20]** [3 20]	**0.5** 1, in (3 6) 2, in (6 12) 4, in (12 20)
Pile slenderness ratio	$\frac{L}{D}$	[10 **20**]	1
Young's Modulus pile–soil ratio	$\frac{E_p}{E_s}$	[50 **500**]	50
Soil hysteretic damping [%]	ξ_s	[**1** 10]	0.25, in (1 1.25) 1.25, in (1.25 10)
Dimensionless frequency	a_o	[0.03 0.25]	0.001
Density pile–soil ratio	$\frac{\rho_p}{\rho_s}$	1.2	
Pile Poisson's ratio	ν_p	0.25	
Soil Poisson's ratio	ν_s	0.40	

computed with a simple model (such as the formulation of a Winkler one), in this work, the correction factor expressions for the flexibility of the source pile are also proposed.

As the flexibilities and interaction factors are complex valued, two fits are performed: one for the absolute value and another one for the argument. This option is chosen over directly fitting the real and imaginary components as it leads to simpler expressions. With these expressions it is pursued to be able to estimate the flexibility of the source pile and interaction factors without the need of executing a meticulous model.

All fits are obtained through a classical least squares regression, considering polynomial of a single or multiple variables (up to a maximum degree of 3) and exponential expressions. The goodness of each fit is evaluated with three commonly used goodness metrics: the sum of squares due to error (SSE), the root mean squared error ($RMSE$) and R-squared (R^2). SSE and $RMSE$ focus on the error magnitude, while R^2 provides insight into the explanatory power of the model. To obtain simple expressions, if two types of fits have similar goodness statistics, the one with fewer parameters is selected.

3. Problem definition

Piles are treated as solid hollow cylindrical foundations embedded in an isotropic homogeneous elastic soil halfspace. This study employs dimensionless variables to enhance the generality of the results. Thus, the vertical flexibility of the source pile and the impedance functions are expressed dimensionlessly based on the pile diameter and the pile's Young's Modulus:

$$F_{ii} D E_s \tag{16}$$

$$\frac{K_G}{D E_s} \tag{17}$$

$$\frac{K_{\theta G}}{D^3 E_s} \tag{18}$$

The dimensionless pile and soil parameters studied in this work as well as their corresponding values are presented in Table 1. The first (upper) part of this table shows the different parameters used to carry out the fitting expressions, being the values in bold text those that are used for the reference case, whereas the others for the correction factor (β) fits. The second (bottom) part of the table lists the dimensionless frequency range and the identical parameters adopted for both the reference case and correction factor fits.

Regarding the parameters considered in Table 1, typical geometric values of jacket pile groups are adopted, covering a large range of pile spacing ratios (from 3 to 20) and pile slenderness ratios (from 10 and 20), representing flexible piles which are typical of this type of pile groups. The Young's Modulus ratio interval is chosen from 50 to 500, corresponding to hollow steel piles in medium-to-soft seabeds. This ratio interval is established considering that the pile Young's Modulus is the equivalent of a cylindrical hollow steel pile with soil mass in its inside. For that purpose, a pile thickness (t_p) of 1.30% of the diameter is selected. This value has been obtained following the pile thickness API's recommendation [27] (see Eq. (19)), where a pile thickness of 1.6% and 1.2% is obtained for a pile diameter of 1 m and 3 m respectively. Soil hysteretic damping spans from 1 to 10%, covering the interval between 2 and 5% that is the commonly employed for seabed profiles.

$$t_p \geq 6.35 + \frac{D}{100} \text{ [mm]} \tag{19}$$

Concerning the same parameters that are adopted in all fits (both in the reference case and in the interaction correction factor fits, presented in the second part of Table 1), the dimensionless frequency (a_o) interval considered ranges from 0.03 to 0.25. The upper value corresponds to a diameter equal to a quarter of the wave length, being within the range of application of the beam-soil continuum model. The density pile–soil ratio adopted is the equivalent density of a cylindrical hollow steel pile with soil mass in its inside, considering a pile thickness of 1.30% of the diameter, in coherence with the Young's Modulus ratio interval. Poisson's ratios of 0.40 and 0.25 are selected for the soil and pile accordingly, usual values of sandy and clays seabed profiles and structural steel. A null hysteretic damping coefficient is assumed for the structural steel of the pile.

With respect to the values adopted to obtain the reference fits (indicated in bold text in Table 1), a pile slenderness ratio of 20, Young's Modulus ratio of 500 and soil damping of 1% are chosen. The flexibilities of the source pile and interaction factors for this reference case ($\hat{F}_{ii}$ and $\hat{\alpha}_{ji}$) are fitted by employing a wide range of pile spacing ratios, from 3 to 20 with steps of 0.5. The other values shown are used to obtain the fitting curves of the correction factors for the flexibility of the source pile and interaction factors (β_F^P and β_α^P). As it can be observed, the reference values are the upper (for the pile slenderness and Young's Modulus ratios) or lower limit (for the soil damping) of the considered intervals. In this way, the reference case is a limit configuration from which the others are obtained.

To validate the proposed procedure in terms of group impedances, three pile regular configurations (of 3, 4 and 5 piles) are studied, where each pile is located at each vertex of the polygon (see Fig. 3). All pile groups are assumed to be rigidly connected between them, a properly assumption for pile groups of jacket-supported OWTs. This rigid connection could be a unique structural element or several elements, such as a cap mass or beam framing joining the piles.

4. Results and discussion

With the aim of addressing the proposed objectives, the results presented in this section are organised into two parts: analysis of the reference case and analysis of correction factors.

In Section 4.1 the reference case is studied. First, the proposed fitted reference expressions to compute the vertical flexibilities of the source pile and interaction factors are shown. The vertical flexibility of the source pile and some interaction factors for different pile spacings are represented, comparing the results obtained with the fitted expressions with those directly computed with the continuum model. Then, the dynamic vertical and rocking impedances are analysed for this reference scenario. The impedances directly determined by the rigorous model are compared with those obtained by the interaction factor superposition method. The superposition is applied for the flexibilities and interaction factors directly obtained with the continuum model and with the proposed fitted expressions. In this way, the validity of both the superposition method and the fitted expressions is tested up.

In Section 4.2, the correction factors used to complete and include the dependency of the other parameters within the overall flexibility and interaction factor expressions are presented. First, the dependency

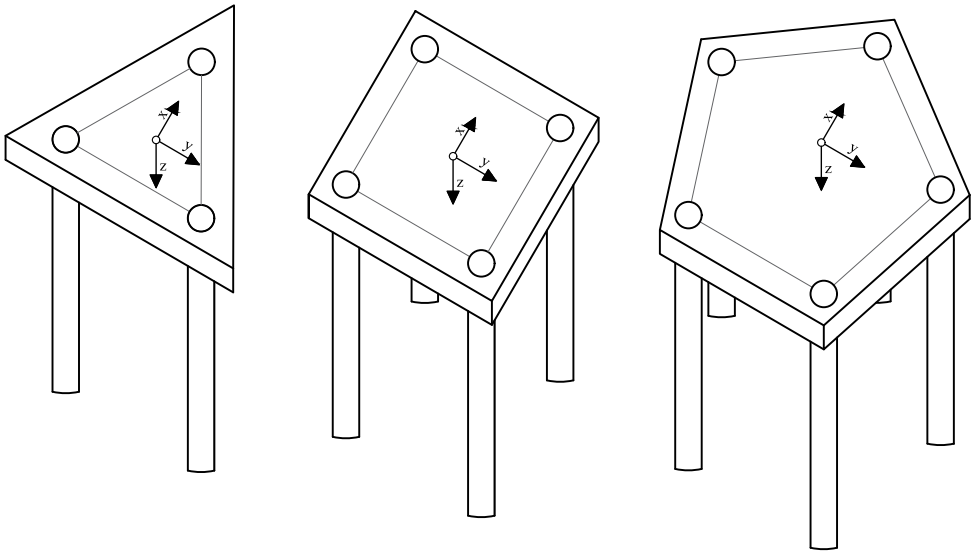

Fig. 3. Polygonal configurations of pile groups for jacket-supported OWTs studied in this work.

of these correction factors is analysed and their proposed fitted expressions are shown. Next, the effect of each correction factor is individually studied, by comparing the vertical and rocking group impedances obtained through the superposition of the fitted expressions, with the superposition of the direct model flexibilities and interaction factors. Afterwards, at the end of this Section 4.2, three cases with different configuration of parameters are studied comparing the model and fitting superposition results in order to analyse the correction as a whole.

4.1. Reference case

4.1.1. Proposed and fitted expressions

The fits obtained for the vertical flexibility of the source pile and interaction factor of the reference case ($L/D = 20$, $E_p/E_s = 500$ and $\xi_s = 1\%$) are exposed in Table 2. For the absolute value and argument of the flexibility of the source pile an exponential and polynomial expression of degree 1 are proposed, whereas for the interaction factor fits a multidegree polynomial expression of degrees 1 and 2 are suggested. The goodness statistics of each fit are also presented in Table 2, being SSE the sum of squares due to error, R^2 the R-squared statistic and $RMSE$ the root mean squared error. As it is exposed, all reference expressions have excellent goodness statistics, since all SSE and $RMSE$ take low values, as well as all R^2 are close to unity. All fits are chosen as a compromise between evaluating their simplicity and the accuracy of their results. For this reference case it is important to obtain expressions with acceptable goodness characteristics, because the complete expressions are based on these reference fits (see Eqs. (14) and (15)).

Fig. 4 shows the dimensionless flexibility of the source pile and the interaction factors for different pile spacing ratios ($S/D = 4, 6$ and 10) against the dimensionless frequency. The dimensionless flexibilities of the source pile are depicted in the first row and the interaction factors in the other ones. The real and imaginary parts are presented in the first and second column respectively. With different colours the results obtained through the fitting expressions (red curves), the model (blue curves) and with the Dobry and Gazetas [11] interaction factor expression (see Eq. (20), green curve) are distinguished. In Eq. (20) the term i refers to the imaginary unit ($\sqrt{-1}$). As it is shown in this equation, the interaction factor proposed by Dobry and Gazetas depends on the pile spacing ratio, the dimensionless frequency and the soil damping. In Fig. 4 it can be seen that the flexibilities of the source pile and interaction factors computed with the proposed fitted expressions align with those directly determined with the continuum model. The interaction factors obtained also matches well with the expression proposed by Dobry and Gazetas, especially for big pile spacing ratios. The flexibility of the source pile shows a slight curved variation over the frequency range, while the interaction factor presents the expected oscillatory behaviour. For the interaction factor, as pile spacing increases the oscillation amplitude and frequency (both in the real and imaginary parts) diminishes. The increase of the pile spacing produces a less interference among piles, as well as soil has more time to deform and dissipate the wave energy, leading to a lower resonant frequency.

$$\alpha_{ji}^{DG} = \left(2\frac{S}{D}\right)^{-\frac{1}{2}} e^{2\pi a_0 \frac{S}{D}(\mathrm{i}-\xi_s)} \tag{20}$$

4.1.2. Vertical and rocking dynamic impedances

In Fig. 5 the dimensionless vertical group impedances (y-axis) for the three, four and five pile groups are shown against the dimensionless frequency (x-axis) for the reference case. Results for each pile configuration are depicted in two columns: the real (stiffness component) and imaginary (damping component) part in the first and second column respectively. Group impedances for different pile spacing ratios ($S/D = 4, 6, 8$ and 10) are arranged by rows. With different colours the results directly obtained through the model (Direct-Model, black curves) are distinguished from those computed applying the superposition method. With a blue and red curve the impedances obtained by superimposing the flexibilities and interaction factors determined through the model ($\hat{\mathrm{F}}, \hat{\alpha}$-Model) and the fitted expressions ($\hat{\mathrm{F}}, \hat{\alpha}$-Fitting) are shown, while with a green curve the results computed by elastic superposition using the model flexibilities of the source pile and Dobry and Gazetas interaction factors (Eq. (20)) are represented. Following the same distribution, Fig. 6 shows the dimensionless rocking group impedances.

It can be observed that the impedances obtained through the interaction factor superposition method are generally similar to those directly computed through the model, both in the vertical and rocking impedances. For the vertical group impedances (Fig. 5) and the lowest pile separation ratio ($S/D = 4$), it can be appreciated a phase difference between the direct model maximum results and the maximum obtained

Table 2
Fitted expressions of the reference case.

Fitted expression/Type	Fitting parameters		Fitting characteristics	
$\mathrm{Abs}(\hat{F}_{ii}(a_o)) = \mathrm{a}e^{\mathrm{b}a_o}\frac{1}{DE_s}$	a	$7.96 \cdot 10^{-2}$	SSE	$4.86 \cdot 10^{-4}$
	b	-3.35	R^2	$9.81 \cdot 10^{-1}$
Exponential of 1 degree			$RMSE$	$1.50 \cdot 10^{-3}$
$\mathrm{Arg}(\hat{F}_{ii}(a_o)) = \mathrm{p}_1 a_o + \mathrm{p}_2$	p_1	-2.71	SSE	$4.42 \cdot 10^{-2}$
	p_2	$-4.01 \cdot 10^{-1}$	R^2	$9.93 \cdot 10^{-1}$
Linear regression			$RMSE$	$1.42 \cdot 10^{-2}$
$\mathrm{Abs}(\hat{\alpha}_{ji}(a_o, \frac{S}{D})) = \mathrm{p}_{00} + \mathrm{p}_{10}a_o + \mathrm{p}_{01}\frac{S}{D} + \mathrm{p}_{11}a_o\frac{S}{D} + \mathrm{p}_{02}\left(\frac{S}{D}\right)^2$	p_{00}	$4.20 \cdot 10^{-1}$	SSE	$6.13 \cdot 10^{-1}$
	p_{10}	$-1.96 \cdot 10^{-1}$	R^2	$9.79 \cdot 10^{-1}$
	p_{01}	$-2.89 \cdot 10^{-2}$	$RMSE$	$8.90 \cdot 10^{-3}$
	p_{11}	$-1.40 \cdot 10^{-3}$		
Multivariate polynomial of 1 and 2 degrees	p_{02}	$7.72 \cdot 10^{-4}$		
$\mathrm{Arg}(\hat{\alpha}_{ji}(a_o, \frac{S}{D})) = \mathrm{p}_{00} + \mathrm{p}_{10}a_o + \mathrm{p}_{01}\frac{S}{D} + \mathrm{p}_{11}a_o\frac{S}{D} + \mathrm{p}_{02}\left(\frac{S}{D}\right)^2$	p_{00}	$-1.02 \cdot 10^{-1}$	SSE	1.39
	p_{10}	1.34	R^2	1
	p_{01}	$-2.51 \cdot 10^{-2}$	$RMSE$	$1.34 \cdot 10^{-2}$
	p_{11}	-6.29		
Multivariate polynomial of 1 and 2 degrees	p_{02}	$1.14 \cdot 10^{-4}$		

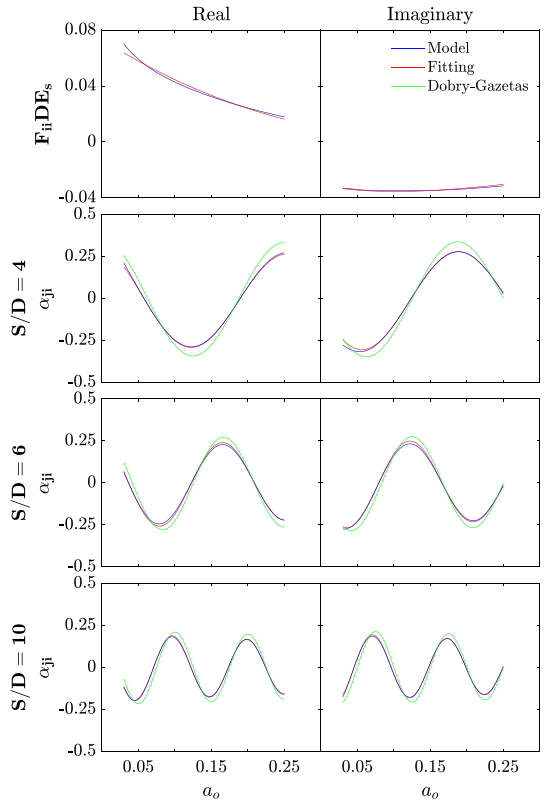

Fig. 4. Flexibility of the source pile and interaction factor for the reference case. (For interpretation of the references to colour in this figure legend, the reader is referred to the web version of this article.)

through the superposition method of the model and fitted flexibilities of the source pile and interaction factor. This maximum occurs at lightly higher frequencies when the interaction between all piles of the group is considered (Direct-Model results). This effect is due to the scattering of waves produced by the presence of all piles, which is only considered in the direct-model results (black curve). This occurs to a greater extent for the smallest pile spacing ($S/D = 4$), while for larger pile spacings this phase difference tends to decrease (note that for the $S/D = 6$ this phase difference practically does not exist). In this way, it is verified that the adjacent piles to the pile pair do not significantly affect the interplay between the pair for wavelengths larger than six times the pile diameter, assumption that was already established in [11]. Despite this difference between the vertical dynamic impedances obtained through the direct model and those of the interaction factor superposition method given for the $S/D = 4$, results computed by superposition reproduce quite well the impedance functions over the entire frequency range. Thus, for this type foundations, with large pile spacing ratios ($S/D \geq 4$), the interaction factor superposition can be employed to compute accurately enough the vertical and rocking impedance functions. The vertical impedances got with the superposition of the Dobry and Gazetas interaction factors show differences with respect to the fitting and model impedances. These differences are mainly appreciated at the impedance peaks, in which a phase and a magnitude difference are produced, conducting to greater peaks. Such peak differences are reduced as the number of piles of the group decreases and the pile spacing ratio increases. Regarding the rocking group stiffnesses and dampings (Fig. 6), the impedances determined through the fitted interaction factors and flexibilities of the source pile match well with the ones obtained through the continuum model. Only some discrepancies can be found at very low or high frequencies. In this case, the differences of the rocking impedances computed with the Dobry and Gazetas interaction factors with respect to the fitting and model results are lower than those given in the vertical impedances. As it was expected, both in the vertical and rocking impedances, a more pronounced group behaviour is observed with the increase of the number of piles. Increasing pile separation ratio produces a reduction in the vertical impedances and a growth of the rocking ones. Furthermore, with the increase of the pile spacing, more number of peaks appears in both the vertical and rocking impedances. Note that for a same frequency range more multiples of the wavelength fit within a greater pile separation. A similar trend is observed when the number of piles increases for the rocking impedances, producing more number of peaks. All these last comments agree well with the conclusions of the classical works (such as [4]). It is worth noting that, for comparison purposes, the rocking impedance functions obtained through the direct continuum model are computed assuming a pile group with hinged heads. This assumption is made to completely remove any contribution of the lateral mode of the piles. However, for the studied configurations, the rocking impedance of the group is mainly governed by the axial stiffness of the piles and, therefore, the results can be extended to groups with rotationally fixed pile heads.

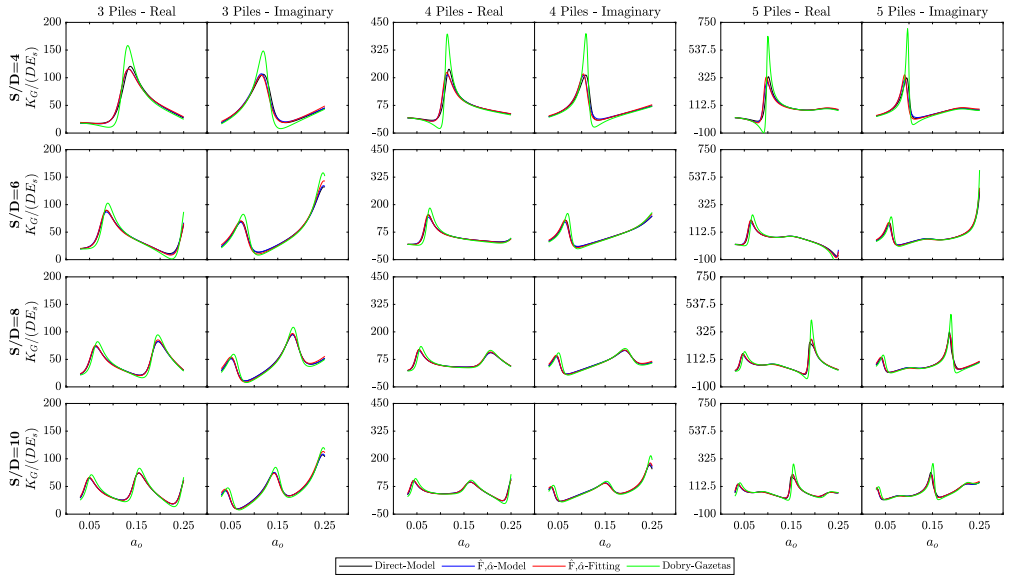

Fig. 5. Vertical group impedances for the reference case. (For interpretation of the references to colour in this figure legend, the reader is referred to the web version of this article.)

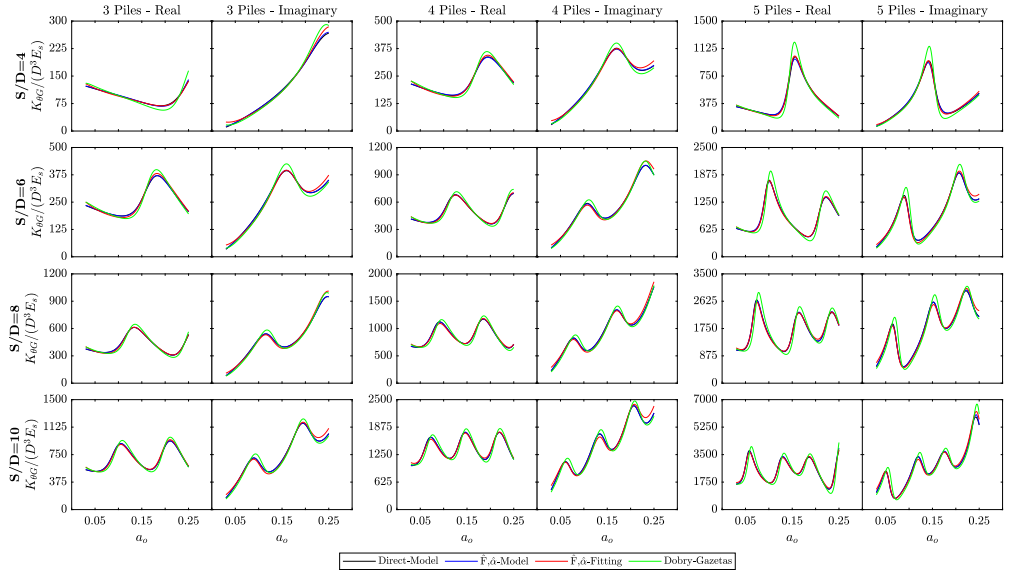

Fig. 6. Rocking group impedances for the reference case. (For interpretation of the references to colour in this figure legend, the reader is referred to the web version of this article.)

4.2. Inclusion of correction factors

As previously mentioned in Section 2.2, with the aim of including the dependency of more parameters in the expressions, some correction factors are also fitted to adjust the reference case expressions. To fulfil this objective, firstly, the influence of the pile slenderness, Young's Modulus ratios and the soil damping is studied for each correction factor. Once this influence is analysed, it is studied how well this correction factor reproduces the variation due to each parameter.

4.2.1. Correction factors for the vertical flexibilities of the source pile

To analyse the flexibilities of the source pile variation with respect to the reference case when some of the system parameters change, Fig. 7 represents the correction factor for the flexibility of the source pile (β_F) against the dimensionless frequency. Each row shows these correction factors for each analysed parameter: the pile slenderness ratio, the Young's Modulus pile–soil ratio and the soil damping. The real and imaginary components of these correction factors are presented in columns. Different colours are used to show the correction factors for diverse values of each parameter. In Fig. 7 it can be observed that the pile slenderness and the Young's Modulus ratios, have a remarkable

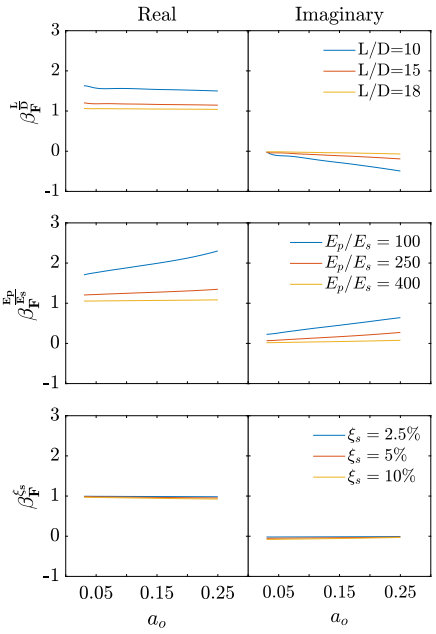

Fig. 7. Correction factors for the flexibility of the source pile against dimensionless frequency. (For interpretation of the references to colour in this figure legend, the reader is referred to the web version of this article.)

influence on the flexibility of the source pile as the results differ from those obtained for the reference case ($L/D = 20$ and $E_p/E_s = 500$). In terms of the soil damping there are no significant differences with respect to the reference case, both in the real and imaginary components. As regards the pile slenderness ratio influence, it can be seen that lower pile slenderness increases the flexibility, as the pile–soil interaction surface decreases. This is because the influence of the pile length on the dimensionless vertical dynamic flexibility of the pile is larger than that of the pile diameter. Besides, a phase difference is produced for low pile lengths as the frequency increases. Respecting the Young's Modulus ratio, low values (less pile stiffness with respect to the soil one) imply higher flexibilities and phase differences in the entire frequency range.

In Table 3 the correction factor fits for the flexibilities of the source pile are presented. The expressions are fitted in terms of the dimensionless frequency and the parameter that each correction factor adjusts. All fits are multivariate polynomial expressions of degrees 1 and 2 (for the pile slenderness ratio and soil damping correction factors) and 1 and 3 (for the Young's Modulus pile–soil correction factor). According to the metrics presented in Table 3, all fitted expressions present a high level of accuracy for reproducing the model's results. Although the variation of the correction factor for the flexibility of the source pile in terms of the soil damping is very small (see Fig. 7), this correction factor is also fitted, since the assumption of not rectifying the flexibility of the source pile with the variation of this parameter affects in a significantly way the results when the soil damping is greater than 5% (this fact will be shown and commented in Section 4.2). All expressions are obtained evaluating their simplicity and accuracy of the fits.

4.2.2. Interaction correction factors

In Fig. 8 the interaction correction factor for each parameter P is presented versus the dimensionless frequency. The interaction correction factors for the pile slenderness ratio are depicted in the firsts two columns (real and imaginary part), in which the results corresponding to a ratio of 10, 15 and 18 are arranged in the first, second and third rows respectively. In the following two columns the interaction correction factors for the Young's Modulus ratio are shown, for values of 100, 250 and 400 in each row. Finally, the interaction correction factors corresponding to the soil damping are represented in the last two columns, for soil dampings of 2.5, 5 and 7.5%. Different colours are used to distinguish the correction factors for different pile spacing ratios. In Fig. 8 it can be observed that the interaction correction factors for the pile slenderness, Young's Modulus ratios and soil dampings, show a considerable dependency of the dimensionless frequency and pile spacing ratio, except for large pile slenderness and Young's Modulus ratios and the imaginary component of pile damping correction factor. Furthermore, the variation of the soil damping interaction correction factor with the dimensionless frequency and the pile separation is uniform, however, for the pile slenderness and Young's Modulus ratios it is not. This fact can be seen for the smaller values of the pile slenderness and Young's Modulus ratios, where the variation of the interaction correction factor is not uniform with the frequency, above all for larger pile spacing ratios.

In Table 4 the fitted expressions obtained for the interaction correction factor of each parameter are shown. On the one hand, the correction factors for the pile slenderness and Young's Modulus ratios are fitted in terms of the dimensionless frequency and the parameter that is rectified. The pile spacing dependency is not directly included as a variable in theses expressions, but it is implicitly within them, because the results corresponding to each pile spacing are used to obtain the expressions. On the other hand, the soil damping correction factor is fitted in terms of the product of the dimensionless frequency and pile spacing ratio, and the soil damping. Thus, the dimensionless frequency, pile spacing ratio and soil damping dependency is explicitly reproduced within the soil damping interaction correction factor. The expressions of the pile slenderness and Young's Modulus correction factors were also attempted to be fitted in terms of this product, but they led to worse results. All fits are multivariate polynomial functions of up 2 degrees. However, the arguments of the interaction correction factor for the Young's Modulus ratio and soil damping are not considered, since their fittings turned out to give superficial functions very close to zero, so this assumption allows to simplify the expressions leading to similar results. The characteristics of these fits are inferior to those described previously (reference case and correction factor fits for the flexibilities of the source pile, Tables 2 and 3), especially for the pile slenderness and Young's Modulus ratios, because the pile spacing dependency is not directly reproduced in these expressions.

4.2.3. Vertical and rocking impedances

In order to analyse how these correction factors (both for the flexibility of the source pile and interaction factor) allow to adjust the reference case, this section is organised as follows: Firstly, it is studied how each correction factor fixes the variation of its respective parameter, this is done by only varying the parameter that is analysed maintaining the others with the reference case values; finally, some cases in which all parameters are modified at the same time are analysed. For simplification purpose, only the results corresponding to the 4-pile group are shown, for the 3 and 5-pile groups, similar conclusions are obtained.

– **Influence of pile slenderness ratio**

Fig. 9 shows the dimensionless vertical impedances of a 4-pile group for different pile spacing ($S/D = 4, 6, 8$ and 10) and pile slenderness ratios ($L/D = 10, 15$ and 18) against the dimensionless frequency. In these results only the pile slenderness and pile spacing ratios are varied, all other parameters are kept invariant adopting the values of the reference case ($E_p/E_s = 500$ and $\xi_s = 1\%$). Results for each pile spacing and pile slenderness ratio are arranged by rows and pair of columns respectively. At the first column of each pair the real component is presented while in the second one the imaginary part. With different

Table 3
Fitted expressions of the correction factors for the flexibilities of the source pile.

Fitted expression	Fitting parameters		Fitting characteristics	
$\mathrm{Abs}(\beta_F^{\frac{L}{D}}(a_o,\frac{L}{D})) = p_{00} + p_{10}a_o + p_{01}\frac{L}{D} + p_{11}a_o\frac{L}{D} + p_{02}\left(\frac{L}{D}\right)^2$	p_{00}	3.05	SSE	$1.98\cdot10^{-1}$
	p_{10}	$-1.91\cdot10^{-1}$	R^2	$9.98\cdot10^{-1}$
	p_{01}	$-1.93\cdot10^{-1}$	$RMSE$	$9.00\cdot10^{-3}$
	p_{11}	$6.55\cdot10^{-3}$		
Multivariate polynomial of 1 and 2 degrees	p_{02}	$4.55\cdot10^{-3}$		
$\mathrm{Arg}(\beta_F^{\frac{L}{D}}(a_o,\frac{L}{D})) = p_{00} + p_{10}a_o + p_{01}\frac{L}{D} + p_{11}a_o\frac{L}{D} + p_{02}\left(\frac{L}{D}\right)^2$	p_{00}	$5.48\cdot10^{-2}$	SSE	$1.89\cdot10^{-2}$
	p_{10}	-2.54	R^2	$9.99\cdot10^{-1}$
	p_{01}	$-7.26\cdot10^{-3}$	$RMSE$	$2.80\cdot10^{-3}$
	p_{11}	$1.27\cdot10^{-1}$		
Multivariate polynomial of 1 and 2 degrees	p_{02}	$2.26\cdot10^{-4}$		
$\mathrm{Abs}(\beta_F^{\frac{E_p}{E_s}}(a_o,\frac{E_p}{E_s})) = p_{00} + p_{10}a_o + p_{01}\frac{E_p}{E_s} + p_{11}a_o\frac{E_p}{E_s} + p_{02}\left(\frac{E_p}{E_s}\right)^2 + p_{12}a_o\left(\frac{E_p}{E_s}\right)^2 + p_{03}\left(\frac{E_p}{E_s}\right)^3$	p_{00}	2.98	SSE	7.49
	p_{10}	5.50	R^2	$9.90\cdot10^{-1}$
	p_{01}	$-1.75\cdot10^{-2}$	$RMSE$	$5.83\cdot10^{-2}$
	p_{11}	$-2.76\cdot10^{-2}$		
	p_{02}	$5.39\cdot10^{-5}$		
	p_{12}	$3.42\cdot10^{-5}$		
Multivariate polynomial of 1 and 3 degrees	p_{03}	$-5.42\cdot10^{-8}$		
$\mathrm{Arg}(\beta_F^{\frac{E_p}{E_s}}(a_o,\frac{E_p}{E_s})) = p_{00} + p_{10}a_o + p_{01}\frac{E_p}{E_s} + p_{11}a_o\frac{E_p}{E_s} + p_{02}\left(\frac{E_p}{E_s}\right)^2 + p_{12}a_o\left(\frac{E_p}{E_s}\right)^2 + p_{03}\left(\frac{E_p}{E_s}\right)^3$	p_{00}	$1.82\cdot10^{-1}$	SSE	$1.05\cdot10^{-1}$
	p_{10}	$3.21\cdot10^{-1}$	R^2	$9.93\cdot10^{-1}$
	p_{01}	$-4.78\cdot10^{-4}$	$RMSE$	$6.90\cdot10^{-3}$
	p_{11}	$3.41\cdot10^{-3}$		
	p_{02}	$-1.07\cdot10^{-6}$		
	p_{12}	$-8.52\cdot10^{-6}$		
Multivariate polynomial of 1 and 3 degrees	p_{03}	$2.73\cdot10^{-9}$		
$\mathrm{Abs}(\beta_F^{\xi_s}(a_o,\xi_s)) = p_{00} + p_{10}a_o + p_{01}\xi_s + p_{11}a_o\xi_s + p_{02}\xi_s^2$	p_{00}	1.00	SSE	$9.87\cdot10^{-4}$
	p_{10}	$2.48\cdot10^{-2}$	R^2	$9.99\cdot10^{-1}$
	p_{01}	$-3.02\cdot10^{-3}$	$RMSE$	$7.05\cdot10^{-4}$
	p_{11}	$-3.22\cdot10^{-2}$		
Multivariate polynomial of 1 and 2 degrees	p_{02}	$-4.85\cdot10^{-5}$		
$\mathrm{Arg}(\beta_F^{\xi_s}(a_o,\xi_s)) = p_{00} + p_{10}a_o + p_{01}\xi_s + p_{11}a_o\xi_s + p_{02}\xi_s^2$	p_{00}	$1.61\cdot10^{-2}$	SSE	$2.40\cdot10^{-3}$
	p_{10}	$-4.14\cdot10^{-2}$	R^2	$9.99\cdot10^{-1}$
	p_{01}	$-1.54\cdot10^{-2}$	$RMSE$	$1.10\cdot10^{-3}$
	p_{11}	$3.56\cdot10^{-2}$		
Multivariate polynomial of 1 and 2 degrees	p_{02}	$1.33\cdot10^{-4}$		

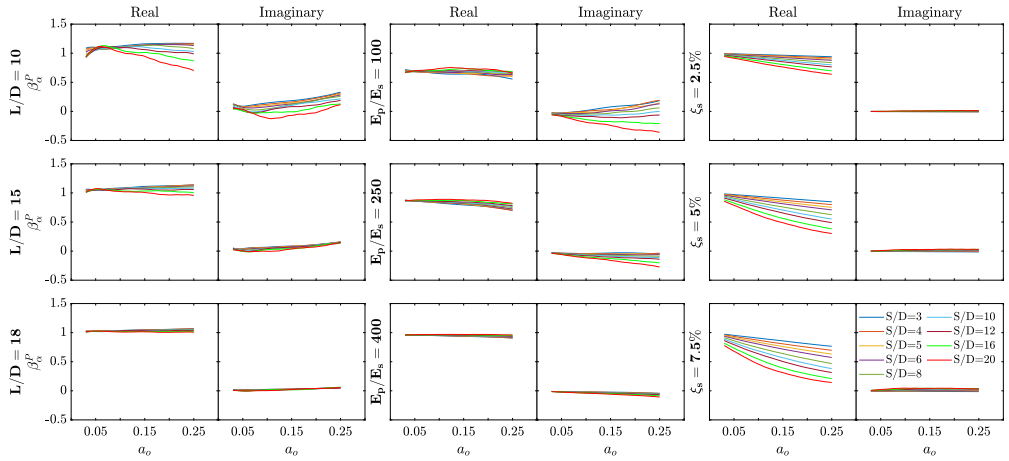

Fig. 8. Interaction correction factors against dimensionless frequency. (For interpretation of the references to colour in this figure legend, the reader is referred to the web version of this article.)

colours the following curves are presented: the impedances obtained through superposition of the flexibilities and interaction factors of the fitted expressions (red curve, F, α-Fitting); those computed by using the flexibilities and interaction factors of the model (blue curve, F, α-Model); the reference case impedances determined with their corresponding fits (green dashed curve, $\hat{\mathrm{F}}$, $\hat{\alpha}$-Fitting); and the impedances got by superimposing the fitted flexibilities of the source pile (adjusted through their correction factors) with the fitted interaction factors of the reference case (cyan dashed curve, F, $\hat{\alpha}$-Fitting). In Fig. 9 it can be observed that the impedances computed through the fitted interaction factors and flexibilities of the source pile agree well with the model ones. The biggest differences between these occur at the first peak of the impedances (both in the real and imaginary parts), in which the fitting peak is above of the model one (except the case with the

Table 4
Fitted expressions of the interaction correction factors.

Fitted expression	Fitting parameters		Fitting characteristics	
$\mathrm{Abs}(\beta_{a}^{\frac{L}{D}}(a_o, \frac{L}{D})) = \mathrm{p}_{00} + \mathrm{p}_{10}a_o + \mathrm{p}_{01}\frac{L}{D} + \mathrm{p}_{11}a_o\frac{L}{D} + \mathrm{p}_{02}\left(\frac{L}{D}\right)^2$	p_{00}	$9.21 \cdot 10^{-1}$	SSE	$5.06 \cdot 10$
	p_{10}	$9.45 \cdot 10^{-2}$	R^2	$2.75 \cdot 10^{-1}$
	p_{01}	$2.64 \cdot 10^{-2}$	$RMSE$	$4.81 \cdot 10^{-2}$
	p_{11}	$1.37 \cdot 10^{-3}$		
Multivariate polynomial of 1 and 2 degrees	p_{02}	$-1.17 \cdot 10^{-3}$		
$\mathrm{Arg}(\beta_{a}^{\frac{L}{D}}(a_o, \frac{L}{D})) = \mathrm{p}_{00} + \mathrm{p}_{10}a_o + \mathrm{p}_{01}\frac{L}{D} + \mathrm{p}_{20}a_o^2 + \mathrm{p}_{11}a_o\frac{L}{D}$	p_{00}	$2.23 \cdot 10^{-3}$	SSE	$1.95 \cdot 10$
	p_{10}	1.01	R^2	$7.15 \cdot 10^{-1}$
	p_{01}	$1.85 \cdot 10^{-3}$	$RMSE$	$2.98 \cdot 10^{-2}$
	p_{20}	2.54		
Multivariate polynomial of 2 and 1 degrees	p_{11}	$-8.35 \cdot 10^{-2}$		
$\mathrm{Abs}(\beta_{a}^{\frac{E_p}{E_s}}(a_o, \frac{E_p}{E_s})) = \mathrm{p}_{00} + \mathrm{p}_{10}a_o + \mathrm{p}_{01}\frac{E_p}{E_s} + \mathrm{p}_{11}a_o\frac{E_p}{E_s} + \mathrm{p}_{02}\left(\frac{E_p}{E_s}\right)^2$	p_{00}	$6.11 \cdot 10^{-1}$	SSE	$3.08 \cdot 10$
	p_{10}	$-1.23 \cdot 10^{-2}$	R^2	$8.93 \cdot 10^{-1}$
	p_{01}	$1.03 \cdot 10^{-3}$	$RMSE$	$3.94 \cdot 10^{-2}$
	p_{11}	$-5.04 \cdot 10^{-4}$		
Multivariate polynomial of 1 and 2 degrees	p_{02}	$-3.12 \cdot 10^{-7}$		
$\mathrm{Arg}(\beta_{a}^{\frac{E_p}{E_s}}(a_o, \frac{E_p}{E_s})) = 0$				
$\mathrm{Abs}(\beta_{a}^{\xi_s}(a_o\frac{S}{D}, \xi_s)) = \mathrm{p}_{00} + \mathrm{p}_{10}a_o\frac{S}{D} + \mathrm{p}_{01}\xi_s + \mathrm{p}_{20}(a_o\frac{S}{D})^2 + \mathrm{p}_{11}a_o\frac{S}{D}\xi_s$	p_{00}	1.08	SSE	$2.71 \cdot 10$
	p_{10}	$-8.54 \cdot 10^{-2}$	R^2	$9.68 \cdot 10^{-1}$
	p_{01}	$-1.66 \cdot 10^{-2}$	$RMSE$	$3.89 \cdot 10^{-2}$
	p_{20}	$1.98 \cdot 10^{-2}$		
Multivariate polynomial of 2 and 1 degrees	p_{11}	$-2.41 \cdot 10^{-2}$		
$\mathrm{Arg}(\beta_{a}^{\xi_s}(a_o\frac{S}{D}, \xi_s)) = 0$				

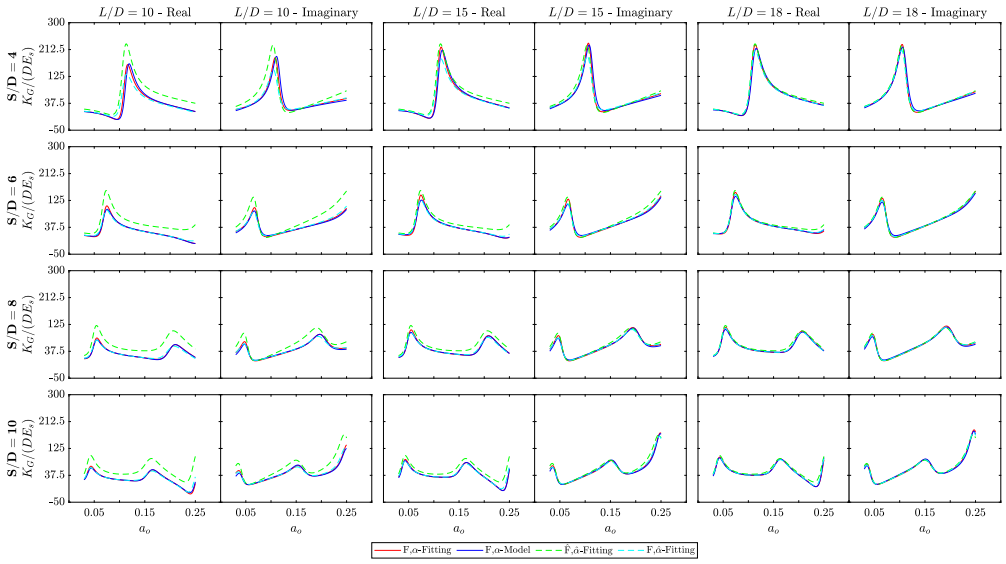

Fig. 9. Vertical 4-pile group impedances for different pile slenderness ratios. (For interpretation of the references to colour in this figure legend, the reader is referred to the web version of this article.)

lowest pile separation and slenderness ratios, $S/D = 4$ and $L/D = 10$). This difference tends to decrease when the pile slenderness and spacing ratios increase. Furthermore, the variations that are produced with the change of the pile slenderness ratio are correctly reproduced with the fits. This fact can be observed when the reference case curve (green dashed lines) is compared with the results corresponding to the pile slenderness variation (continuous lines), especially for the lowest pile slenderness ratio. Note that if the interaction factor expression proposed by Dobry and Gazetas [11] (see Eq. (20)) were used, similar results would be computed for the different pile slenderness ratios, as the expression does not depend on this ratio. Although the pile spacing ratio has not been included as a variable in the fitted expressions of the correction factor, the variation in the results produced by the alteration of the pile spacing ratio is properly reproduced by adjusting the fitted expression of the reference case. Despite the interaction correction factor fits of the pile slenderness ratio have low goodness characteristics (see Table 4), the fitting results match well with the model ones. This is because the flexibility of the source pile (that it is better fitted (see Table 3) has a greater impact on the total dynamic response than the interaction factor). This fact can also be seen when only the flexibility of the source pile is rectified with its correction factors (cyan dashed line), where for separations larger than four times the pile diameter, similar results between this assumption and the superposition of the model flexibilities and interaction factors are obtained. Thus, the contribution of the adjustment of the flexibility of the source pile is quite bigger than the interaction factor one. For the lowest value

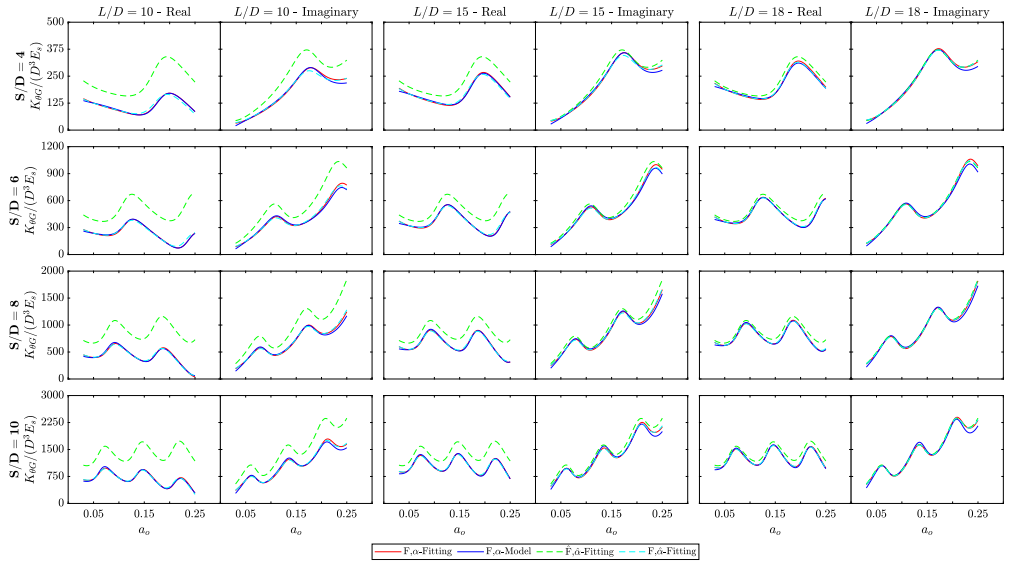

Fig. 10. Rocking 4-pile group impedances for different pile slenderness ratios. (For interpretation of the references to colour in this figure legend, the reader is referred to the web version of this article.)

of the pile spacing ratio it can be observed a phase difference and a considerable difference between this assumption and the model results at the peak impedances, this is due to the greater relevance of pile–pile interaction as the pile spacing ratio decreases.

Fig. 10 shows the dimensionless rocking impedances versus the dimensionless frequency, for different pile slenderness and pile spacing ratios and for the 4-pile group. Results are arranged in the same way as used for the vertical impedances (Fig. 9). The rocking impedances obtained with the superposition of the flexibilities and interaction factors of the proposed expressions match very well with those superimposed with the model flexibilities and interaction factors. In this case, the main differences between the fitting and model results occur at the larger frequencies ($a_o \geq 0.20$) and in the imaginary component, giving slightly greater results the impedances obtained with the fitted expressions. Moreover, the rocking impedances show a greater dependency of the pile slenderness and pile spacing ratios. Note how the differences observed with respect to the reference case are greater than those obtained in the vertical impedances. For these rocking impedances, the assumption of only rectifying the flexibility of the source pile leads to good results, even for the smallest pile spacing ratio. Both in the vertical and rocking impedances, the dynamic vertical group response rises with the increase of the pile slenderness ratio.

– **Influence of Young's Modulus ratio**

In the same way as previously made for analysing the pile slenderness variation (Figs. 9 and 10), Figs. 11 and 12 show the dimensionless vertical and rocking impedances for different Young's Modulus ($E_p/E_s = 100, 250$ and 500) and pile spacing ratios ($S/D = 4, 6, 8$ and 10), maintaining all other parameters invariant with the values of the reference case ($L/D = 20$ and $\xi_s = 1\%$). The results are presented in the same way that it was exposed for the pile slenderness ratio, showing the impedances for several Young's Modulus ratios in pairs of columns. The vertical impedances obtained through the fitted interaction factors and flexibilities of the source pile align well with the results obtained from the model (see Fig. 11). Only at intermediate Young's Modulus ratios ($E_p/E_s = 100$ and 250) some differences at the first peak and high dimensionless frequencies appear. As it can be observed, the assumption of not considering a correction factor for the argument of the interaction factor in the Young's Modulus ratio practically does not affect the results. As in the previous case (variation of pile slenderness ratio), the alteration due to the Young's Modulus ratio is well captured without adding the pile spacing ratio as a variable in the interaction correction factor fit. Besides, it can be seen that there is a considerable influence of the Young's Modulus ratio in the final results, above all for the lower values of this ratio, in which significant differences can be appreciated comparing the reference case (green dashed line) with the continuous lines. This variation could not be reproduced with the interaction factor expression suggested by Dobry and Gazetas [11] (see Eq. (20)), since this one does not depend on the Young's Modulus ratio. In this case, more differences appear when only the flexibility of the source pile is adjusted with the correction factors (cyan dashed line). These differences can be seen for the lower pile spacing and Young's Modulus ratios, especially, at the first peak, in which a magnitude and phase difference with respect to the continuous lines can be observed. For the rocking impedances (Fig. 12) more differences between the fitting and model curves can be observed, particularly for the higher values of the pile spacing and Young's Modulus ratios, even so the impedances obtained with the fits are quite close to the model ones. When only the adjustment of the flexibility is considered through its correction factors, good results are obtained, although some discrepancies can be seen for the lowest pile spacing and Young's Modulus ratios. What is more, for both the vertical and rocking impedances, larger values of impedances are obtained as the Young's Modulus pile–soil ratio increases.

– **Influence of soil damping**

The dimensionless vertical and rocking impedances of the 4-pile group for different soil dampings ($\xi_s = 2.5, 5$ and 7.5%) and pile spacing ratios ($S/D = 4, 6, 8$ and 10) are depicted in Figs. 13 and 14 respectively, the other parameters are kept invariant with the values of the reference case ($L/D = 20$ and $E_p/E_s = 500$). Results are shown in the same disposal than the previously used for the pile slenderness and Young's Modulus ratios, but now each pair of columns presents the impedances for each soil damping. Similar conclusions than the previously commented for the pile slenderness and Young's Modulus ratios are also drawn for the soil damping variation: the impedances computed with the fitted interaction factors and flexibilities of the source pile match very well with those of the model in both the vertical

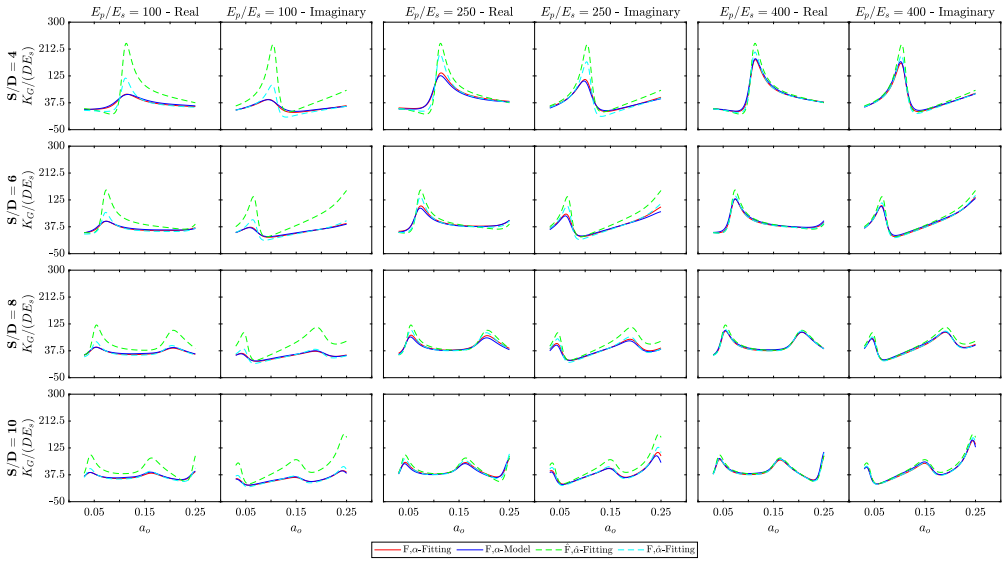

Fig. 11. Vertical 4-pile group impedances for different Young's Modulus ratios. (For interpretation of the references to colour in this figure legend, the reader is referred to the web version of this article.)

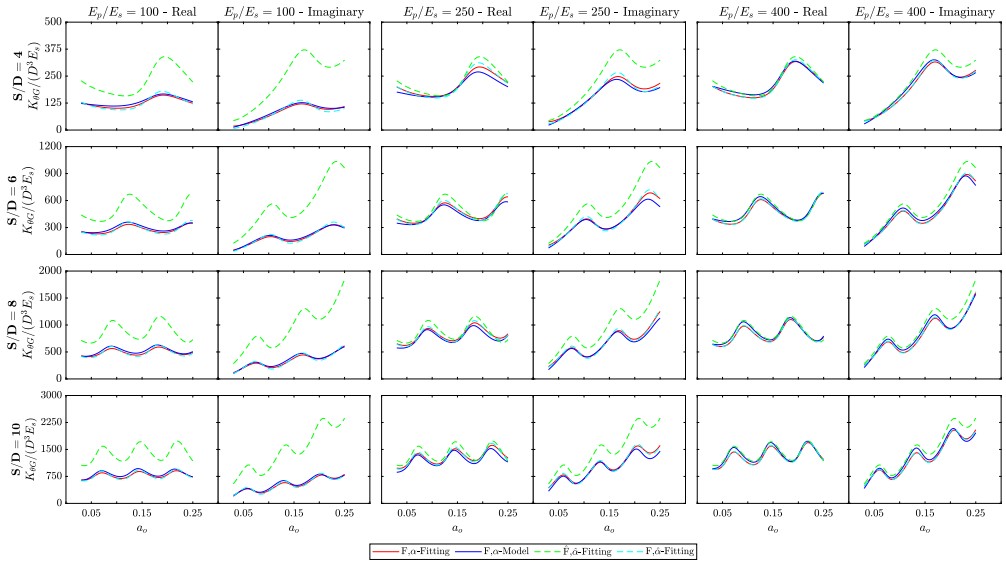

Fig. 12. Rocking 4-pile group impedances for different Young's Modulus ratios. (For interpretation of the references to colour in this figure legend, the reader is referred to the web version of this article.)

and rocking impedances. The larger differences between these two are produced at the first vertical impedance peak and at the highest frequencies in the imaginary component of the rocking impedances. As it can be observed the variation of the soil damping does not significantly affect the vertical and rocking impedances for soil dampings lower than 5%. Nonetheless, for damping values higher than 5%, there are significant differences between the peaks of the reference curve and the peaks of the other curves. The assumption of only considering the correction factors for the flexibility of the source pile allows to obtain good impedances, except for the smallest pile spacing ratio and the soil dampings larger or equal to 5%. For these cases, the contribution of the interaction factor rectification is considerable in order to correctly reproduce the impedance peaks and the frequencies at they occur. Moreover, greater vertical and rocking dynamic impedances are obtained as the soil damping drops off. This fact is due to the attenuation of the pile–pile interaction produced by the increase of the soil damping.

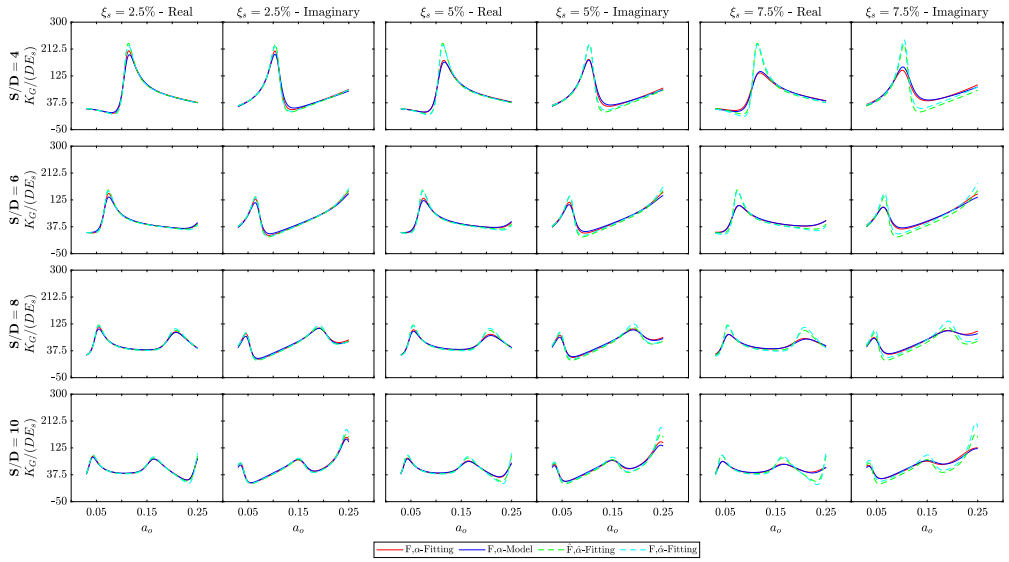

Fig. 13. Vertical 4-pile group impedances for different soil dampings. (For interpretation of the references to colour in this figure legend, the reader is referred to the web version of this article.)

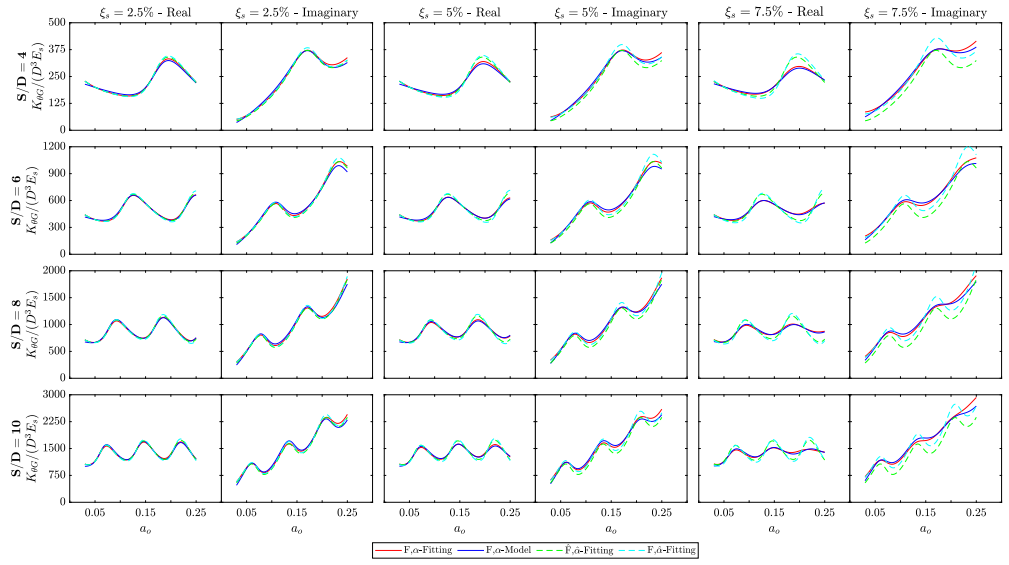

Fig. 14. Rocking 4-pile group impedances for different soil dampings. (For interpretation of the references to colour in this figure legend, the reader is referred to the web version of this article.)

– **Variation of the three parameters**

Figs. 15 and 16 show the dimensionless vertical and rocking impedances of the 4-pile group against the dimensionless frequency for three different parameter configurations, where the pile slenderness, Young's Modulus ratios and soil dampings are modified at the same time. Specifically, the three studied configurations are: $L/D = 14$, $E_p/E_s = 100$, and $\xi_s = 2\%$; $L/D = 16$, $E_p/E_s = 200$, and $\xi_s = 4\%$; and $L/D = 18$, $E_p/E_s = 400$, and $\xi_s = 5\%$. The results for each configuration are disposed by pair of columns, where the real and imaginary components are represented in the first and second column respectively. The impedances for three different pile spacing ratios ($S/D = 6, 8$ and 10) are arranged by rows. The same curve colours and line traces than those previously used are employed to distinguish the results of the fits and the model. As it is shown, in the first configuration (firsts two columns of Figs. 15 and 16), the fitting and model continuous curves are a little separated from each other, especially for the rocking stiffness (real component) and for the larger pile spacing ratios. Nevertheless, the curve shape is correctly reproduced by using the fitted expressions of the flexibilities of the source pile and interaction factors. Note that this first set of parameters is the furthest from the reference case in terms of pile slenderness and Young's Modulus ratios. However, for the second and third parameter configurations, in which the pile slenderness and Young's Moudulus ratios are nearer to the reference case, the fitting

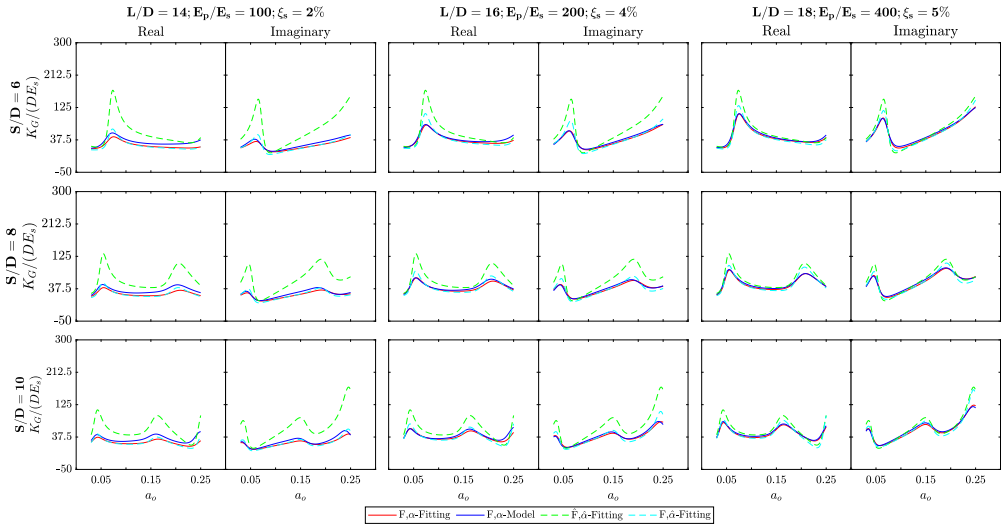

Fig. 15. Vertical 4-pile group impedances for different parameter configurations. (For interpretation of the references to colour in this figure legend, the reader is referred to the web version of this article.)

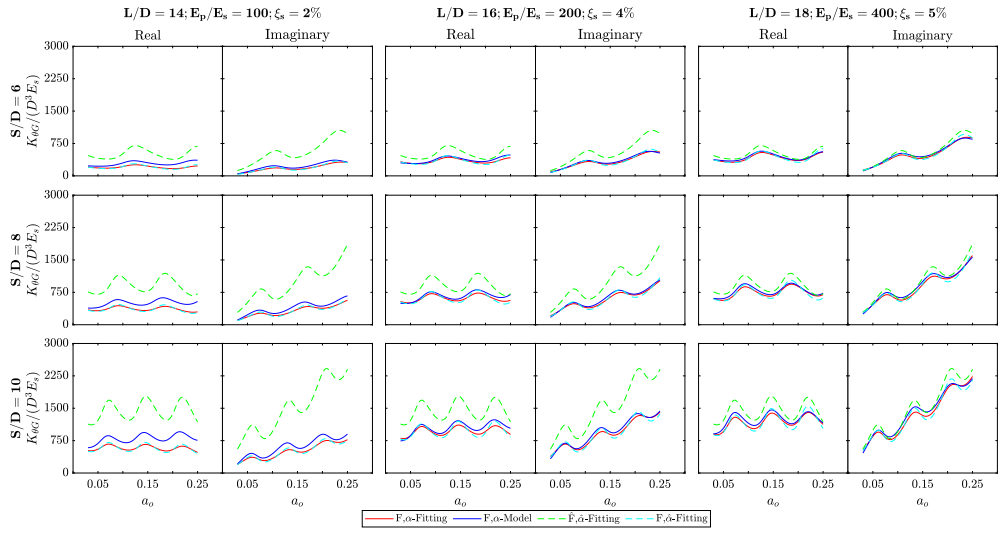

Fig. 16. Rocking 4-pile group impedances for different parameter configurations. (For interpretation of the references to colour in this figure legend, the reader is referred to the web version of this article.)

and model impedances give similar results, both in the vertical and rocking impedances. The impedances computed through the fitted interaction factors and flexibilities of the source pile are commonly lower than those of the model at the entire dimensionless frequency range. For large pile spacing ratios and in the rocking impedances, more differences can be appreciated. Nonetheless, fits generally reproduce well the variation of the group impedances of the reference case. When only the flexibility of the source pile is rectified with the correction factors, it can be seen relevant discrepancies in the peaks of the vertical impedances. These differences are lower in the rocking impedances, but they are noticeable in the two last configurations, which are those that have a greater soil damping.

5. Conclusions

This paper studies the interaction factor superposition method for pile groups of jacket-supported OWTs. The results obtained from this method are compared with those computed by a previously developed continuum model [8]. Ready-to-use expressions are proposed by performing curve fittings for the flexibilities of the source pile and interaction factors directly determined with the continuum model for a wide variety of jacket pile groups parameters. The influence of the dimensionless frequency, pile separation ratio, pile slenderness ratio, Young's Modulus ratios and soil damping is studied and included in the expressions. The validity of these expressions are analysed throughout the work. The following conclusions are drawn:

- The interaction factor superposition method correctly reproduces the vertical and rocking group impedances for the regular pile configurations characteristic of jacket foundations. Thus, for this type of pile groups with large pile spacing ratios, the assumption of only considering the interaction between pile pairs and neglecting the interplay of the other surrounding piles allow to reproduce in a accurately and easily way the dynamic group response. This last consideration is totally fulfilled for pile spacings equal or higher than six times the pile diameter. For lower pile spacings, the rest of piles starts to affect the interaction among the pair of piles, producing differences between the rigorous model and the superposition method.
- Apart from the influence of the dimensionless frequency and separation ratio, the effect of the pile slenderness, Young's Modulus ratios and soil hysteretic damping can be significant in the determination of the impedance functions. The influence of these parameters can be reproduced with the use of correction factors that adapt the flexibilities of the source pile and interaction factors of a reference case. Results obtained with the proposed fitted expressions and correction factors generally reproduce well the dynamic behaviour of pile groups for jacket-supported OWTs. When only one parameter is modified from the reference case, the impedances computed by superimposing the fitted interaction factors and flexibilities of the source pile match quite well with those obtained through the flexibilities and interaction factors of the continuum model. When all parameters are changed at once, greater differences between the results determined with the model and those calculated with the fitted expressions are obtained. Especially when the pile slenderness and Young's Modulus ratios are far from the reference case values ($L/D = 20$ and $E_p/E_s = 500$). However, these differences are acceptable and the curve shape is properly reproduced.
- The assumption of only adjusting the flexibility of the source pile with the proposed correction factors can lead to admissible vertical and rocking impedances. The rocking impedances obtained with this simplification are generally acceptable. Nevertheless, for low values of pile spacing and Young's Modulus ratios, as well as for large values of soil dampings, omitting the influence of these parameters on the interaction factors can lead to significant differences in the vertical impedances, especially in their peak values.

Thus, the dynamic vertical response of jacket pile groups can be estimated applying the interaction factor superposition method and the proposed expressions. The use of this method and the proposed expressions are useful since they can be employed without the need to execute a rigorous model, allowing to obtain the vertical and rocking impedances in a faster and simpler way. These impedances could subsequently be used to reproduce the soil–structure interaction of these type of structures. As future developments it is proposed to carry out a similar work but analysing the horizontal and rocking-horizontal dynamic behaviour of jacket pile groups. Additionally, this study can be extended to more complex soils, such as stratified or saturated soils. Furthermore, it could be interesting to evaluate the superposition method by employing more complex techniques, such as machine learning, that could improve the proposed expressions. For instance, artificial neural networks combined with the proposed superposition procedure could result in more accurate impedance functions. Artificial networks could be used to predict the own vertical flexibilities and interaction factors, considering all relevant soil and pile variables at once. Then, the impedance functions would be computed applying elastic superposition.

CRediT authorship contribution statement

Eduardo Rodríguez-Galván: Writing – original draft, Visualization, Software, Methodology, Conceptualization. **Guillermo M. Álamo:** Writing – review & editing, Supervision, Software, Conceptualization. **Juan J. Aznárez:** Writing – review & editing, Supervision, Funding acquisition, Conceptualization. **Orlando Maeso:** Writing – review & editing, Supervision, Conceptualization.

Declaration of competing interest

The authors declare that they have no known competing financial interests or personal relationships that could have appeared to influence the work reported in this paper.

Acknowledgements

This research has been funded by Ministerio de Ciencia e Innovación and Agencia Estatal de Investigación (MCIN/AEI/10.13039/501100011033) of Spain through research project PID2020-120102RBI00 and predoctoral research scholarship PRE2021-099200 (E. Rodríguez-Galván), also funded by FSE+. This research has been partially supported by ACIISI, Spain-Gobierno de Canarias and European FEDER Funds Grant EIS 2021 04.

Data availability

Data will be made available on request.

References

[1] Council GWE. Global offshore wind report 2023. Brussels, Belgium: GWEC 2023.
[2] Musial W, Spitsen P, Duffy P, Beiter P, Shields M, Mulas Hernando D, Hammond R, Marquis M, King J, Sathish S. Offshore wind market report: 2023 edition. Tech. rep., National Renewable Energy Laboratory (NREL), Golden, CO (United States); 2023.
[3] Jalbi S, Bhattacharya S. Concept design of jacket foundations for offshore wind turbines in 10 steps. Soil Dyn Earthq Eng 2020;139:106357.
[4] Kaynia AM. Dynamic stiffness and seismic response of pile groups (Ph.D. thesis), Massachusetts Institute of technology; 1982.
[5] Kaynia AM, Kausel E. Dynamics of piles and pile groups in layered soil media. Soil Dyn Earthq Eng 1991;10(8):386–401.
[6] Dezi F, Carbonari S, Leoni G. A model for the 3D kinematic interaction analysis of pile groups in layered soils. Earthq Eng Struct Dyn 2009;38(11):1281–305.
[7] Dezi F, Carbonari S, Morici M. A numerical model for the dynamic analysis of inclined pile groups. Earthq Eng Struct Dyn 2016;45(1):45–68.
[8] Álamo GM, Martínez-Castro AE, Padrón LA, Aznárez JJ, Gallego R, Maeso O. Efficient numerical model for the computation of impedance functions of inclined pile groups in layered soils. Eng Struct 2016;126:379–90.
[9] Wang P, Huang Y, Zhao M, Cheng X, Du X. Analytical solution for simplifying the pile-soil interaction to a spring-damping system under horizontal vibration. Soils Found 2024;64(3):101469.
[10] Poulos HG. Analysis of the settlement of pile groups. Geotech 1968;18(4):449–71.
[11] Dobry R, Gazetas G. Simple method for dynamic stiffness and damping of floating pile groups. Geotech 1988;38(4):557–74.
[12] Gazetas G, Makris N. Dynamic pile-soil-pile interaction. Part I: Analysis of axial vibration. Earthq Eng Struct Dyn 1991;20(2):115–32.
[13] Mylonakis G, Gazetas G. Settlement and additional internal forces of grouped piles in layered soil. Geotech 1998;48(1):55–72.
[14] Makris N, Gazetas G. Dynamic pile-soil-pile interaction. Part II: Lateral and seismic response. Earthq Eng Struct Dyn 1992;21(2):145–62.
[15] Rotta Loria AF, Laloui L. The interaction factor method for energy pile groups. Comput Geotech 2016;80:121–37.
[16] Gazetas G, Fan K, Kaynia AM. Dynamic response of pile groups with different configurations. Soil Dyn Earthq Eng 1993;12(4):239–57.
[17] Torshizi MF, Saitoh M, Álamo GM, Goit CS, Padrón LA. Influence of pile radius on the pile head kinematic bending strains of end-bearing pile groups. Soil Dyn Earthq Eng 2018;105:184–203.
[18] Zheng C, Cui Y, Kouretzis G, Luan L. Scattered wave effects on the vertical dynamic response of pile groups embedded in layered soil. Comput Geotech 2023;158:105361.
[19] Sales MM, Curado TS. Interaction factor between piles: limits on using the conventional elastic approach in pile group analysis. Soil. Rocks 2018;41(1):49–60.
[20] Mylonakis G. Contributions to static and seismic analysis of piles and pile-supported bridge piers. State University of New York at Buffalo; 1995.

[21] Abhinav KA, Saha N. Coupled hydrodynamic and geotechnical analysis of jacket offshore wind turbine. Soil Dyn Earthq Eng 2015;73:66–79.
[22] Jalbi S, Bhattacharya S. Closed form solution for the first natural frequency of offshore wind turbine jackets supported on multiple foundations incorporating soil-structure interaction. Soil Dyn Earthq Eng 2018;113:593–613.
[23] Plodpradit P, Dinh VN, Kim K-D. Coupled analysis of offshore wind turbine jacket structures with pile-soil-structure interaction using FAST v8 and X-SEA. Appl Sci 2019;9(8):1633.
[24] Romero-Sánchez C, Padrón LA. Influence of wind and seismic ground motion directionality on the dynamic response of four-legged jacket-supported Offshore Wind Turbines. Eng Struct 2024;300:117191.
[25] Quevedo-Reina R, Álamo GM, François S, Lombaert G, Aznárez JJ. Importance of the soil–structure interaction in the optimisation of the jacket designs of offshore wind turbines. Ocean Eng 2024;303:117802.
[26] Álamo GM, Bordón JDR, Aznárez JJ. On the application of the beam model for linear dynamic analysis of pile and suction caisson foundations for offshore wind turbines. Comput Geotech 2021;134:104107.
[27] API RP 2A-WSD. Recommended practice for planning, designing and constructing fixed, offshore plaftorms - working stress design. American Petroleum Institute.

3. Summary, conclusions, and future research directions

3.1 Summary and conclusions
3.2 Future research directions

3.1 Summary and conclusions

This PhD thesis aims to contribute to a better understanding of some unexplored aspects related to the SSI modelling and their influence on the seismic response of OWT pile foundations. In order to achieve this and obtain useful and general conclusions, three exhaustive parametric studies have been carried out:

Initially, the influence of the seabed profile definition on the seismic response of monopile-supported OWTs is studied [54]. The SSI effects are analysed for each seabed profile typology, examining the inertial and kinematic interaction contributions within SSI. One homogeneous and two non-homogeneous soil profiles with equivalent shear-wave velocities from 100 to 300 m/s are evaluated, representing soft to medium seabed stiffnesses. The seismic response of four monopile-supported OWTs from 5 to 15 MW embedded in all these seabed profiles are studied. The seismic response is computed by employing a finite element substructuring model in frequency domain, where the foundation-soil behaviour is reproduced by impedance functions and kinematic interaction factors, obtained by a previously developed continuum model [45]. The earthquake excitation is simulated by considering planar S-waves vertically propagating through the soil, producing a free-field lateral displacement at ground level. Ten different earthquakes are used to determine the system seismic response, which is quantified in terms of mean maximum bending moments and shear forces, and mean acceleration amplification factors at the rotor height. Several submodels together with the fixed base assumption are defined in order to quantify the SSI effects and the contribution of the kinematic and inertial interaction. Firstly, the foundation behaviour (impedance functions and kinematic interaction factors), and the natural frequencies of the 10 MW monopile-supported OWT for each seabed profile are analysed, by considering an equivalent-shear wave velocity of 200 m/s. Subsequently, its foundation behaviour in all considered soils and for the first and second vibration modes is examined. In this point it has been observed that the rotational motion is more influenced by deeper ground properties, while the lateral ground motion is more affected by shallower ones. Therefore, higher lateral impedances and rotational kinematic interaction factors are obtained for homogeneous equivalent soil profiles, whereas larger cross-coupled, rocking impedances, and lateral kinematic interaction factors are computed for non-homogeneous profiles. Thus, as the variation of the elastic properties of the soil is more significant, lower natural frequencies are determined. Secondly, the seismic responses obtained for each SSI submodel and soil profile are explored. From this point, it is concluded that the greatest seismic responses are produced when the overall SSI is considered (both the inertial and kinematic interactions). Furthermore, it is demonstrated the high relevance of including the rotational kinematic interaction factor within SSI. Finally, the influence of contemplating a homogeneous or non-homogeneous soil profile is evaluated. For this purpose, the relative differences of the seismic responses computed in the two non-homogenous soil profiles with respect to those of the homogeneous one are examined. Accordingly, it is concluded that homogeneous soil profiles leads to larger seismic responses than non-homogeneous ones, due to the influence of

the rotational kinematic interaction factor.

Afterwards, the non-linear and inelastic effects of soil-pile interaction on the seismic response of OWT pile foundations and monopile-supported OWTs are evaluated [55]. In this regard, three Beam on Dynamic Winkler Foundation models are assessed: a plastic non-linear model, an elastic non-linear model, and a linear model defined through non-degraded soil properties, which is taken as the reference one. The soil-pile interaction in all these BDWF models is defined by employing the soil resistance and deflection curves established by the API practices [49]. The non-linear and inelastic effects are examined through the analysis of kinematic and inertial interactions. Two types of sandy soils are examined: a very loose and medium dense sand soil, defined following the API recommendations. The finite element method is applied to compute the piles and OWTs seismic responses. The seismic excitation is simulated assuming planar harmonic S-waves vertically propagating throughout an elastic non-homogeneous half-space, which has a linear variation of soil properties with depth, producing a free-field lateral displacement at ground level. Ten different earthquakes scaled with respect to a maximum ground acceleration of 0.6g are used to compute the system seismic response. The seismic response is analysed in terms of mean maximum bending moments, shear forces, and accelerations envelopes. In addition, soil resistance envelopes are also studied to better understand the non-linear and inelastic effects. Firstly, the seismic response of different piles of OWTs, from large to small slendernesses are studied. Kinematic and inertial contributions are evaluated by considering different cap masses, which are established as a proportion δ (ranging from 0 to 1) of the ultimate axial bearing capacity of each pile. The mean maximum envelopes of the piles are analysed for the cases where the kinematic and inertial interaction predominate ($\delta = 0$ and $\delta = 1$, respectively). In addition, with the aim of determining the non-linear and inelastic effects, the relative differences of the maximum responses of the two non-linear model with respect to those of the linear one are evaluated. From this analysis, it is concluded that when the kinematic interaction prevails, similar results between models are obtained, whereas when the inertial interaction starts to be activated, differences between models can be observed. In any case, the non-degraded linear model conducts to higher seismic responses, followed by the elastic non-linear one. Lastly, the seismic response of three monopile-supported OWTs (from 5 to 15 MW) and their respective monopiles with a cap mass equivalent to the superstructure weight is studied for each BDWF model. It is observed that similar results between models are obtained, due to the superstructure mass is not enough to activate the inertial interaction effects in the studied cases.

Finally, the application of the superposition method to estimate the vertical and rocking impedance functions of OWT pile groups is evaluated by performing an extensive dimensionless parametric study [56]. In this third parametric study the contribution of the main parameters involved in the problem (frequency, pile and soil characteristics) are examined by using a wide range of realistic pile group configurations. Some expressions dependent of these dimensionless variables are fitted and proposed. The proposed expressions enable a simple and rapid determination of the

source pile flexibilities and interaction factors, without the requirement of executing any other advance solution. These expressions are based on a reference case scenario with several fitted correction factors, which allow for correcting the reference expressions taking into account the contribution of the different involved parameters. To carry out the fitting of these expressions, the source pile flexibilities and interaction factors are computed through a continuum model [45]. Once the source pile flexibilities and the interaction factors are obtained, the group impedances are determined by applying superposition. Firstly, the superposition method's applicability is evaluated for a reference case. For this purpose, the vertical and rocking impedance functions obtained applying superposition from the fitting expressions are compared to those directly computed through the direct continuum model, and with those determined applying superposition with the source flexibilities and interaction factors of the continuum model. Additionally, the impedance functions obtained by superimposing the interaction factors of the Dobry and Gazetas [36] expression are included. From this analysis it is concluded that the superposition method leads to accurate estimations of the vertical and rocking impedance functions for these pile groups, which are characterised by having large pile spacing ratios. Thus, the proposed expressions together with the superposition method can be used to correctly estimate the vertical and rocking impedance functions. Afterwards, the influence of the different parameters and the validity of their fitted correction factors are examined. It is shown that, in addition to the dimensionless frequency and pile separation ratio contributions, the other pile and soil characteristics might considerably affect the impedance function estimation. To reproduce the effects of these parameters, correction factors can be used over the reference case scenario. Finally, results indicate that the superposition method by using the fitted reference expressions together with the proposed correction factors generally conducts to good dynamic estimations, showing that the correction of the single pile flexibility term is more relevant than that of the pile-to-pile interaction factors.

To summarise, this PhD dissertation has explored some aspects related to SSI modelling and their influence on the seismic and dynamic response of OWT pile foundations. Some useful conclusions to model SSI and to address the design and seismic analysis of these structures have been reached. Among these conclusions the most notable ones are:

- Homogeneous soil profiles lead to more conservative results than non-homogeneous ones for monopile-supported OWTs, due to the great relevance of the rotational kinematic interaction factor within the SSI.
- A linear BDWF model defined through non-degraded soil properties can be used to reproduce the seismic response of OWT pile foundations and monopile-supported OWTs, since it leads to similar and more conservative results than non-linear BDWF models, as the kinematic interaction is the one that predominates within the SSI in this type of structures.
- The superposition method together with the proposed expressions can be applied

to estimate the vertical and rocking impedance functions for OWT pile groups.

All these main conclusions are valuable for the dynamic analysis and design of such structures, as they can simplify the initial design processes or the performing of parametric studies without significantly compromising result accuracy.

Further insights and a more in-depth analysis of the three exhaustive parametric analyses can be found in the respective publications (Chapter 2).

3.2 Future research directions

This section presents several potential directions for future research inspired by the findings of this PhD thesis. These suggestions are mainly based on deeping the exploration of non-linear effects in SSI modelling, which have been preliminarily addressed in the current work. The proposed future research directions are expected to make a meaningful contribution to the understanding and advancement of these effects. Based on the foundational work developed throughout this dissertation, the following research paths are suggested:

- The implementation of a non-linear model of soil for the computation of the free-field displacements under earthquake loading. In this way, the effects of considering a linear and non-linear behaviour of the soil response under seismic wave propagation could be assessed within different BDWF models.
- To develop BDWF models for multiple pile foundations. Thus, the study of the non-linear and inelastic effects of SSI could be addressed on pile group foundations. For this purpose, it might be convenient to first study the superposition method in the lateral behaviour of pile groups. This could provide a better understanding of the interaction factors or p-multipliers that can be applied to BDWF pile group models.
- The improvement of the developed BDWF models, for instance, the inclusion of the vertical behaviour ($t-z$ and $q-z$ curves), would be an interesting point of research to evaluate the non-linear and inelastic effects under inclined seismic waves. In addition, the implementation of $p-y$, $t-z$, $q-z$ curves associated for clay soils would allow further analysis of the non-linear and inelastic effects of SSI in other types of soils. Other interesting improvement would be the inclusion of the sliding or gap at soil-pile interface, thus, the influence of this phenomenon could be addressed.
- The inclusion of the developed BDWF models to more rigorous software capable of precisely simulating the coupled dynamic response of wind turbines, such as OpenFAST [58], which is a non-linear aero-hydro-servo code. This would allow to assess the non-linear effects of SSI taken into account the non-linear behaviour of all OWT components.

A. Resumen en castellano

A Resumen en castellano
A.1 Introducción
A.2 Objetivos
A.3 Publicaciones derivadas de la tesis doctoral
A.4 Justificación
A.5 Conclusiones

Título de la Tesis Doctoral: Avances en el modelado de la interacción suelo-estructura para el análisis sísmico de cimentaciones pilotadas de aerogeneradores marinos. Evaluación paramétrica de la heterogeneidad del suelo, comportamiento no lineal y efectos del grupo.

A.1 Introducción

Las cimentaciones pilotadas son extensamente utilizadas para soportar una gran variedad de estructuras civiles y marinas, como edificaciones, puentes y plataformas marinas. Su uso es particularmente ventajoso en situaciones donde el suelo superficial no tiene capacidad de carga suficiente, puesto que transmiten las cargas a estratos más profundos y resistentes. Su alta capacidad de carga vertical y horizontal, permitiendo reducir notablemente asentamientos, y su viabilidad en condiciones geológicas especiales, son alguna de las ventajas más destacables de este tipo de cimentaciones [1, 2].

Dentro del sector marino, las cimentaciones pilotadas fueron inicialmente empleadas para soportar estructuras de extracción de petróleo. No obstante, en los últimos años, debido a la transición que se está produciendo hacia un futuro energéticamente más sostenible, se han venido utilizando como cimentaciones para aerogeneradores marinos. Atendiendo a los recientes informes de energía eólica y eólica marina de 2025 ([3, 4], respectivamente), 8 nuevos GW de energía eólica marina fueron instalados en 2024, alcanzando una capacidad total de 83,2 GW, equivalente a la demanda eléctrica anual de 73 millones de hogares. Así, 2024 fue el cuarto mejor año en términos de potencia total instalada, siendo 2021, 2023 y 2022 los tres primeros con 21,1, 10,8 y 8,8 GW respectivamente. A pesar de la incertidumbre geopolítica global existente, se espera que esta tendencia positiva siga dándose durante los próximos años, tal y como sucedió después de la crisis derivada de la COVID-19.

Un componente crítico de todo aerogenerador marino es su subestructura (incluyendo su cimentación), que actúa como la conexión entre la turbina eólica y el lecho marino, permitiendo transferir las cargas ambientales, de peso propio, y operacionales al terreno subyacente. La elección de la subestructura está influenciada por diferentes condiciones, como la profundidad del agua, propiedades del lecho marino, dimensiones de la turbina, procedimientos de instalación, transporte y otros factores económicos. Atendiendo a todos estos aspectos existen diversas tipologías de subestructuras con diferentes características que las hacen compatibles con distintos escenarios. Principalmente, las subestructuras pueden clasificarse en dos grupos principales: las flotantes y las cimentadas directamente al lecho marino. Por una parte, las flotantes son adecuadas para grandes profundidades de agua, donde las fijadas al lecho marino no pueden ser instaladas (profundidades mayores a 60-70 m), sin embargo, estas subestructuras están aún en desarrollo, presentando altos costes. Por otra parte, las soluciones fijadas directamente al lecho marino son empleadas para profundidades menores (hasta 60-70 m).

Estas subestructuras fijadas al lecho marino son una tecnología mucho más madura, presentando unos costes totales generales mucho menores que las soluciones flotantes. Por todo esto, esta tipología es la que predomina dentro del sector (representando el 99 % de las subestructuras registradas en 2023, según el informe de mercado de energía eólica marina de 2024 [5]), y se espera que siga predominando en el futuro. Dentro de las subestructuras directamente fijadas al lecho marino existen varias tipologías. En primer lugar, los monopilotes son la tecnología más usada (69.7% de las subestructuras registradas en 2023). Esta consiste en un pilote de gran diámetro que se hinca en el lecho marino, constituyendo la mejor solución en términos de efectividad y costes de instalación para aguas poco profundas. El 75 % de las subestructuras anunciadas para los próximos 72 GW de futuros proyectos de eólica marina corresponden a monopilotes [5], por tanto, esta tecnología seguirá predominando en los próximos años. En segundo lugar, las subestructuras tipo jackets (que representan el 16.8 % de las subestructuras reportadas), son estructuras de acero en celosía empleadas para profundidades de agua mayores. Su representación ha ido incrementando con el paso de los años debido a la necesidad de instalar estas estructuras más lejos de la costa. Este tipo de subestructura es fijada al lecho marino mediante grupos de pilotes o cajones de succión (generalmente de 3 a 5 pilotes o cajones de succión), los cuales se disponen de forma poligonal. Los cajones de succión se caracterizan por una instalación más silenciosa y de mayor simplicidad. No obstante, los grupos de pilotes son la solución de cimentación más común (utilizados en aproximadamente el 80 % de los jackets registrados), ya que pueden ser instalados en una mayor variedad de suelos, y proporcionan mejores características estructurales debido a su mayor esbeltez y rigidez vertical [6]. Seguidamente, se encuentran las subestructuras de encepado y los trípodes. Las subestructuras de encepado consisten en múltiples pilotes hincados en el lecho marino unidos entre sí con un encepado, mientras que la tecnología trípode consiste en una columna central unida rígidamente a tres patas inclinadas que se apoyan en el lecho marino mediante grupos de pilotes o cajones de succión. De esta forma, queda de manifiesto la importante presencia que tienen los pilotes como elementos de cimentación para aerogeneradores marinos.

Los aerogeneradores marinos están constantemente sometidos a cargas dinámicas muy variables: viento, olas y cargas de operación. Todas estas cargas dinámicas inducen vibraciones que podrían causar daños por fatiga o inestabilidad estructural. Además, como consecuencia de la expansión global en la instalación de aerogeneradores marinos, estos se han comenzado a instalar en regiones con mayor riesgo sísmico. Por ello, las cargas sísmicas también se han convertido en un factor esencial a considerar, surgiendo recientemente recomendaciones prácticas para reducir el riesgo sísmico de parques eólicos [7]. Otro aspecto crucial en el diseño de este tipo de estructuras es asegurar que las frecuencias naturales del sistema estén suficientemente alejadas de las frecuencias de operación del rotor, del efecto sombra provocado por la rotación de las aspas, y de las cargas medioambientales que actúan sobre la estructura. Como consecuencia de todo esto, el análisis dinámico de aerogeneradores marinos ha sido extensamente estudiado a lo largo del presente siglo [8–30], y las cargas sísmicas se han venido estudiando e

incorporando en estos análisis dinámicos [8, 10, 11, 14–31], reconociéndose la importancia de su incorporación, puesto que incluso sismos de pequeña intensidad pueden afectar a su respuesta estructural [8, 20, 30, 31].

En los análisis dinámicos de esta estructuras esbeltas comúnmente cimentadas en suelos blandos, la consideración de la interacción suelo–estructura juega un papel fundamental, puesto que su respuesta dinámica se ve significativamente influenciada por dicha interacción, pudiendo dar lugar a respuestas más elevadas y a frecuencias naturales significativamente distintas que las que se obtienen al suponer una base rígida [8–10, 21, 24, 25, 32, 33]. Con respecto al modelado de esta interacción suelo-estructura en cimentaciones pilotadas de aerogeneradores marinos, esta se puede clasificar principalmente en dos grandes categorías: modelos de interacción lineales y no-lineales.

Por una parte, los modelos de interacción suelo-estructura lineales [8, 22–26, 29, 34–41] asumen un comportamiento elástico y lineal en esta interacción, manteniendo las mismas propiedades de rigidez y de amortiguación independientemente de la deformación o de la intensidad de carga. Una aproximación lineal es el método de subestructuración, el cual emplea matrices de impedancias y factores de interacción cinemática que representan la rigidez y amortiguación del conjunto suelo-cimentación, y la filtración de los movimientos del terreno por la cimentación, respectivamente [22, 23, 25, 29]. Otro enfoque lineal es el uso de modelos de parámetros concentrados, los cuales representan el comportamiento dinámico del suelo mediante un sistema equivalente de resortes, amortiguadores y masas concentradas [8, 24, 26]. Estos modelos de parámetros concentrados se basan en ajustar los resultados en frecuencia obtenidos de modelos más complejos, con el objetivo de representar las funciones de impedancias dinámicas del suelo mediante un sistema discreto equivalente. De esta forma, el comportamiento dinámico de referencia del conjunto suelo-cimentación en todos estos enfoques lineales es obtenido mediante formulaciones desarrolladas más complejas, las cuales se basan en diferentes técnicas para reproducir rigurosamente la interacción suelo-cimentación, como el método de elementos finitos, el método de elementos de contorno, otras soluciones en semiespacio elástico, etc. [39, 42–45]. Por otro lado, para grupos de pilotes, donde aparte de la interacción suelo-pilote existe la interacción pilote-suelo-pilote, las funciones de impedancia pueden ser calculadas utilizando otro enfoque conocido como método de superposición [35–40]. Este enfoque permite estimar la respuesta dinámica de un grupo de pilotes sumando las respuestas individuales de cada pilote con las interacciones entre pares de pilotes. La principal ventaja de este método en comparación con otros modelos más desarrollados es su simplicidad, lo que lo convierte en un enfoque interesante para abordar diseños iniciales y estudios paramétricos. La efectividad del método de superposición ha sido explorada en el análisis dinámico de configuraciones de pilotes típicas para edificaciones [36, 39], donde se ha demostrado que el método conduce a estimaciones bastante precisas para separaciones entre pilotes medias y largas. Finalmente, otro enfoque es considerar un comportamiento lineal dentro de modelos de viga sobre cimentación tipo Winkler. En este tipo de modelos, la interacción entre pilote y suelo circundante se realiza mediante resortes independientes dispuestos en paralelo con amortiguadores a lo largo de la longi-

tud del pilote. Dentro de estos modelos tipo Winkler, para grupos de pilotes, los efectos pilote-suelo-pilote se pueden simular mediante el uso de factores de interacción [38, 41]. Las principales ventajas de todos estos modelos que asumen un comportamiento lineal de los medios implicados con respecto a los no-lineales, es su facilidad de definición y su eficiencia computacional, lo que los hacen ideales para abordar diseños preliminares y estudios paramétricos. Con respecto a su uso en el estudio dinámico de aerogeneradores marinos, los modelos lineales son usados frecuentemente ya sea empleando modelos de subestructuración [22, 23, 25, 29], o modelos de parámetros concentrados [8, 24, 26].

Por otra parte, los modelos de interacción suelo-estructura no-lineales permiten modelar el comportamiento no-lineal de la interacción suelo-pilote, permitiendo reproducir la degradación de la rigidez, el comportamiento histerético y la plasticidad en esta interacción. Para ello, se utilizan relaciones de resistencia y deflexión del suelo hiperbólicas ($p-y$), así como reglas de carga y descarga, que necesitan procedimientos iterativos para poder ser resueltas. Por todas estas características, estos modelos son más complejos que los lineales, y son considerados más realistas. Entre los modelos no-lineales más empleados se encuentran los modelos de viga sobre cimentación tipo Winkler, donde para grupos de pilotes los efectos de interacción pilote-suelo-pilote son modelados mediante multiplicadores-p, que son coeficientes de reducción empíricos que se aplican sobre las curvas $p-y$ de un pilote aislado para tener en cuenta los efectos del grupo [46–48]. En cuanto al uso de estos modelos no-lineales en el análisis dinámico de aerogeneradores marinos, las relaciones hiperbólicas $p-y$ normalmente empleadas son las curvas establecidas por la recomendación práctica del API (American Petroleum Institute [49]), ya que su aplicación es recomendada también por el estándar técnico DNV-OS-J101 [50]. Debido a que son modelos más realistas y a que son recomendados por estos estándares, el uso de este tipo de modelos no-lineales de interacción suelo-estructura en el análisis dinámico de aerogeneradores marinos ha incrementado notablemente en los últimos años [9–19, 21, 31].

Ambos enfoques han sido ampliamente empleados y estudiados en el análisis dinámico de aerogeneradores marinos soportados por monopilotes y jackets [8–19, 21–26, 29, 31]. No obstante, ciertos aspectos relacionados con el modelado de la interacción suelo-estructura y sus efectos sobre la respuesta sísmica de cimentaciones pilotadas para aerogeneradores marinos no han sido abordados con la suficiente profundidad, aún existiendo incertidumbres en torno a ellos. Por ejemplo, algunos modelos lineales de interacción suelo-estructura han sido empleados para evaluar la influencia de algunos parámetros como: las dimensiones de los aerogeneradores [8, 25], condiciones de operación [8, 26], o direccionalidad sísmica [26]. No obstante, la influencia de la definición del perfil del lecho marino en la respuesta sísmica de aerogeneradores marinos, así como el análisis de los efectos de interacción suelo-estructura dependiendo de esta definición, no han sido abordados todavía. El estudio de esta influencia supondría una contribución valiosa para abordar las etapas de diseño y el análisis dinámico en este tipo de estructuras, especialmente en situaciones donde la definición del perfil de suelo supone una incertidumbre debida a su inherente complejidad. Además, la interacción suelo-estructura está formada por dos tipos de interacción: la cinemática

e inercial. La interacción cinemática está influenciada por el movimiento del suelo y la interfaz suelo-pilote, mientras que la interacción inercial está principalmente afectada por la masa de la superestructura. La mayoría de los estudios que evalúan los efectos de la interacción suelo-estructura tienden a analizar este fenómeno en su conjunto [8–10, 21, 23–26], sin examinar la contribución de la interacción cinemática e inercial por separado. Una mejor comprensión acerca de estas dos componentes permitiría mejorar el entendimiento del comportamiento dinámico de estas estructuras, así como el modelado de su interacción suelo-estructura. Otro aspecto no abordado es el estudio de la influencia de los efectos no-lineales y plásticos dentro del modelado de la interacción suelo-estructura en comparación con la suposición lineal y elástica. Aunque algunos efectos no-lineales en las propiedades del suelo, como la plasticidad y la degradación de rigidez, han sido estudiados en el análisis dinámico de estas estructuras (ver, por ejemplo, [51]), los efectos no-lineales en el modelado de la interacción suelo-estructura para el análisis dinámico de estos dispositivos no han sido evaluados aún. La comprensión de esta influencia en la interacción suelo-estructura ayudaría a definir el rango de aplicación de los modelos no-lineales y lineales, proporcionando una contribución valiosa en el diseño y análisis dinámico de estos dispositivos. Por último, la aplicabilidad del método de superposición para configuraciones de pilotes típicas de infraestructuras civiles ha sido ampliamente estudiada (ver, por ejemplo, [36, 39]). Sin embargo, la funcionalidad de este método en el análisis dinámico de configuraciones de pilotes para aerogeneradores marinos, las cuales se caracterizan por estar compuestas de disposiciones poligonales de N lados, no ha sido examinada todavía en profundidad. Por tanto, analizar la aplicabilidad de este método contribuiría a determinar si esta metodología supone una alternativa útil en la reproducción de la interacción suelo-estructura para este tipo de estructuras.

A.2 Objetivos

Esta tesis doctoral pretende contribuir al avance en el modelado de la interacción suelo-estructura para el análisis sísmico de aerogeneradores marinos soportados por cimentaciones pilotadas, investigando la influencia de la heterogeneidad del suelo, el comportamiento no-lineal de la interacción suelo-estructura, y los efectos del grupo, mediante una serie de estudios paramétricos. Para conseguir este objetivo principal, se establecen los siguientes objetivos adicionales:

- Analizar la influencia de la definición del perfil del lecho marino en la respuesta sísmica de varios aerogeneradores marinos monopilotados, evaluando los efectos de la interacción suelo-estructura y las componentes cinemáticas e inerciales que la forman.

- Estudiar el impacto de los efectos no-lineales e inelásticos dentro de la interacción suelo-estructura en la respuesta sísmica de cimentaciones pilotadas de aerogeneradores marinos.

- Evaluar la aplicabilidad del método de superposición en el cálculo de funciones de impedancia para grupos de pilotes de aerogeneradores marinos, estudiando una amplia variedad de configuraciones realistas de grupos de pilotes y la influencia de los principales parámetros involucrados en el problema.

La consecución de todos estos objetivos no solo permitiría mejorar el modelado y la comprensión de los fenómenos relacionados con la interacción suelo-estructura en la respuesta sísmica de aerogeneradores marinos, sino que también supondrían una contribución para abordar las etapas de diseño de este tipo de estructuras. A partir de las conclusiones alcanzadas, sería posible identificar los modelos de interacción suelo-estructura e hipótesis más apropiadas para cada escenario específico.

A.3 Publicaciones derivadas de la tesis doctoral

La tesis por compendio está compuesta por las siguientes tres publicaciones en revistas científicas indexadas en el Journal Citation Reports (JCR):

- E. Rodríguez-Galván, G. M. Álamo, C. Medina and O. Maeso. Influence of seabed profile on the seismic response of monopile-supported offshore wind turbines including dynamic soil-structure interaction. Marine Structures, 92:103500, 2023.

- E. Rodríguez-Galván, G. M. Álamo, J. J. Aznárez and O. Maeso. Non-linear behaviour of soil–pile interaction phenomena and its effect on the seismic response of OWT pile foundations. Validity range of a linear approach through non-degraded soil properties. Computers and Geotechnics, 168:106188, 2024.

- E. Rodríguez-Galván, G. M. Álamo, J. J. Aznárez and O. Maeso. An accurate and ready-to-use approach for the estimation of impedance functions of regular pile groups for offshore wind turbine foundations. Vertical and rocking components. Engineering Structures, 323:119288, 2025.

Además, también se ha realizado una contribución a congreso:

- E. Rodríguez-Galván, G. M. Álamo, C. Medina, L. A. Padrón, J. J. Aznárez and O. Maeso. Seismic response of monopile-supported offshore wind turbines embedded in different seabed profiles including dynamic soil-structure interaction. 9th International Conference on Computational Methods in Structural Dynamics and Earthquake Engineering (COMPDYN), 2023.

A.4 Justificación

La respuesta dinámica de aerogeneradores marinos es un problema complejo que debe ser evaluado considerando la interacción entre todas las partes que la forman: torre, subestructura, cimentación y suelo. Para llevar a cabo estos análisis dinámicos son necesarios modelos numéricos. La incorporación de la interacción suelo-estructura ha demostrado ser un factor determinante para reproducir correctamente la respuesta dinámica y realizar el diseño de estas estructuras. Sin embargo, aunque la interacción suelo-estructura haya sido objeto de estudio en los últimos años, todavía existen una serie de aspectos que demandan más estudio. Por esto, esta tesis se centra en analizar ciertos aspectos relacionados con el modelado y los efectos de la interacción suelo-estructura en el análisis sísmico de cimentaciones pilotadas de aerogeneradores marinos, con el objetivo de contribuir a una mejor comprensión de este fenómeno para realizar el análisis dinámico y el diseño de estas estructuras. Para cumplir este objetivo, a lo largo de la tesis se analizan diversos modelos numéricos de interacción suelo-estructura, junto con los efectos y parámetros asociados con estos, a través de tres estudios paramétricos:

En primer lugar, se estudia la influencia del perfil de lecho marino sobre la respuesta sísmica de aerogeneradores marinos monopilotados de distinta potencia (desde 5 hasta 15 MW), analizando la influencia de la interacción suelo-estructura y de las interacciones cinemática e inerciales que la forman [54]. Con el objetivo de evaluar los fenómenos de interacción suelo-estructura y la contribución de la interacción cinemática e inercial, distintos submodelos son evaluados. Además de contribuir a un mejor entendimiento de los efectos de la interacción suelo-estructura en la respuesta sísmica de aerogeneradores monopilotados en distintos perfiles de suelo, este estudio también es una importante contribución para el diseño de estas estructuras, debido a la complejidad que existe en la definición del suelo marino en situaciones donde no existen estudios geotécnicos.

En segundo lugar, se evalúa la contribución del comportamiento no-lineal y plástico de la interacción suelo-estructura en la respuesta sísmica de cimentaciones pilotadas para aerogeneradores marinos y aerogeneradores marinos monopilotados [55]. Para esto, tres modelos de interacción suelo-estructura basados en modelos de viga de cimentación Winkler son desarrollados: un modelo plástico no-lineal, un modelo elástico no-lineal y un modelo no-degradado equivalente lineal. Se estudia la respuesta sísmica de varias cimentaciones monopilotadas en dos tipos de suelos empleando los tres modelos desarrollados, analizando la contribución de los efectos cinemáticos e inerciales dentro de la interacción suelo-estructura. Finalmente, se examina la respuesta sísmica de varios aerogeneradores monopilotados de distinta potencia (entre 5 y 15 MW) mediante cada uno de los tres modelos de interacción suelo-estructura. La evaluación de los efectos no-lineales e inelásticos en la interacción suelo-estructura comparando los tres modelos con un modelo elástico lineal, suponen un avance en el modelado de esta interacción, proporcionando conclusiones útiles en la selección de la hipótesis de interacción más adecuada a utilizar en procesos de diseño y análisis sísmicos.

Finalmente, se analiza la aplicación del método de superposición en la determinación de las funciones de impedancia verticales y de cabeceo para cimentaciones de grupos de pilotes de aerogeneradores marinos [56]. Se ha seleccionado el análisis del término de impedancia de cabeceo debido al papel fundamental que desempeña esta componente en la respuesta sísmica de este tipo de estructuras, tal como se evidenció en el primer estudio paramétrico desarrollado dentro de esta tesis [54]. Este análisis se realiza para una amplia variedad de grupos de pilotes, analizando la influencia de los principales parámetros involucrados en el problema. Además, se proponen una serie de expresiones dependientes de estos parámetros para estimar las respuesta de un solo pilote y las interacciones pilote-suelo-pilote. Estas expresiones, junto con el método de superposición, permiten estimar las funciones de impedancia sin la necesidad de disponer de un modelo riguroso. Así, el método de superposición y las expresiones propuestas constituyen un enfoque útil para estimar rápidamente las funciones de impedancia de interacción suelo-estructura, lo cual puede ser efectivo para abordar diseños preliminares de este tipo de estructuras o estudios paramétricos.

Aunque en esta tesis se han analizado una gran variedad de modelos de interacción suelo-estructura y aspectos relacionados con esta interacción, el marco metodológico del presente trabajo sigue una misma dirección: la comparación y el análisis de distintos modelos de interacción suelo-estructura, específicamente diseñados o seleccionados para estudiar los fenómenos claves objetos de investigación. Esta comparación se realiza mediante estudios paramétricos en los que se evalúa una amplia gama de configuraciones y variables relevantes dentro del problema, con el fin de obtener conclusiones generales que contribuyan a mejorar el modelado de la interacción suelo-cimentación de estas estructuras.

A.5 Conclusiones

Esta tesis doctoral tiene como objetivo contribuir a una mejor comprensión de algunos aspectos no explorados relacionados con el modelado de la interacción suelo-estructura y su influencia en la respuesta sísmica de cimentaciones pilotadas para aerogeneradores marinos. A tal efecto, se han realizado tres estudios paramétricos con la finalidad de obtener conclusiones generales y útiles.

Inicialmente, en el primer trabajo se analiza la influencia del tipo de perfil de lecho marino en la respuesta sísmica de aerogeneradores monopilotados. Con este fin, se estudian tres tipos de perfiles de suelo: uno homogéneo, y dos no-homogéneos, con velocidades de propagación de ondas de cizalla equivalentes consideradas entre 100 y 300 m/s, representando una gran variedad de lechos marinos desde blandos a medios [54]. Se evalúa la respuesta sísmica de cuatro aerogeneradores marinos monopilotados de distinta potencia nominal (desde 5 a 15 MW) en todos estos suelos. Para ello, se considera un modelo de subestructuración de elementos finitos en el dominio de la frecuencia, donde el comportamiento del conjunto suelo-monopilote se realiza mediante funciones de impedancias y factores de interacción cinemática, utilizando un

modelo continuo previamente desarrollado para su cálculo [45]. La excitación sísmica se representa mediante ondas de corte que se propagan verticalmente produciendo un movimiento de campo libre en la superficie del lecho marino. La respuesta sísmica se cuantifica en términos de momentos máximos, fuerzas cortantes máximas, y factores de amplificación de aceleraciones, todos ellos calculados realizando la media de las respuestas obtenidas para 10 sismos diferentes. Para analizar la influencia de la interacción suelo-estructura, y de las componentes cinemática e inercial dentro de esta, se evalúan distintos submodelos de interacción suelo-estructura. Primero, para el aerogenerador de 10 MW se analiza el comportamiento de su cimentación y las frecuencias naturales del conjunto estructural. En este análisis se observa que el movimiento de rotación está principalmente influenciado por las cotas más profundas del suelo, mientras que el movimiento lateral lo está por las más superficiales, obteniéndose mayores impedancias laterales y factores de interacción de cabeceo en los suelos homogéneos, mientras que en los no-homogéneos se dan mayores impedancias de rotación, cruzadas y factores de interacción cinemática laterales. Por tanto, a medida que la variación de las propiedades elásticas del suelo es más significativa, se obtienen menores frecuencias naturales. Seguidamente, se evalúan las respuestas sísmicas en cada submodelo y para cada aerogenerador y suelo. Concluyéndose que las mayores respuestas se dan cuando la interacción suelo-estructura es considerada en su conjunto, y que el factor de interacción cinemática de cabeceo es la componente más relevante dentro de esta interacción para este tipo de estructuras. Finalmente, se aborda la influencia de considerar un perfil no-homogéneo frente a uno homogéneo, concluyéndose que la suposición homogénea conduce a resultados más conservadores, debido a la alta influencia del factor de interacción cinemática de cabeceo para este caso.

En el segundo trabajo se estudia la influencia de los efectos no-lineales y plásticos en la interacción suelo-estructura [55]. Con este objetivo, se analizan y comparan tres modelos de interacción suelo-pilote: un modelo plástico no-lineal, uno elástico no-lineal y otro elástico lineal definido a partir de las propiedades no degradadas del suelo, escogiendo este último como referencia. Todos estos modelos se basan en el modelo de viga de cimentación tipo Winkler y en las curvas de resistencia-deflexión del suelo establecidas por la recomendación práctica API [49]. A lo largo del trabajo se evalúan los efectos no-lineales e inelásticos analizando las interacciones cinemáticas e inerciales. Se estudian dos tipos de suelo arenosos, uno muy suelto y otro medio denso. Los pilotes y aerogeneradores se modelan mediante el método de elementos finitos. La excitación sísmica se modela mediante ondas de corte armónicas se propagan verticalmente a través de un semiespacio elástico no-homogéneo con variación lineal de las propiedades elásticas del suelo con la profundidad. La respuesta sísmica se cuantifica en términos de envolventes medias de máximos momentos flectores, fuerzas cortantes y aceleraciones, utilizando 10 sismos escalados con respecto a una aceleración máxima de 0,6g. En primer lugar, se analiza la respuesta sísmica de diferentes pilotes de aerogeneradores marinos, desde larga a corta esbeltez. Los efectos cinemáticos e inerciales son cuantificados utilizando distintas masas de encepado, definidas como una proporción δ (desde 0 hasta 1) de la capacidad de carga última vertical de cada pilote.

Además, los efectos no-lineales e inelásticos se cuantifican en términos de diferencias relativas de los dos modelos de interacción no-lineales con respecto al equivalente lineal. De este análisis se concluye que se obtienen resultados similares entre los tres modelos de interacción suelo-estructura cuando los efectos cinemáticos predominan, mientras que cuando la interacción inercial es activada se empiezan a ver diferencias entre modelos. No obstante, el modelo lineal equivalente conduce a resultados más conservadores, seguido del modelo no-lineal elástico. Finalmente, se estudian las respuestas sísmicas de los aerogeneradores marinos monopilotados, y el de sus respectivos monopilotes. Se concluye que los tres modelos de interacción conducen a resultados muy similares, ya que la masa de la superestructura no es suficiente como para activar los efectos inerciales en los casos analizados.

Finalmente, en el tercer trabajo se evalúa la aplicabilidad del método de superposición en la estimación de las impedancias verticales y de cabeceo para grupos de pilotes de aerogeneradores marinos, realizando un extenso estudio paramétrico adimensional [56]. En este tercer trabajo se estudia la contribución de los principales parámetros involucrados en el problema (frecuencia y características de pilote y suelo), analizando una amplia gama de configuraciones realistas de grupos de pilotes. Se proponen y ajustan algunas expresiones dependientes de estos principales parámetros que permiten determinar directamente las flexibilidades del pilote aislado y los factores de interacción sin necesidad de disponer de un modelo riguroso para su cálculo. Estas expresiones están basadas en un caso de referencia, junto con unos factores correctores que permiten reproducir la influencia individual de los distintos parámetros. Las flexibilidades del pilote fuente y los factores de interacción necesarios para ajustar todas estas expresiones, fueron obtenidos a partir de un modelo continuo previamente desarrollado [45]. Para estudiar la eficacia del método de superposición y las expresiones propuestas, las funciones de impedancias obtenidas mediante superposición utilizando estas expresiones son comparadas con las impedancias directamente calculadas mediante el modelo continuo. Primero, se estudió la aplicabilidad del método para el caso de referencia, demostrándose que la superposición y las expresiones propuestas conducen a estimaciones precisas de las impedancias verticales y de cabeceo para estos grupos de pilotes, caracterizados por disponer de grandes separaciones entre pilotes. Seguidamente, se analiza la influencia de los distintos parámetros y la validez de los ajustes de los factores correctores. De esto se concluye que, además de la frecuencia adimensional y del ratio de separación entre pilotes, las demás características relacionadas con el pilote y suelo (esbeltez del pilote, relación de rigidez y amortiguamiento) pueden afectar notablemente a la estimación de las funciones de impedancia. Además, se observa que los factores de corrección se pueden emplear sobre el caso de referencia para reproducir la influencia de cada uno de estos parámetros. Finalmente, se comprueba que el uso de los ajustes de los factores correctores conducen a buenas estimaciones, demostrándose que la corrección del término de flexibilidad del pilote aislado es más influyente que la corrección del término relacionado con el factor de interacción entre pilotes.

Así, la presente tesis ha explorado ciertos aspectos con respecto al modelado y los efectos de la interacción suelo-estructura en la respuesta sísmica de cimentaciones pi-

lotadas de aerogeneradores marinos, obteniéndose algunas conclusiones valiosas para abordar el diseño y análisis sísmico de estas estructuras. Las conclusiones más relevantes de entre todas las obtenidas son:

- La consideración de un perfil de suelo homogéneo da lugar a respuestas sísmicas más conservadoras que la suposición de un suelo heterogéneo, debido a la gran relevancia que adquiere el factor de interacción cinemática de cabeceo.
- Para reproducir la respuesta sísmica de cimentaciones pilotadas de aerogeneradores marinos y de aerogeneradores marinos monopilotados, se puede emplear un modelo de interacción suelo-pilote lineal definido a partir de las propiedades no degradadas del suelo. Debido a que esta suposición conlleva a resultados similares y más conservadores que los modelos de interacción no-lineales, ya que la interacción cinemática es la que predomina dentro de la interacción suelo-monopilote en este tipo de estructuras.
- El método de superposición, junto con las expresiones propuestas, pueden ser empleados para determinar las funciones de impedancias verticales y de cabeceo para grupos de pilotes de aerogeneradores marinos.

Un estudio más detallado de cada uno de los problemas analizados, acompañado de conclusiones más específicas, se presentan en las publicaciones que integran esta tesis.

REFERENCES

[1] B. M. Das. Principles of Foundation Engineering. Cengage Learning, Boston, MA, 8th edition, 2015.

[2] M. J. Tomlinson and J. Woodward. Pile Design and Construction Practice. CRC Press, Taylor & Francis Group, Boca Raton, FL, 6th edition, 2015.

[3] G. W. E. Council. Global Wind Report 2025. Technical report, Global Wind Energy Council (GWEC), April 2025.

[4] G. W. E. Council. Global Offshore Wind Report 2025. Technical report, Global Wind Energy Council / Pacific Northwest National Laboratory, June 2025.

[5] A. McCoy, W. Musial, R. Hammond, D. Hernando, P. Duffy, P. Beiter, P. Pérez, R. Baranowski, G. Reber and P. Spitsen. Offshore wind market report: 2024 edition. Technical Report NREL/TP-5000-90525, National Renewable Energy Laboratory (NREL), U.S. Department of Energy, Golden, CO, 2024.

[6] S. Jalbi and S. Bhattacharya. Concept design of jacket foundations for offshore wind turbines in 10 steps. Soil Dynamics and Earthquake Engineering, 139:106357, 2020.

[7] Det Norske Veritas (DNV). DNV-RP-0585: Seismic design of wind power plants. Technical report, Det Norske Veritas, August 2021. Recommended Practice, Edition 2021-08.

[8] L. A. Padrón, S. Carbonari, F. Dezi, M. Morici, J. D. R. Bordón and G. Leoni. Seismic response of large offshore wind turbines on monopile foundations including dynamic soil–structure interaction. Ocean Engineering, 257:111653, 2022.

[9] S. Bisoi and S. Haldar. Dynamic analysis of offshore wind turbine in clay considering soil–monopile–tower interaction. Soil Dynamics and Earthquake Engineering, 63:19–35, 2014.

[10] S. Shi, E. Zhai, C. Xu, K. Iqbal, Y. Sun and S. Wang. Influence of pile-soil interaction on dynamic properties and response of offshore wind turbine with monopile foundation in sand site. Applied Ocean Research, 126:103279, 2022.

[11] A. Ali, R. De Risi and A. Sextos. Seismic assessment of wind turbines: How crucial is rotor-nacelle-assembly numerical modeling? Soil Dynamics and Earthquake Engineering, 141:106483, 2021.

[12] S. Bisoi and S. Haldar. Design of monopile supported offshore wind turbine in clay considering dynamic soil–structure-interaction. Soil Dynamics and Earthquake Engineering, 73:103–117, 2015.

[13] S. Haldar, J. Sharma and D. Basu. Probabilistic analysis of monopile-supported offshore wind turbine in clay. Soil Dynamics and Earthquake Engineering, 105:171–183, 2018.

[14] L. Wang and T. Ishihara. A new foundyn module in openfast to consider foundation dynamics of monopile supported wind turbines using a site-specific soil reaction framework. Ocean Engineering, 266:112692, 2022.

[15] F. Liang, Z. Yuan, X. Liang and H. Zhang. Seismic response of monopile-supported offshore wind turbines under combined wind, wave and hydrodynamic loads at scoured sites. Computers and Geotechnics, 144:104640, 2022.

[16] D. H. Kim, S. G. Lee and I. K. Lee. Seismic fragility analysis of 5 MW offshore wind turbine. Renewable energy, 65:250–256, 2014.

[17] W. Jiang, C. Lin and M. Sun. Seismic responses of monopile-supported offshore wind turbines in soft clays under scoured conditions. Soil Dynamics and Earthquake Engineering, 142:106549, 2021.

[18] W. Jiang and C. Lin. Lateral responses of monopile-supported offshore wind turbines in sands under combined effects of scour and earthquakes. Soil Dynamics and Earthquake Engineering, 155:107193, 2022.

[19] R. Mo, R. Cao, M. Liu and M. Li. Effect of ground motion directionality on seismic dynamic responses of monopile offshore wind turbines. Renewable Energy, 175:179–199, 2021.

[20] P. Wang, M. Zhao, X. Du, J. Liu and C. Xu. Wind, wave and earthquake responses of offshore wind turbine on monopile foundation in clay. Soil Dynamics and Earthquake Engineering, 113:47–57, 2018.

[21] Y. Yang, M. Bashir, C. Li and J. Wang. Analysis of seismic behaviour of an offshore wind turbine with a flexible foundation. Ocean Engineering, 178:215–228, 2019.

[22] A. M. Kaynia. Effect of kinematic interaction on seismic response of offshore wind turbines on monopiles. Earthquake Engineering & Structural Dynamics, 50(3):777–790, 2021.

[23] A. M. Kaynia, D. M. Pedersen, H. Askheim and C. Romero-Sánchez. Implementation of seismic soil-structure interaction in openfast and application to an offshore wind turbine on jacket structure. Marine Structures, 103:103832, 2025.

[24] C. Romero-Sánchez and L. A. Padrón. Influence of wind and seismic ground motion directionality on the dynamic response of four-legged jacket-supported offshore wind turbines. Engineering Structures, 300:117191, 2024.

[25] C. Medina, G. M. Álamo and R. Quevedo-Reina. Evolution of the seismic response of monopile-supported offshore wind turbines of increasing size from 5 to 15 MW including dynamic soil-structure interaction. Journal of Marine Science and Engineering, 9(11):1285, 2021.

[26] C. Romero-Sánchez and L. A. Padrón. Seismic response of jacket-supported offshore wind turbines for different operational modes considering earthquake directionality. Ocean Engineering, 311:118798, 2024.

[27] N. Alati, G. Failla and F. Arena. Seismic analysis of offshore wind turbines on bottom-fixed support structures. Philosophical Transactions of the Royal Society A: Mathematical, Physical and Engineering Sciences, 373(2035):20140086, 2015.

[28] M. James and S. Haldar. Seismic vulnerability of jacket supported large offshore wind turbine considering multidirectional ground motions. In Structures, volume 43, 407–423. Elsevier, 2022.

[29] C. Medina, G. M. Álamo and L. A. Padrón. Contribution of the rotational kinematic interaction to the seismic response of monopile-supported offshore wind turbines. Ocean Engineering, 280:114778, 2023.

[30] W. Wang, Z. Gao, X. Li and T. Moan. Model test and numerical analysis of a multi-pile offshore wind turbine under seismic, wind, wave, and current loads. Journal of Offshore Mechanics and Arctic Engineering, 139(3):031901, 2017.

[31] S. K. Patra and S. Haldar. Seismic response of monopile supported offshore wind turbine in liquefiable soil. Structures, 31:248–265, 2021.

[32] L. Arany, S. Bhattacharya, J. H. Macdonald and S. J. Hogan. Closed form solution of eigen frequency of monopile supported offshore wind turbines in deeper waters incorporating stiffness of substructure and SSI. Soil Dynamics and Earthquake Engineering, 83:18–32, 2016.

[33] R. Quevedo-Reina, G. M. Álamo, S. François, G. Lombaert and J. J. Aznárez. Importance of the soil–structure interaction in the optimisation of the jacket designs of offshore wind turbines. Ocean Engineering, 303:117802, 2024.

[34] G. M. Álamo, J. D. R. Bordón, J. J. Aznárez and O. Maeso. Relevance of soil-pile tangential tractions for the estimation of kinematic seismic forces: Formulation and setting of a winkler approach. Applied Mathematical Modelling, 59:1–19, 2018.

[35] H. Poulos. Analysis of the settlement of pile groups. Geotechnique, 18(4):449–471, 1968.

[36] R. Dobry and G. Gazetas. Simple method for dynamic stiffness and damping of floating pile groups. Geotechnique, 38(4):557–574, 1988.

[37] G. Gazetas and N. Makris. Dynamic pile-soil-pile interaction. Part I: Analysis of axial vibration. Earthquake Engineering & Structural Dynamics, 20(2):115–132, 1991.

[38] N. Makris and G. Gazetas. Dynamic pile-soil-pile interaction. Part II: Lateral and seismic response. Earthquake Engineering & Structural Dynamics, 21(2):145–162, 1992.

[39] A. M. Kaynia. Dynamic stiffness and seismic response of pile groups. Ph.D. thesis, Massachusetts Institute of Technology, 1982.

[40] A. F. R. Loria and L. Laloui. The interaction factor method for energy pile groups. Computers and Geotechnics, 80:121–137, 2016.

[41] G. Mylonakis and G. Gazetas. Settlement and additional internal forces of grouped piles in layered soil. Géotechnique, 48(1):55–72, 1998.

[42] A. M. Kaynia and E. Kausel. Dynamics of piles and pile groups in layered soil media. Soil Dynamics and Earthquake Engineering, 10(8):386–401, 1991.

[43] F. Dezi, S. Carbonari and G. Leoni. A model for the 3D kinematic interaction analysis of pile groups in layered soils. Earthquake Engineering & Structural Dynamics, 38(11):1281–1305, 2009.

[44] F. Dezi, S. Carbonari and M. Morici. A numerical model for the dynamic analysis of inclined pile groups. Earthquake Engineering & Structural Dynamics, 45(1):45–68, 2016.

[45] G. M. Álamo, A. E. Martínez-Castro, L. A. Padrón, J. J. Aznárez, R. Gallego and O. Maeso. Efficient numerical model for the computation of impedance functions of inclined pile groups in layered soils. Engineering Structures, 126:379–390, 2016.

[46] A. M. Dodds and G. R. Martin. Modeling pile behavior in large pile groups under lateral loading. Technical Report MCEER-07-0004, Multidisciplinary Center for Earthquake Engineering Research (MCEER), University at Buffalo, The State University of New York, Buffalo, NY, April 16 2007.

[47] D. A. Brown, C. Morrison and L. C. Reese. Lateral load behavior of pile group in sand. Journal of geotechnical engineering, 114(11):1261–1276, 1988.

[48] K. Jones, M. Sun and C. Lin. Numerical analysis of group effects of a large pile group under lateral loading. Computers and Geotechnics, 144:104660, 2022.

[49] American Petroleum Institute (API). Recommended Practice for Planning, Designing and Constructing Fixed Offshore Platforms—Working Stress Design (RP 2A-WSD). American Petroleum Institute, Washington, D.C., 21st edition, 2000. With errata and supplements from 2002, 2005, and 2007.

[50] Det Norske Veritas (DNV). DNV-OS-J101: Design of Offshore Wind Turbine Structures. Technical report, Det Norske Veritas, May 2014. Offshore Standard, Edition 2014-05.

[51] X. Cheng, T. Wang, J. Zhang, P. Wang, W. Tu and W. Li. Dynamic response analysis of monopile offshore wind turbines to seismic and environmental loading considering the stiffness degradation of clay. Computers and Geotechnics, 155:105210, 2023.

[52] L. A. Padrón, J. J. Aznárez and O. Maeso. BEM–FEM coupling model for the dynamic analysis of piles and pile groups. Engineering Analysis with Boundary Elements, 31(6):473–484, 2007.

[53] J. D. R. Bordón, G. M. Álamo, L. A. Padrón, J. J. Aznárez and O. Maeso. MultiFEBE: A multi-domain finite element–boundary element solver for linear mixed-dimensional mechanical problems. SoftwareX, 20:101265, 2022.

[54] E. Rodríguez-Galván, G. M. Álamo, C. Medina and O. Maeso. Influence of seabed profile on the seismic response of monopile-supported offshore wind turbines including dynamic soil-structure interaction. Marine Structures, 92:103500, 2023.

[55] E. Rodríguez-Galván, G. M. Álamo, J. J. Aznárez and O. Maeso. Non-linear behaviour of soil–pile interaction phenomena and its effect on the seismic response of OWT pile foundations. Validity range of a linear approach through non-degraded soil properties. Computers and Geotechnics, 168:106188, 2024.

[56] E. Rodríguez-Galván, G. M. Álamo, J. J. Aznárez and O. Maeso. An accurate and ready-to-use approach for the estimation of impedance functions of regular pile groups for offshore wind turbine foundations. Vertical and rocking components. Engineering Structures, 323:119288, 2025.

[57] E. Rodríguez-Galván, G. M. Álamo, C. Medina, L. A. Padrón, J. J. Aznárez and O. Maeso. Seismic response of monopile-supported offshore wind turbines embedded in different seabed profiles including dynamic soil-structure interaction. 9th International Conference on Computational Methods in Structural Dynamics and Earthquake Engineering (COMPDYN), 2023.

[58] National Renewable Energy Laboratory. OpenFAST Documentation. Release v3.5.2, 2024. https://openfast.readthedocs.io/en/main/. Code published at https://github.com/OpenFAST/openfast.

INSTITUTO UNIVERSITARIO
SIANI
INGENIERIA COMPUTACIONAL

Edificio Central del Parque Tecnológico
Campus Universitario de Tafira
35017 Las Palmas de Gran Canaria
e-mail: info@siani.es · www.siani.es